2012

A pneumatic semi-active control methodology for vibration control of air spring based suspension systems

William Daniel Robinson
Iowa State University

A pneumatic semi-active control methodology for vibration control of air spring based suspension systems

by

William Daniel Robinson

A dissertation submitted to the graduate faculty

in partial fulfillment of the requirements for the degree of

DOCTOR OF PHILOSOPHY

Major: Mechanical Engineering

Program of Study Committee:
Atul G. Kelkar, Major Professor
Jerald M. Vogel
James E. Bernard
Judy M. Vance
Greg R. Luecke
Brian L. Steward

Iowa State University

Ames, Iowa

2012

DEDICATION

To my wonderful wife and life partner, Charlyn, and to our wonderful children, Bill, Greg, David, and Ann.

TABLE OF CONTENTS

LIST OF FIGURES

LIST OF TABLES

ABSTRACT

This research investigates a pneumatic suspension system containing an air spring, air flow valve, and an accumulator, where the spring and damping functions are combined into one package. The spring and accumulator provide the spring characteristics, and the computer controlled adjustable valve provides the damping characteristics by automatically adjusting the air flow between the air spring and the accumulator.

An extensive analysis and investigation of the plant dynamics is performed. A dynamic plant model is developed and tuned to experimental data. The plant model is then used in the design of a semi-active control system. A detailed description of the model tuning procedure is provided.

Based upon the insights gained through analysis and system identification, a semi-active control methodology is developed, which exploits certain unique features of the system. Three potential controllers are developed and compared, where each controller uses different measurement feedback signals. However, all three controllers measure direct force generation through a pressure feedback signal. Both experimental and simulation data for the controllers is provided.

The first controller uses an LQI (Linear Quadratic Impulse) optimal solution, based on Covariance Control Theory, to generate an optimal "active" damping control force, along with a Set-Point plus PI tracking controller to adjust the valve opening to cause the system to track this desired force during a switching event or control window of opportunity.

The second controller uses a Modified Skyhook solution to generate the ideal tracking signal, along with a Set-Point plus PI tracking controller. The LQI controller is used in simulation (offline) to aid in setting the skyhook gain on the Modified Skyhook controller.

The third controller uses a Relative Displacement solution to generate the ideal tracking signal, along with a Set-Point plus PI tracking controller. The LQI controller is used (offline) to aid in setting the gain on the Relative Displacement controller. This controller is probably the most useful for vehicular applications, since only *relative* coordinates and a pressure are required for feedback.

It was found that all three controllers could track an optimally generated “active” signal during the switching event, provided the proper gains were chosen.

CHAPTER 1. INTRODUCTION

The rapid expansion of computer technology and the decreasing costs of computer processing equipment over the past several decades have allowed the proliferation of onboard computer systems for monitoring and controlling various aspects of vehicular performance. This has led to the research and application of advanced software control algorithms that continuously monitor and adjust various system parameters to enable optimum system performance over a wide range of operating conditions.

Vehicle suspension systems are one particular area of research and application that have benefited significantly from advanced methods of computer control. Before the computer revolution, vehicle suspension systems were typically classified as passive, which implies that computer control algorithms were not used. Research and development on these systems usually revolved around the development of better passive system components tuned to a specific disturbance environment. Computer control algorithms are typically applied to suspension systems that are classified as either active or semi-active. These types of systems have the ability to continuously adjust to varying disturbance environments or road inputs. The algorithms automatically seek to minimize in some respect the vibration that is imparted to a suspended mass as the disturbance environment changes over time. This is accomplished by using electrical sensors that monitor various elements of the system, and then issuing commands to physical actuators that adjust system parameters and/or impart energy to the system. By minimizing the vibration level imparted to an operator, the comfort level is increased and human fatigue is decreased, which ultimately leads to safer operation of the vehicle. In addition, by reducing the dynamic forces imparted to the suspension and vehicle, structural fatigue is diminished, which leads to longer life of the system components. The great majority of research on active and semi-active systems have revolved around some type of adjustable dampers or force actuators that directly impact damping of the suspended mass.

This thesis will present an in-depth analysis and correlated model of the plant (system) and an advanced semi-active control methodology to provide optimal vibration control for a pneumatic suspension composed of a mass suspended by an air spring connected to an accumulator through an adjustable air control valve. This chapter will provide an overview of

suspension system types and background information leading to the motivation for the methodology presented in this thesis. Subsequent chapters will develop the analysis, model, and control methodology, which will then be demonstrated with system simulations, and verified with experimental test results.

1.1 Basic Suspension Types

Suspension systems can be broadly classified as passive, active, and semi-active. A survey, bibliography, and classification of the dynamic analysis and control design aspects of advanced vehicle suspension systems before 1995 is found in [1]. This section will describe and compare each of the three basic suspension types. Relevant background and research information will be provided. Subsequent sections will describe the specific pneumatic system configuration under study, and provide a motivation for the control methodology presented in a later chapter.

To introduce the basic concepts, a single degree-of-freedom system will be used for each type suspension. If one is studying vehicle tire suspensions, usually a minimum of two degrees-of-freedom are used, one for the tire and one for the sprung mass. More complex full vehicle suspension models would use whatever degrees-of-freedom are appropriate to represent the particular dynamics under study. For designing seat suspensions, such as might be used in large over-the-road trucks, single degree-of-freedom models are usually sufficient for the initial study. Later in this thesis, it will be seen that a single degree-of-freedom is sufficient to describe and to use for controller development for the particular type pneumatic system that will be presented.

1.1.1 Passive Suspensions

The passive type suspension generally consists of spring and damper elements as shown in Figure 1.1. No computer control is associated with this type of suspension. The suspension characteristics are fixed by the mass, spring, and damper elements, although some passive systems may have limited adjustments for the spring and/or damper elements. Passive suspensions do not automatically change or optimize their spring or damper characteristics based upon a changing environment. Therefore, they are most effective over a narrow range

of disturbance inputs. The suspensions are designed based on a nominal mass load and disturbance environment expected to be most encountered over the design life of the suspension. Due to relatively low costs of manufacturing and maintenance when compared to the other system types, passive suspensions currently represent the majority of vehicular suspensions in use today. Research and development on passive systems has typically focused on improving and optimizing individual system elements, such as the shock absorber.

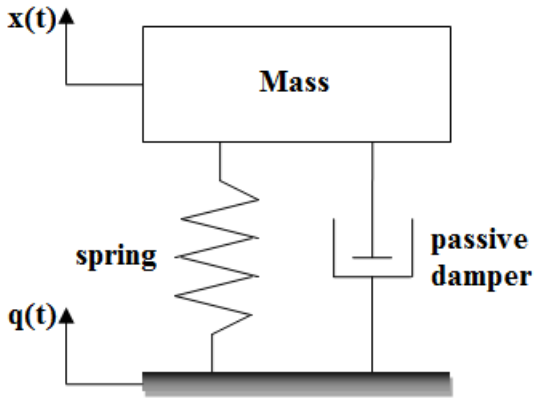

Figure 1.1 Passive system

To compare the various types of suspension, it is instructive to view simple representative equations of each system type. It should be understood that suspension systems are inherently nonlinear, and proper design must take into account the nonlinear nature of the suspension elements. However, to avoid unnecessary complexity while describing the basic ideas, linear system elements will be used.

If an idealized linear model is assumed to represent the system shown in Figure 1.1, then a linear, second order differential equation describing the system is

$$m\ddot{x} + b\dot{x} + kx = b\dot{q} + kq \tag{1.1}$$

where x, $\dot{x}$, and $\ddot{x}$ are the absolute displacement, velocity, and acceleration of the mass, respectively, and q, $\dot{q}$ are the displacement and velocity of the base. The coefficients m, b, and k represent the sprung mass, damping coefficient, and spring rate, respectively. The damping coefficient b includes the shock absorber effect in addition to any other inherent system damping, which is considered small relative to the damping force provided by the

physical shock absorber. The base motion terms located on the right-hand side of (1.1) are considered external disturbances acting on the system.

1.1.2 Active Suspensions

Active suspensions are typically composed of a spring element and some type of force actuator as shown in Figure 1.2. For present purposes, the damper element represented by the damping constant b_s represents the inherent system damping, not a separate shock absorber (damper) as was the case of the passive suspension. The primary damping or energy dissipation is provided by the active force actuator, and thus replaces the passive damper shown in Figure 1.1. Theoretically, both the spring and the damper could be replaced by a force actuator; however, this is not typical due to practical system constraints. At a minimum, some type of spring is usually necessary to provide support, even in the most advanced system designs.

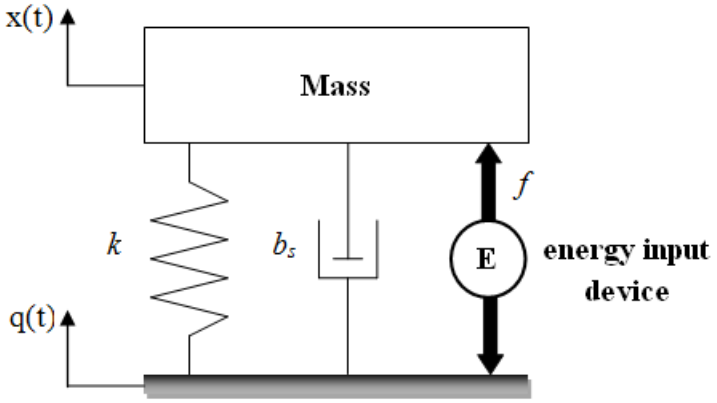

Figure 1.2 Active suspension

Assuming, as before, a linear idealized model, the differential equation representing the active suspension can be written as:

$$m\ddot{x} + b_s\dot{x} + kx = b_s\dot{q} + kq + f \tag{1.2}$$

where f is an external continuously varying force provided by the actuator, and the other terms are as previously defined. Equation (1.2) is expressed in a form such that the right-hand side consists of external influences on the system - base displacement and external force inputs. The external force, which is produced by a powered actuator, is capable of supplying

energy to the system. The left-hand side consist of terms representing inherent system characteristics – mass, damping (energy dissipation), and spring influence (energy storage). For active suspensions, a mathematical control law is developed and implemented in software on a real-time computer processor, which drives the actuator and thus determines the force *f*, which may become a function of several variables depending on the sensory input and the structure of the controller.

The literature has not been entirely consistent on what constitutes an active suspension. As acknowledged in [1] some authors and manufacturers have generalized "active" to refer to any system that employs a power supply and signal processing or is electronically modulated. This has included semi-active systems as well as other types. In their classification of advanced suspensions, the authors define two types of active suspension based on the capability of the force actuator – high frequency or broadband, also referred to as fully active, and low frequency or band-limited, also referred to as slow active. For purposes of this thesis, the term "active suspension" includes both of these type systems, and no further distinction is necessary.

An example of a recent innovation in broadband active suspensions is the Bose Corporation automotive suspension system as shown in Figure 1.3. Each suspension module contains a coiled spring of which its only function is to provide support. The primary actuation in each module is provided by a linear electromagnetic motor powered by amplifiers. The motors are capable of extending and retracting at rates great enough to virtually eliminate all vibrations to the passenger cabin. A module is attached to each wheel of the automobile. Proprietary advanced computer algorithms control the complete system. In addition to vibration control, the system also controls pitch and roll during braking, accelerating, and cornering. Another interesting feature claimed by the manufacturer is that the power amplifiers are regenerative, where power flows to the motors when required during an event, such as hitting a pothole, and then the motors act as generators after the event returning power back through the actuators. It is claimed that the power requirements are less than a typical automobile air conditioning system.

In addition to the active chassis suspension, Bose recently introduced an active seat suspension for large trucks as shown in Figure 1.4, which is based on the same technology as

the Bose active chassis suspension. According to Bose, the seat suspension runs off the truck battery and consumes no more energy than that needed by a 50-watt light bulb.

Figure 1.3 Bose active suspension

Figure 1.4 Bose active seat

1.1.3 Semi-active Suspension

A semi-active suspension is typically composed of a spring type element and a damper that is continuously adjustable as represented in Figure 1.5. The damper characteristic $\boldsymbol{\beta}$ is continuously variable and is controlled by a computer algorithm. Since the adjustable damper is not capable of supplying energy to the system, the system performance is limited compared to the capability of the active suspension. However, unlike an active suspension, the semi-active suspension is mathematically stable, since only the damping value is adjusted and no energy can be added to the system. Semi-active suspensions provide an alternative to active systems when the performance improvement of the semi-active system over the passive system is adequate. In addition, a semi-active suspension may be less costly and potentially more reliable than an active suspension.

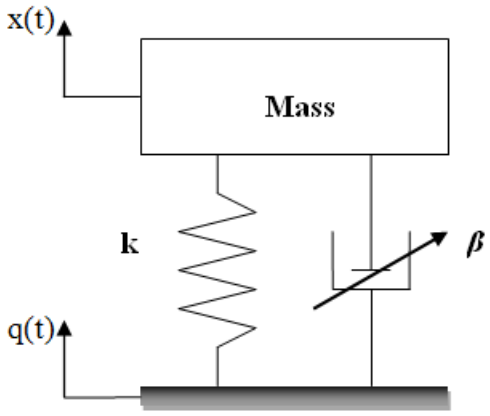

Figure 1.5 Semi-active suspension

The linear idealized model for this system is:

$$m\ddot{x} + (\beta + b_s)\dot{x} + kx = (\beta + b_s)\dot{q} + kq \tag{1.3}$$

where β varies over time as defined by a control law. In keeping with the prior convention, the external inputs are placed on the right-hand side of the equality, and the inherent system characteristics are placed on the left-hand side. For the semi-active suspension, a system characteristic (in this case, a damping coefficient) is controlled by the computer. The inherent system damping b_s has been separated from the primary damping mechanism. In other words,

if β equals to zero, the system would still have some amount of natural damping, smaller than the maximum achievable value of β.

The linear equation as written assumes that the damping force is a linear function of the relative velocity with slope equal to the damping coefficient. This is easier to see if (1.3) is rewritten in terms of a summation of forces as follows:

$$m\ddot{x} + f_d + f_s = 0 \tag{1.4}$$

where f_d is the damping force defined as

$$f_d = (\beta + b_s)(\dot{x} - \dot{q}) \tag{1.5}$$

and f_s is the spring force defined as

$$f_s = k(x - q) \tag{1.6}$$

where $(x - q)$ and $(\dot{x} - \dot{q})$ are the relative displacement and relative velocity, respectively.

In reality, the damping and spring forces are nonlinear. However, for passive suspension design, it is common to assume linearity over a certain range, depending on the design issue under study and the construction of the particular device. For control algorithm development, assumed linearity may not be appropriate for some semi-active system designs, due to the physics of the device that provides the damping force. In addition, the damping mechanism may not provide a force that is strictly a function of the relative velocity; it could also be some nonlinear function of both relative velocity and relative displacement. Sometimes a piece-wise linear assumption may be sufficient, as is the case for some systems using an MR (Magneto-Rheological) damper. In other systems, such as the pneumatic system that will be studied in this thesis, where the damping is a function of the mass flow of air through an orifice, assuming that the primary damping mechanism is a linear function of the relative velocity of the suspended mass may be problematic, as will be demonstrated in this thesis.

1.2 Pneumatic Suspensions

1.2.1 Air Springs

Pneumatic components, such as air springs, have long been used as vibration isolation and leveling devices. They are typically used where it is desired to have a higher spring rate in a smaller package than can be provided by an equivalent steel spring. They can also provide load leveling functions by adding or removing air. From the standpoint of vehicle suspensions, air springs can be found in many types of vehicles, such as automobiles, large trucks, buses, railway vehicles, construction and agricultural vehicles. In large truck applications, air springs can be used for cab and seat suspensions in addition to truck and trailer chassis suspensions. In addition, air springs are also used in factory operations.

An air spring (or air bag) is basically a column of air confined within a rubber and fabric container. Air springs are designed and manufactured in various shapes and sizes to meet a wide variety of applications as shown in Figure 1.6. Two common types are the reversible sleeve or rolling lobe and the convoluted or bellows as shown in Figure 1.7. A reversible sleeve type air spring contains a piston over which the elastomeric material moves as the height of the air spring changes in relation to load variations. Thus the piston plunges in and out of the air cavity. The convoluted air spring contains one or more lobes. There is no piston associated with this type air spring. In general, the reversible sleeve air spring has an advantage over the convoluted by the fact that the piston can be shaped to fine tune the spring rate. In addition, it is possible with the reversible sleeve design to maintain a constant load for a given internal pressure over a range of heights [2].

Figure 1.6 Assortment of air springs

Figure 1.7 Reversible sleeve and convoluted designs

As the name implies, an air spring is typically a replacement for the traditional steel spring in a suspension system. Depending on the application, advantages of the air spring over a steel spring are often cited in the literature. Some of the advantages enumerated in [2] are as follows:

1) An air spring has variable load-carrying capability. If a higher load needs to be accommodated, air can be added to the spring (automatically or manually) to increase the pressure and at the same time maintain the required height of the suspension.
2) The spring rate of an air spring can be adjusted. This happens, for example, when an additional load is applied and air is added to the spring to maintain a specified height. The internal pressure increases to accommodate the load, but without a significant shift in the suspension natural frequency.
3) The height of the load can be adjusted when necessary by increasing or decreasing the amount of air in the air spring. This allows for load leveling operations, or for the "squatting" capabilities such as are found in some transit bus applications.
4) An air spring has low friction dynamics. Since there is a flexible elastomeric member separating the rigid attachment points of the suspension, the air spring can move in six degrees of freedom without the resistance and squeaks associated with conventional steel spring suspensions.

1.2.2 Air Suspensions

For passive vibration suppression applications, the air spring's engineering function is the same as a steel spring, where a force is generated as a function of the displacement of the

load. Since both air springs and steel springs contain relatively small amounts of damping, they are typically used in conjunction with separate dampers or shock absorbers. Although, integrated air spring and damper units are available for some applications as shown in Figure 1.8, the spring and damper functions are typically separate. In many cases, air or some other gas is the fluid medium for the air spring, and a hydraulic fluid is the medium for the damper.

Figure 1.8 Separate and integrated components

In this thesis, the separate functions of spring and damper will be combined into a system that contains an air spring, valve, and accumulator. The sizing of the air spring and the accumulator provide the spring function, and the valve provides the damping function by controlling the air flow between the spring and the accumulator. A computer algorithm will control the opening and closing of the valve to optimize the damping provided by the system. The details and model of this system are provided in the next chapter.

CHAPTER 2. PLANT MODEL

2.1 Introduction

To effectively synthesize a controller, it is first necessary to gain a thorough understanding of the plant (system not including controller) dynamics to be controlled. Thanks to modern computer technology, in today's industrial environment, a virtual model of the plant is typically constructed as part of an MBD (Model Based Design) and simulation based process. Using a combination of analytical control design methodologies and computer simulations, controllers can be effectively synthesized and tested in a virtual environment before generating the final code and deploying on the physical hardware.

Modeling of a physical system is an abstraction from reality. More specifically, using the language of science, modeling is a *mathematical* abstraction from reality. A model is not to be confused with reality, or with the actual physical system, although it can provide useful insight depending on the fidelity of the model. In addition to using the laws of physics – for example, the laws of the conservation of energy, gravity, and momentum; the modeler makes approximations, assumptions, and engineering and scientific judgments when constructing a system model. In this sense, the act of modeling is an art as well as a science. An engineer or scientist always works, whether consciously or unconsciously, according to a particular paradigm (in the sense of Thomas Kuhn [3]). This paradigm (sometimes defined as a "world view" and "thinking inside a box") has been shaped through education, training, experience, and certain environmental factors, such as particular industry cultures, customs, and norms. It is not uncommon for two engineers to construct different models of the same physical system, especially as the system becomes more complex. This does not necessarily mean that one model is correct and the other is incorrect. By definition, in the engineering sense, a model is not meant to be exactly equivalent to the physical system.

Engineering models are typically constructed from first principles (e.g., Newton's, Laws of Motion), mathematical system identification that relies on test data, or a combination of both. Based upon many years of physical system modeling experience in industrial environments, for the sake of efficiency and economic considerations, it is the author's opinion that a model should be constructed as simply as possible to answer the questions that

are being asked. It is not necessary to have five decimal places of accuracy if zero decimal place accuracy is sufficient. In many situations, even if it is possible to develop extremely accurate models of a physical system or process using first principles, the engineer seldom has accurate knowledge of all parameters required by the model. There could be various reasons for this ignorance. If, for example, a component of a system is purchased from a supplier, due to proprietary considerations, the supplier may be unwilling to supply the appropriate information. At other times, the supplier may actually be ignorant of his own product's parameters. Some parameters may require extensive testing to obtain accurate values, which might not be economically justified. Regardless of the reasons for having incomplete information, the engineer still has to design and build a product that works and meets the customer's expectations of price, performance, utility, quality and safety.

There is another important consideration that significantly impacts the modeling process, the type of model, and the accuracy. This is something that is not typically considered, and is thus overlooked when pontificating about the modeling process and the economics and efficiency of modeling. This consideration is the *tool set* employed by the modeler to construct the model.

In today's corporate and academic environment, the tool set typically consist of a suite of software programs. These programs create a particular type of environment in which to interact and build models. The software contains the mathematical building blocks to be used for model construction, which frees the engineer to focus on the design task instead of becoming mired in developing and debugging computer code to solve the physical system equations. However, the engineer is limited to this environment and the underlying code that controls the environment. Many times the software was developed by mathematicians and computer programmers who might be paradigm deficient when it comes to properly understanding how the engineer actually goes about the task of modeling. Thus, the engineer, metaphorically speaking, enters into a virtual idealized world that has artificial boundaries created by the software developers.

This artificial virtual world always has limitations that impact the type and accuracy of the models that are allowed to be constructed. The engineer is limited to the fidelity of the mathematics of the underlying building blocks, and to the pre-determined rules of interaction

of the blocks. Although most programs allow the user to interface their own equations to the artificial environment, the modeler is placed in a position similar to an automobile owner considering having a problem fixed on his vehicle. If it requires the complete tear down of the engine to replace a simple part, then the owner might think twice about how bad he wants to fix the problem, given the time and expense required. If the automobile is still running and serving a useful purpose, although less efficiently, the owner might decide to ignore the problem. In a similar way, if the modeler desires to obtain a more accurate model, but it requires many hours of programming and debugging, she might think twice about just how accurate the model needs to be.

Given the above considerations, this chapter will focus on constructing and analyzing a model of the physical system to be controlled. The primary purpose of the model is to ultimately aid in developing a controller to control the vibration of the system. This ultimate purpose serves as a guide in determining the fidelity required for both the model and the correlation to test data. With this in mind, an appropriate model will be developed.

As previously mentioned, the air spring and accumulator provide the spring function for the system, and the air flow controlled by the valve provides the damping function. The ultimate objective is to develop a computer control algorithm, running in real-time, that will automatically adjust the valve to provide optimal damping to the system. This chapter will focus on developing and analyzing the system equations of motion to gain insight and a deeper understanding of the dynamics to be controlled.

First, a nonlinear dynamic model based upon first principles will be constructed. The model will be tuned based on test data. The equations will be used to simulate the system with the aid of commercially available software (Simulink). From the nonlinear set of equations, an idealized set of linear equations will be extracted and analyzed. The linear equations will provide additional insight into the system dynamics, which is more difficult to obtain by studying only the nonlinear model. Once a thorough understanding of the plant is obtained, a later chapter will be concerned with the development of the control methodology.

2.2 System Equations

2.2.1 Nonlinear Equations

A schematic of the plant is provided in Figure 2.1. The system consists of a mass supported by a reversible sleeve air spring. The opposite end of the air spring is attached to a shaker table. A solenoid operated valve with an adjustable orifice connects the air spring volume to a fixed-volume accumulator. The shaker table provides the base motion, causing the mass to vibrate in the vertical direction. The internal volume of the air spring changes as the mass oscillates. This causes air to flow back and forth between the air spring and the accumulator. The valve orifice opening can be adjusted by sending a current to the solenoid, thus restricting the flow of air between the air spring and the accumulator.

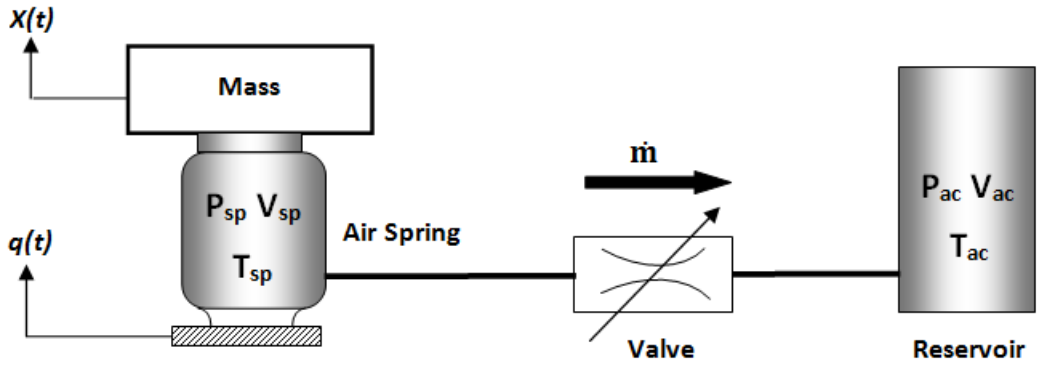

Figure 2.1 Open loop system schematic

Some of the following derivations and some of the results are similar to those contained in [4]. However, the following differences are noted:

1) The experimental results and correlations reported in this research are specific to a reversible sleeve air spring, whereas the experimental results reported in the reference are primarily focused on a bellows type spring.
2) The derivations here use a different equation for the mass air flow through the valve. This *does not* imply that the equation used in this research is somehow "superior" to the equation used in the reference. The equation here was chosen early in the project phase, before any additional knowledge of the system was gained or a firm research direction was established, to facilitate the collection of test data, due to its compact

formulation and the fact that the equation applies to both subcritical and critical flow regimes. However, after gaining a more complete understanding of the system to be controlled later in this research, it was determined that any legitimate mass flow equation formulation could be used here for purposes of developing controllers, provided it is tuned to actual experimental data.

3) A different model for relating the internal air spring pressure to the force generated to move the suspended mass is proposed in this paper, whereas the reference paper used a "fictitious" variable mass support area to make this conversion.
4) New results and interpretations, along with a more in-depth analysis are presented in this thesis.
5) The focus of the reference paper research was on development of dimensional analysis to aid in the design of a passive system. However, this research will be concerned with the development of a tuned and validated plant model that is amenable to the model-based synthesis of semi-active controller designs.

Air Spring Equation

With reference to Figure 2.1, mathematical quantities are defined positive in the direction of the arrows depicted in Figure 2.1. The mass flow rate of air *into* the air spring volume can be written as

$$\dot{m} = -\frac{d}{dt}\left(\rho_{sp} V_{sp}\right) \tag{2.1}$$

The variables ρ_{sp} and V_{sp} are the density and volume of air, respectively. The negative sign corresponds to the sign convention, which assumes air flow through the nozzle as positive when flowing from left to right (i.e., out of the air spring and into the accumulator). Since both density and volume are time dependent, differentiating (2.1) produces

$$\dot{m} = -\dot{\rho}_{sp} V_{sp} - \rho_{sp} \dot{V}_{sp} \tag{2.2}$$

An isentropic (constant entropy) process will be assumed, where the relationship between density and pressure at two states of the system is expressed as

$$\frac{\rho_{sp}}{\rho_{sp(e)}} = \left(\frac{P_{sp}}{P_{sp(e)}}\right)^{1/n} \tag{2.3}$$

The variables $\rho_{sp(e)}$ and $P_{sp(e)}$ represent the air density and absolute pressure in the air spring at equilibrium. The constant n is the polytropic exponent defined as the ratio of specific heats (Cp/Cv) of the gas. For air, the numerical value for n is equal to 1.3947. For typical calculations, n may be rounded to 1.4 without significant loss of accuracy.

From the ideal gas law, the density at equilibrium can be expressed as

$$\rho_{sp(e)} = \frac{P_{sp(e)}}{RT_{sp(e)}} \tag{2.4}$$

where R is the specific gas constant and $T_{sp(e)}$ is the absolute temperature in the air spring at equilibrium. Substituting (2.4) into (2.3) and differentiating with respect to time produces

$$\dot{\rho}_{sp} = \frac{1}{nRT_{sp(e)}}\left(\frac{P_{sp}}{P_{sp(e)}}\right)^{\frac{1-n}{n}} \dot{P}_{sp} \tag{2.5}$$

By substituting (2.5) into (2.2) and rearranging terms produces a first order differential equation for pressure in the air spring as

$$\dot{P}_{sp} = -\frac{nRT_{sp(e)}}{V_{sp}}\left(\frac{P_{sp}}{P_{sp(e)}}\right)^{\frac{n-1}{n}} \dot{m} - \frac{nP_{sp}}{V_{sp}}\dot{V}_{sp} \tag{2.6}$$

Accumulator Equation

Noting that the accumulator volume is constant, applying (2.1) produces the mass flow rate into the accumulator as

$$\dot{m} = \dot{\rho}_{ac}V_{ac} \tag{2.7}$$

This leads to first order differential equation for pressure in the accumulator expressed as

$$\dot{P}_{\mathrm{ac}} = \frac{nRT_{\mathrm{ac(e)}}}{V_{\mathrm{ac}}}\left(\frac{P_{\mathrm{ac}}}{P_{ac(e)}}\right)^{\frac{n-1}{n}} \dot{m} \tag{2.8}$$

Note that at equilibrium, the pressures in the air spring and accumulator are equal ($P_{sp(e)} = P_{ac(e)}$, and the mass flow rate is zero ($\dot{m} = 0$). Also, the temperatures are assumed constant and equal at equilibrium ($T_{ac(e)} = T_{sp(e)}$).

Valve Equation

An expression for the mass flow rate through a valve can be developed by considering the flow of a compressible fluid through an orifice plate. The construction of proportional air flow valves typically have some sort of orifice opening that is being controlled. However, the valve manufacturers may accomplish this in a variety of ways. Therefore, the actual resistance to air flow through the valve may consist of more than just the orifice opening. For example, there may be passageways of varying lengths within the valve. In addition, the flow of air may experience bending through angles and so forth. These additional valve elements must be considered to accurately model air flow through a valve. Unfortunately, as previously mentioned in the introduction to this chapter, suppliers may consider the internal details of construction of the valve to be proprietary information. Also, any tests results provided by a supplier should always be validated. Therefore, it is recommended that any valve be tested by the user under environmental conditions similar to what is expected in the field before committing to a particular design.

In addition to valve design, other restrictions to air flow between the air spring and the accumulator may be present. For example, additional piping and connections will most likely exist. These elements will need to be accounted for if an accurate model is desired.

Given the above considerations, and to simplify the resulting equations, the approach that is considered here is to use an equation representing compressible air flow through a restriction, and include an additional tuning factor to match actual test data, which should approximate the additional considerations mentioned above.

An equation representing restricted air flow was developed in [5] in terms of the measured upstream total pressure and temperature and the measured downstream pressure. If static pressure and temperature are measured in lieu of total pressure, the difference in result is usually negligibly small. A formulation was developed that would account for both critical and subcritical flow. The mass flow rate is given by [5]:

$$\dot{m} = \frac{\varphi C A P_u \, \beta}{\sqrt{T_u}} \tag{2.9}$$

For convenience, and to avoid confusion with other variables, φ has been substituted for K, and β has been substituted for N in the reference paper. φ, which is taken as a constant, is a

function of the polytropic exponent *n* for air, and β is a restriction factor, which is a function of *n* and the up-stream and down-stream pressures. Tabular values are provided in the reference paper for β (or *N*). The variables are defined as follows, where all units are SI.

$$\varphi = \left[\frac{n^2}{n-1}\left(\frac{2}{n+1}\right)^{(n+1)/(n-1)}\right]^{1/2} = 1.2855\sqrt{g/c_p}$$

$C = C_a C_d$

$A =$ effective orifice area (m^2)

$P_u =$ upstream (high side) pressure (Pa)

$$N = \sqrt{\frac{X}{X_c}\left[\frac{X_c+1}{X+1}\right]^{\left(\frac{n+1}{n-1}\right)}} = 3.8772\sqrt{X(X+1)^{\left(\frac{n-1}{n+1}\right)}}$$

$T_u =$ upstream temperature (K)

$g =$ acceleration due to gravity (m/s^2)

$c_p =$ specific heat at constant pressure (J/(kg-K))

$C_a = 0.038$ valve tuning coefficient determined experimentally (see test results below)

$C_d =$ coefficient of discharge

$X = r^{\left(\frac{n-1}{n}\right)} - 1$

$X_c = (n-1)/2$

$r = P_u/P_d$

$P_d =$ downstream (low side) pressure (Pa)

$n =$ polytropic exponent

The properties for air used in the above calculations will be taken as defined for "Normal Air," which contains sufficient moisture and an average amount of CO_2 such that its specific weight at standard conditions (P = 14.70 lbs/in^2, T = 68^0F) is exactly 0.075 lbs/ft^3. This leads to the following values:

$$c_p = 1017.3\ \frac{J}{kg-K}$$

$$n = 1.39470$$

Mass Equation

Using Newton's Second Law of Motion with the assumed coordinate directions shown in Figure 2.2, the force balance on the suspended mass can be expressed as

$$M\ddot{x} = f_p - W_g - f_b \tag{2.10}$$

where f_p, W_g, and f_b are the air spring force, weight of the mass, and bag damping force, respectively. Note that the bag damping force f_b , in addition to air bag material (or fabric) damping, also includes any natural system damping that is *not* produced by air flow through the valve. In other words, all additional damping not provided by air flow through the valve has been lumped into this term. This damping is also assumed to be linear damping, which is a further engineering approximation or assumption. Analysis of test data establishes this value.

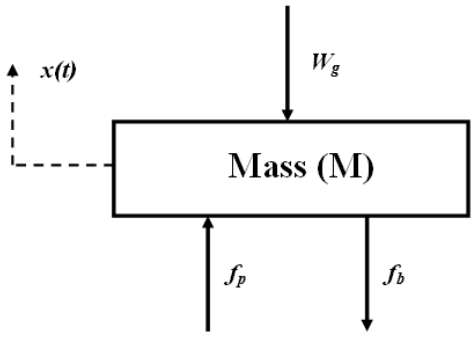

Figure 2.2 Mass force balance

Expanding the force balance (2.10) produces

$$M\ddot{x} = (P_w - P_{wo})A_s - W_g - c_b(\dot{x} - \dot{q}) \tag{2.11}$$

where

P_w = pressure that transmits directly to mass support

P_{wo} = pressure at equilibrium

A_s = effective mass support area

c_b = bag damping coefficient

$(\dot{x} - \dot{q})$ = relative velocity

W_g = weight

For the reversible sleeve air spring, the assumption is that the effective support area, as shown in Figure 2.3, is constant. However, the volume beneath the support plate expands and contracts as the pressure increases and decreases. A reading of [4] might tend to confuse the reader of the validity of this assumption, since the author uses a variable "fictitious" area. A different approach will be used in this thesis, which is developed below.

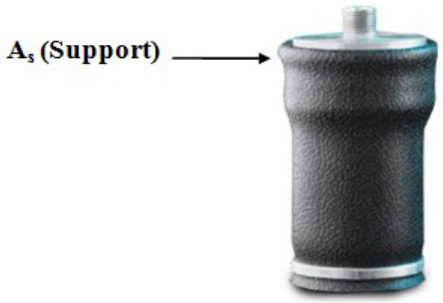

Figure 2.3 Air spring support area

Additional Considerations

Equations (2.6), (2.8), (2.9), and (2.11) represent the fundamental non-linear differential equations for the system. However, to effectively use them to construct a computer simulation, a few other details need to be addressed.

First, it is assumed that all simulations and analyses start from the equilibrium position, unless otherwise specified. Therefore, $x(t)$ is the displacement of the mass measured from the equilibrium position (i.e., $x(0) = \dot{x}(0) = \ddot{x}(0) = 0$). The acceleration of the mass is then produced by a *change in forces* acting on the mass with respect to the equilibrium position. With this understanding, (2.11) can be replaced by

$$M\ddot{x} = P_w A_s - c_b(\dot{x} - \dot{q}) \tag{2.12}$$

Second, the volume V_{sp} of the air spring needs to be determined. The volume is highly irregular and nonlinear, and is specific to the particular model and type of air spring. For modeling purposes, the volume can be considered a nonlinear function of the height and pressure. Unfortunately, it is difficult to directly measure the volume. As a practical matter, the volume is usually indirectly determined based on other measurements, and must be experimentally determined for the particular air spring under study. Previous research has

suggested that for engineering purposes the volume can be assumed a function of height only without significant loss in accuracy [4]. Current research reported in this thesis will also work with this assumption. Intuitively, this seems appropriate particularly for a reversible sleeve air spring, since the air spring fabric rides up and down over a piston. The volume V_{ac} of the accumulator (reservoir) is constant and known.

Finally, note that to obtain the proper sign (direction) for $\dot{m}$, (2.9) is replaced by

$$\dot{m} = sign(P_{sp} - P_{ac}) \frac{KCAP_u N}{\sqrt{T_u}}$$

2.2.2 Nonlinear Simulation Equations

With the appropriate substitutions, a summary of the final set of equations for numerical simulation purposes can now be expressed as

$$\dot{P}_{sp} = -\frac{nRT}{V_{spr}} \left(\frac{P_{sp}}{P_{sp(e)}} \right)^{\frac{n-1}{n}} \dot{m} - \frac{nP_{sp}}{V_{sp}} \dot{V}_{sp} \tag{2.13}$$

$$\dot{P}_{ac} = \frac{nRT}{V_{ac}} \left(\frac{P_{ac}}{P_{ac(e)}} \right)^{\frac{n-1}{n}} \dot{m} \tag{2.14}$$

$$\dot{m} = sign(P_{sp} - P_{ac}) \frac{KCAP_u N}{\sqrt{T_u}} \tag{2.15}$$

$$M\ddot{x} = P_w A_s - c_b \dot{h} \tag{2.16}$$

where pressures P_{sp} (air spring) and P_{ac} (accumulator) are absolute. P_w is the gauge pressure that directly transmits the force to the suspended mass. The subscript *e* indicates equilibrium condition. Units of measure are standard SI units. The differential equations have the following set of initial conditions:

$P_1(t_0) = P_2(t_0) = P_e$

$x(t_0) = \dot{x}(t_0) = 0$

and the following variables are defined:

$h = x - q + h_e$, height of air spring

$\dot{h} = \dot{x} - \dot{q}$

$V_{sp} = V(h)$, experimentally determined

$P_w = P_w(P_{sp})$, gauge pressure acting on mass, experimentally determined function of P_{sp}

A_s, air spring support area

$T_u = \mathrm{T} = \text{constant}$

$P_u = \max(P_1, P_2)$

2.2.3 Pressure Composition

At this point one other issue needs to be addressed before proceeding with the linear analysis. Before the equations can be solved, the relationship between P_{sp} and P_w needs to be established. This is not a straight forward relationship, and will need to be established with test data.

To account for this difference in pressures, the authors of [4] applied a "fictitious" mass support area that varied as a function of displacement to translate the total pressure to what is "seen" by the suspended mass. No explanation was given for this "magic," which is counterintuitive to the fact that the mass support area does not change as a function of displacement. The results here clearly indicate physically what is happening.

Since physical modeling of the air spring material is beyond the scope of this research, the operating paradigm that is proposed is that the total measured pressure P_{sp} inside the air spring will be considered to be composed of two parts. Part of the total measured pressure is a reaction to the forces generated in the flexible air spring material as it expands or contracts. The other part of total pressure is a reaction to the vertical force induced by the suspended weight, distributed over A_s. One way to intuitively think about this, in a static sense, is to consider that the air spring is pumped up with an initial amount of air, which expands the air spring fabric, which in turn creates an initial internal air pressure in the air spring before the suspended weight is added. Therefore, there is a certain amount of elastic energy stored in the air spring material, due to its elastic behavior, as it stiffens and the volume expands. As external weight is then added, the internal pressure increases, but the air spring also changes shape and the internal volume changes. Part of the air pressure created is due to the elastic behavior (resistance) of the fabric, and part of the pressure is due to supporting the weight.

Figure 2.4 provides a decomposition of the total pressure versus the supported weight. The data was collected by removing weights from the sled, and recording the corresponding air spring pressure. The total pressure curve (top curve) is the measured air spring gauge pressure and is equal to the sum of the two lower curves. The pressure due to the suspended mass (bottom curve) is equal to the weight of the mass distributed over the effective air spring support area, and the pressure associated with the air bag elasticity is equal to the total measured gauge pressure minus the pressure due to the suspended mass.

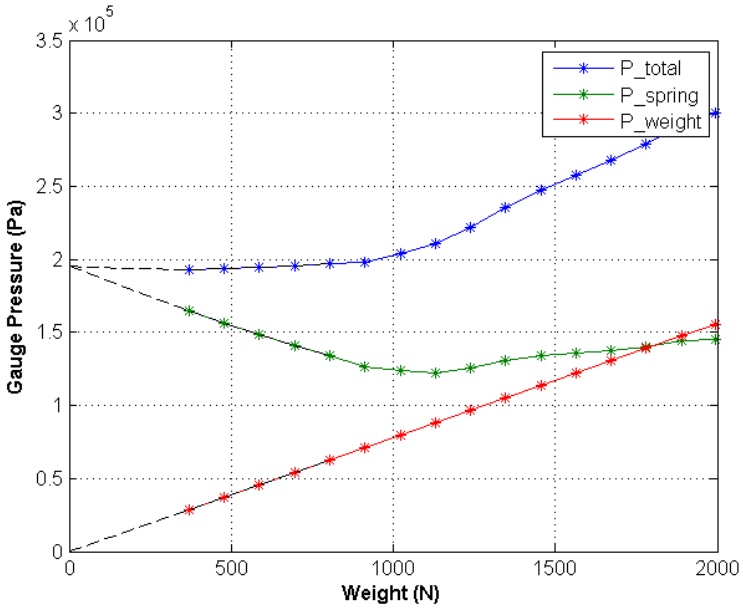

Figure 2.4. Pressure composition, experimental data

The dashed portions of the curves represent extrapolation points. Since the test structure is constructed such that the air spring cannot be completely unloaded due to the sled attachment, a cubic fit to the data allowed extrapolation down to zero weight. Note that, as expected, when there is no supported weight, the total measured gauge pressure is equal to the initial inflation pressure (approximately 29 psi). As previously mentioned, this pressure is produced by the resistance of the air bag as the fabric elastically expands as air is pumped into the bag.

Therefore, the total internal absolute pressure will be represented as

$$P_1 = P_w + P_s + P_{atm} \tag{2.17}$$

where P_s is the gauge pressure associated with the elastic behavior of the fabric, and P_w is the pressure needed to support the weight. If (2.17) is multiplied through by the support area A_s, the following is obtained:

$$F_1 = F_w + F_s + F_{atm} \tag{2.18}$$

where F_1 is the total air spring force (absolute pressure) composed of the force F_w acting directly on the suspended mass, and the force F_s associated with elastic energy in the bag material.

To completely understand the behavior of the air spring, additional techniques and analysis should be employed. In particular, it is recommended that future research consider using finite element techniques applied to the air bag material, coupled with the thermodynamic relations, to better understand the complete behavior of the system.

More will be discussed on this topic of pressure composition in the section on static test results later in the thesis.

2.2.4 Linearized Dynamics

As previously stated, a thorough understanding of the plant dynamics is necessary for developing an effective control algorithm. Analyzing a set of linear equations, which have been constructed from the nonlinear plant equations, can provide useful insight into system dynamics without having to resort strictly to nonlinear numerical simulations.

Equation (2.13) can be expanded in a Taylor series. Keeping only the first order terms leads to

$$\begin{aligned} \dot{P}_{sp} = \dot{P}_{sp(e)} + \left.\frac{\partial \dot{P}_{sp}}{\partial P_{sp}}\right|_e \left(P_{sp} - P_{1e}\right) + \left.\frac{\partial \dot{P}_{sp}}{\partial V_{sp}}\right|_e \left(V_{sp} - V_{sp(e)}\right) \ldots \\ + \left.\frac{\partial \dot{P}_{sp}}{\partial \dot{V}_{sp}}\right|_e \left(\dot{V}_{sp} - \dot{V}_{sp(e)}\right) + \left.\frac{\partial \dot{P}_{sp}}{\partial \dot{m}}\right|_e \left(\dot{m} - \dot{m}_e\right) \end{aligned} \tag{2.19}$$

The subscript e indicates evaluation at the equilibrium conditions, where $\dot{P}_{sp(e)} = \dot{m}_e = \dot{V}_{sp(e)} = 0$. Performing the operations in (2.19) leads to

$$\dot{P}_{sp} = -\frac{nRT}{V_{sp(e)}}\dot{m} - \frac{nP_{sp(e)}}{V_{sp(e)}}\dot{V}_{sp} \tag{2.20}$$

As previously stated, $V_{sp} = V_{sp}(h)$; therefore, $\dot{V}_{sp}$ can be linearized and expressed as

$$\dot{V}_{sp} = \left(\frac{dV_{sp}}{dh}\right)\left(\frac{dh}{dt}\right) = v\dot{h} \tag{2.21}$$

where $v = dV_{sp}/dh$. Equation (2.20) can now be expressed as

$$\dot{P}_{sp} = -\frac{nRT}{V_{sp(e)}}\dot{m} - \frac{nvP_{sp(e)}}{V_{sp(e)}}\dot{h} \tag{2.22}$$

Similarly, expanding (2.14) in a Taylor series leads to

$$\dot{P}_{ac} = \frac{nRT}{V_{ac(e)}}\dot{m} \tag{2.23}$$

Obtaining a linear expression for $\dot{m}$ is not as straightforward as in the above procedure. Equation (2.15) produces a slope that is vertical at the origin, which leads to infinite derivatives, as shown in Figure 2.5. Therefore, a different approach will need to be used if it is desired to perform a linear analysis. The approach that will be taken is to approximate (or assume) a sloped line through the origin, such that a linear analysis can be applied. By doing this, an engineering approximation (or assumption) is being introduced, which is not purely accurate in a mathematical sense, but still allows useful information to be obtained from a linear analysis, as will be demonstrated below. Also, since the linear analysis will be used only in a *qualitative* sense to arrive at some boundary conditions, and to produce linearized frequency response (relative amplitude), instead of accurately predicting mass flow, and thus will not be used in the nonlinear simulation, this approximation should not be a concern.

Therefore, instead of using (2.15), the mass flow rate can alternatively be expressed as

$$\dot{m} = \frac{1}{R_f}\left(P_{sp} - P_{ac}\right) \tag{2.24}$$

where R_f is a linear flow resistance coefficient, and (2.24) is linear in form.

Equations (2.15) and (2.24) can be brought into conformity by equating the two equations and solving for R_f, which produces

$$R_f = \frac{(P_u - P_d)\sqrt{T_u}}{KCAP_uN} \tag{2.25}$$

where P_{sp} and P_{ac} have been replaced by P_u and P_d, respectively, where P_u is the upstream (high side) pressure and P_d is the downstream (low side) pressure, and T_u is assumed constant.

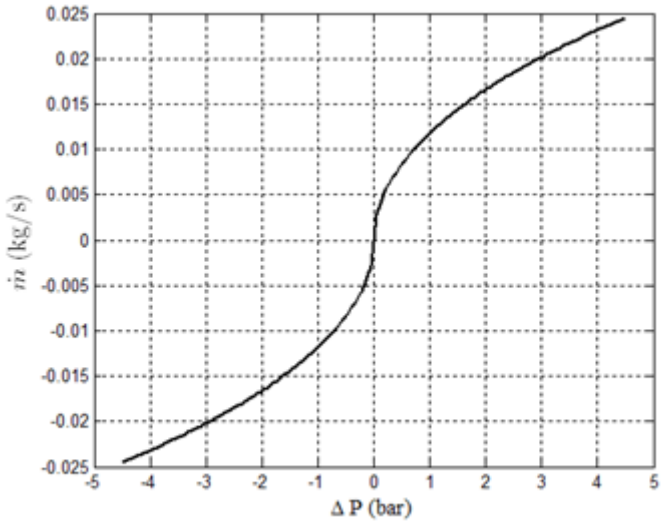

Figure 2.5 Mass flow rate vs. pressure drop

For linear analysis, such as a frequency response, R_f is held constant for each frequency sweep. As the resistance R_f increases, the mass flow rate $\dot{m}$ decreases. This is equivalent to closing the valve. In other words, $R_f \longrightarrow \infty$ implies $\dot{m} \longrightarrow 0$. From a steady-state frequency response perspective, R_f is both amplitude (pressure drop) and valve opening dependent, by virtue of the fact that the pressure drop appears in the numerator, and the valve opening area appears in the denominator. This allows the mass flow rate to be expressed over a significant range of pressure drops for linear analyses. A typical curve of R_f versus pressure drop for representative values of orifice area opening percentages is shown in Figure 2.6. These curves were generated for pressure ratios (P_u/P_d) of 1.1 to 1.8, with $P_d = P_{sp(e)}$. Similarly, Figure 2.7 provides a chart of R_f relative to the orifice opening area percentages for various values of pressure drop.

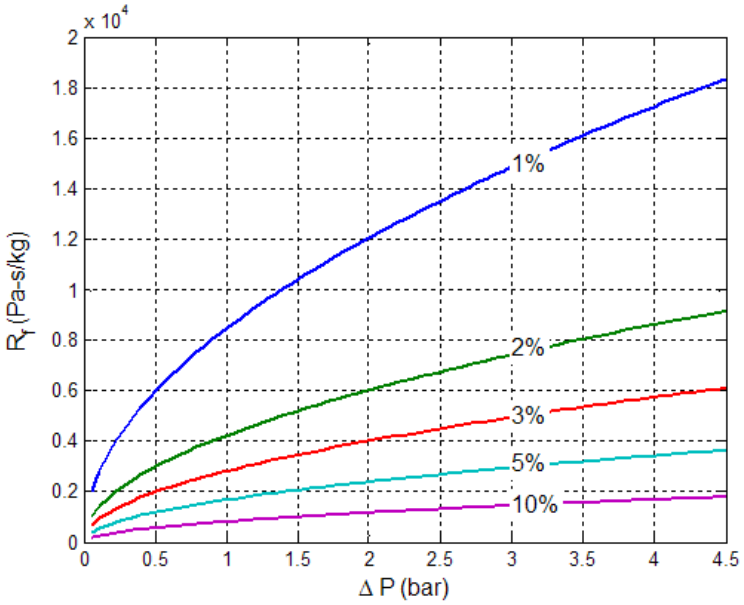

Figure 2.6 Resistance coefficient vs. pressure drop

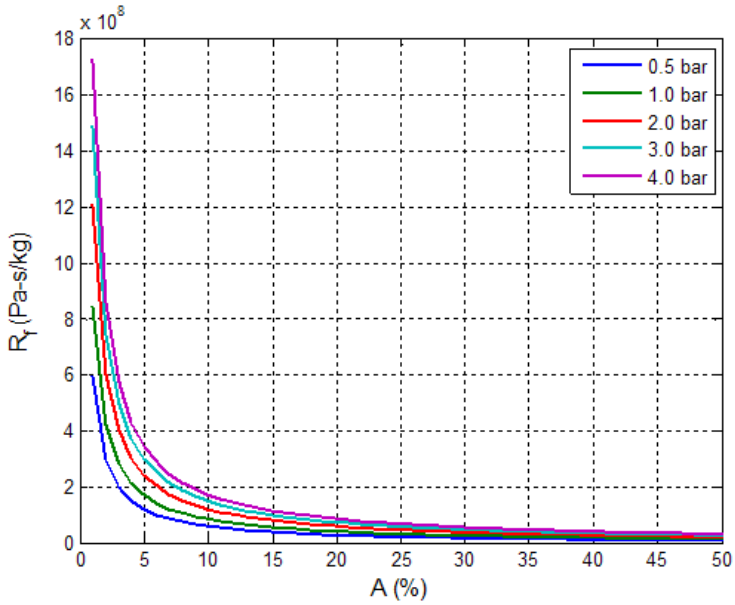

Figure 2.7 Resistance coefficient vs. area percent

It is interesting to note that the above charts approximate straight lines with constant slopes when plotted as log-log charts. Using natural logarithms to represent the results in Figure 2.6 leads to the logarithm chart shown in Figure 2.8. Each curve has a slope equal to 0.508, which is primarily influenced by the polytropic exponent. Similarly, the results in Figure 2.7 can be plotted as shown in Figure 2.9. Each curve has a slope equal to -1.0,

indicating a direct linear logarithmic relationship between the resistance coefficient and the valve opening area.

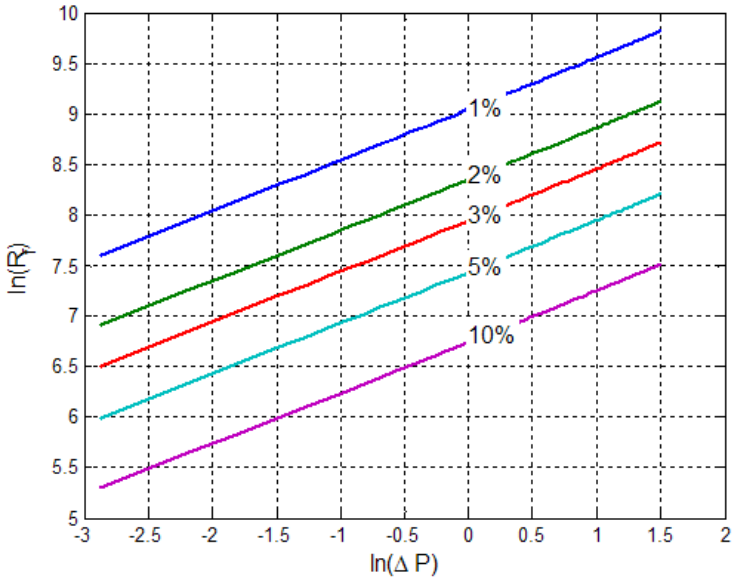

Figure 2.8 Resistance coefficient vs. pressure drop

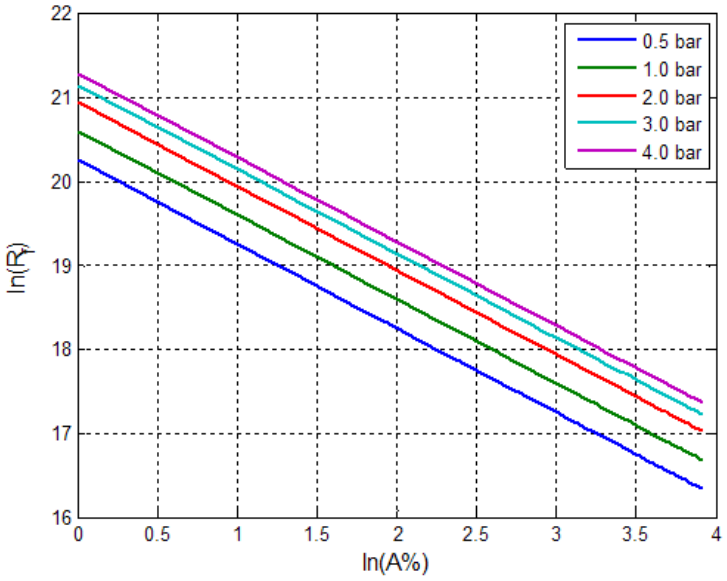

Figure 2.9 Resistance coefficient vs. area percent

Since R_f is a function of the pressure drop and the valve opening, a three dimensional log-log plot can be made of R_f with respect to the change in opening orifice area and the

pressure drop as shown in Figure 2.10. Note that R_f approximates a plane in logarithm space over some domain.

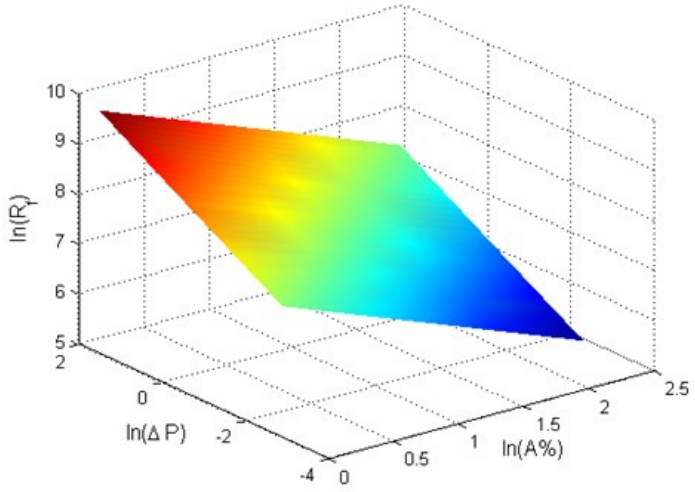

Figure 2.10 Resistance coefficient vs. ΔP and A%

The equation for a plane can be expressed as:

$$a(x - x_0) + b(y - y_0) + c(z - z_0) = 0 \tag{2.26}$$

where (a, b, c) are the coordinates of a vector normal to the plane, and (x_0, y_0, z_0) are the coordinates of a point in the plane. Therefore, selecting any three points to form two vectors, taking the cross product to form the normal vector, and then substituting into (2.26), an equation for the plane is created. R_f can be estimated from this equation once the equation has been established for a particular valve.

For example, suppose P_i represents three points ($i = 1,2,3$) defined as

$$P_i = (x_i, y_i, z_i) = \left(\ln(\text{A\%}), \ln(\Delta P_i), \ln\left(R_{fi}\right)\right)$$

A normal vector to the plane, which has scalar components, (a, b, c), can then be defined by the cross product

$$\vec{N} = \vec{P}_{1\to 2}\ X\ \vec{P}_{1\to 3}$$

where $\vec{P}_{1\to 2}$ and $\vec{P}_{1\to 3}$ define the vectors connecting points P_1 to P_2 and P_1 to P_3, respectively. Once (2.26) has been generated, R_f can be calculated as follows:

$$\ln(R_f) = \frac{-a(\ln(A\%) - x_0) - b(\ln(\Delta P) - y_0)}{c} \tag{2.27}$$

This leads to

$$R_f = e^{ln(R_f)} \tag{2.28}$$

where the right-hand side of (2.27) is substituted for the exponent on the right-hand side of (2.28).

These results were not directly used for controller development in this thesis, but are presented for future research interests, which are needed to fully exploit the results.

The set of linearized dynamical equations can now be summarized as follows:

$$\dot{P}_{sp} = -\frac{nRT}{V_{sp(e)}}\dot{m} - \frac{n\nu P_{sp(e)}}{V_{sp(e)}}\dot{h} \tag{2.29}$$

$$\dot{P}_{ac} = \frac{nRT}{V_{ac(e)}}\dot{m} \tag{2.30}$$

$$\dot{m} = \frac{1}{R_f}\left(P_{sp} - P_{ac}\right) \tag{2.31}$$

$$M\ddot{x} = P_w(A_s) - c_b\dot{h} \tag{2.32}$$

2.3 Linear Analysis

The linear dynamics representation led to an interesting observation: namely, the resistance to air flow through the valve is not only a function of the valve opening area, but is also dependent on the amplitude of oscillation. This will also be demonstrated later in the nonlinear analysis.

2.3.1 Boundary Conditions and System Natural Frequencies

Pressure Force versus Spring Height Relationships

Suppose the total internal force in (2.18) is differentiated to produce

$$\dot{F}_1 = \dot{P}_1 A_s \tag{2.33}$$

Substituting (2.29) into (2.33) leads to:

$$\dot{F}_1 = -\frac{nRTA_s}{V_{sp(e)}}\dot{m} - \frac{n\nu P_{sp(e)}A_s}{V_{sp(e)}}\dot{h} \tag{2.34}$$

Two boundary conditions will now be considered. The first condition approximates a closed valve, where R_f approaching infinity (infinite resistance) implies $\dot{m}$ approaching zero:

$$\left(R_f \longrightarrow \infty\right) \Rightarrow (\dot{m} \longrightarrow 0) \tag{2.35}$$

and the second condition approximates an open valve as

$$\left(R_f \longrightarrow 0\right) \Rightarrow \left\{(P_{sp} - P_{ac}) \longrightarrow 0\right\} \longrightarrow \left\{P_{sp} = P_{ac}\right\} \tag{2.36}$$

Consider the closed valve condition. Apply (2.35) to (2.34) to obtain

$$\dot{F}_1 = -\frac{n\nu P_{sp(e)} A_s}{V_{sp(e)}} \dot{h} \tag{2.37}$$

which relates the change in force to the change in height, which is a force versus deflection relationship. Therefore, (2.37) can be expressed as

$$\dot{F}_1 = -K_{sp}\dot{h} \tag{2.38}$$

where K_{sp} is defined as the air spring stiffness with no accumulator effects:

$$K_{sp} = \frac{n\nu P_{1e} A_s}{V_{1e}} \tag{2.39}$$

For the second condition (2.36), the pressure drop theoretically approaches zero, which implies $P_{sp} = P_{ac}$, and the mass oscillates as though it is connected to both volumes without resistance to air flow through the valve. This condition is approximated by the valve fully open. However, in practice, if the valve happens to be overly restrictive to air flow in the open position, the true stiffness could be higher than calculated.

It should be commented at this point that a fully open valve only approaches the condition where both volumes are connected. As mentioned previously, there may be additional resistances, such as piping and connections in the system, which create resistance to air flow. In addition, the valve itself will have some amount of resistance when fully open. The amount of resistance at the fully open condition will be dependent on valve design and size.

Applying condition (2.36) to (2.30) produces

$$\dot{P}_{ac} = \dot{P}_{sp} = \frac{nRT}{V_{ac(e)}}\dot{m} \tag{2.40}$$

Solving for $\dot{m}$ and substituting the result into (2.29) leads to

$$\dot{P}_{sp} = -\frac{nRT}{V_{sp(e)}}\left(\frac{V_{ac(e)}}{nRT}\right)\dot{P}_{sp} - \frac{n\nu P_{sp(e)}A_s}{V_{sp(e)}}\dot{h} \tag{2.41}$$

Rearranging terms and cancelling variables produces

$$\dot{P}_{sp}\left(1 + \frac{V_{ac(e)}}{V_{sp(e)}}\right) = -\frac{n\nu P_{sp(e)}A_s}{V_{sp(e)}}\dot{h}$$

which leads to

$$\dot{P}_{sp}\left(\frac{V_{sp(e)} + V_{ac(e)}}{V_{sp(e)}}\right) = -\frac{n\nu P_{sp(e)}A_s}{V_{sp(e)}}\dot{h}$$

Further manipulation produces

$$\dot{P}_{sp} = -\left(\frac{V_{sp(e)}}{V_{sp(e)} + V_{ac(e)}}\right)\frac{n\nu P_{sp(e)}A_s}{V_{sp(e)}}\dot{h}$$

which leads finally to

$$\dot{P}_{sp} = -\left(\frac{n\nu P_{sp(e)}A_s}{V_{sp(e)} + V_{ac(e)}}\right)\dot{h} \tag{2.42}$$

Multiplication of (2.42) by the mass support area produces the equation relating change in force to change in height of the air spring expressed as

$$\dot{F}_1 = -K_{sys}\dot{h} \tag{2.43}$$

where K_{sys} is the stiffness of the system when both volumes (air spring and accumulator) are influencing vibration, defined as

$$K_{sys} = \frac{n\nu P_{sp(e)}A_s}{V_{sp(e)} + V_{ac(e)}} \tag{2.44}$$

To simplify notation, the following quantities are defined:

$$C_{sp} = \frac{V_{sp(e)}}{nRT}, \qquad C_{ac} = \frac{V_{ac(e)}}{nRT}$$

Also, note the following relationship

$$\frac{C_{sp}}{C_{sp}+C_{ac}}=\frac{K_{sys}}{K_{sp}}$$

Making the appropriate substitutions from above into the pressure rate equations produces

$$\begin{aligned}\dot{P}_{sp} &= -\frac{1}{C_{sp}R_f}\left(P_{sp}-P_{ac}\right)-\frac{n\nu P_{sp(e)}A_s}{V_{sp(e)}}\dot{h}\\ \dot{P}_2 &= -\frac{1}{C_{ac}R_f}\left(P_{sp}-P_{ac}\right)\\ F &= A_sP_{sp}\end{aligned} \tag{2.45}$$

where F_1 is replaced by F for convenience. Expressing these equations in state space format produces

$$\begin{bmatrix}\dot{P_{sp}}\\ \dot{P}_{ac}\end{bmatrix}=\begin{bmatrix}-1/C_{sp}R_f & 1/C_{sp}R_f\\ 1/C_{ac}R_f & -1/C_{ac}R_f\end{bmatrix}\begin{bmatrix}P_{sp}\\ P_{ac}\end{bmatrix}+\begin{bmatrix}-n\nu P_{sp(e)}A_s/V_{sp(e)}\\ P_{ac}\end{bmatrix}\dot{h}$$
$$F=\begin{bmatrix}A_s & 0\end{bmatrix}\begin{bmatrix}P_{sp}\\ P_{ac}\end{bmatrix} \tag{2.46}$$

where the equations represent deviations about equilibrium.

Using familiar notation for state space format produces

$$\begin{aligned}\dot{x} &= [A]x+[B]u\\ y &= [C]x\end{aligned} \tag{2.47}$$

Comparing (2.47) to (2.46), with obvious definitions for matrices A, B, and C, the Laplace transform of (2.46) produces the transfer function between the air spring force and the height of the air spring as

$$\frac{F(s)}{h(s)}=Cs(sI-A)^{-1}B \tag{2.48}$$

where I is the appropriately dimensioned identity matrix. Carrying out the operation symbolically and performing some algebraic manipulation produces the transfer function

$$\frac{F(s)}{h(s)}=\frac{-K_{sys}\left(C_{ac}R_fs+1\right)}{C_{ac}R_f\frac{K_{sys}}{K_{sp}}s+1} \tag{2.49}$$

Note that the mass has not yet been included in the formulation.

It is instructive to look at the extreme or limiting conditions. First, observe the static gain for $s \longrightarrow 0$, which produces

$$\lim_{s\to 0}\left|\frac{F(s)}{h(s)}\right| = \left|\frac{-C_{sp}K_{sp}}{C_{sp}+C_{ac}}\right| = K_{sys} \tag{2.50}$$

Second, divide the numerator and denominator of (2.49) by s, and observe the limiting condition $s \longrightarrow \infty$, which produces

$$\lim_{s\to \infty}\left|\frac{F(s)/s}{h(s)/s}\right| = K_{sp} \tag{2.51}$$

For the steady state frequency response, substituting $s = j\omega$, which is the complex frequency, into (2.49) produces the transfer function as a function of frequency. The first limiting condition (2.50) implies that, at low frequencies, the system oscillates under the influence of both volumes combined. In other words, the system stiffness at low frequencies is composed of contributions from both the air spring volume and the accumulator volume.

The second limiting condition (2.51) implies that, at high frequencies, the system primarily vibrates under the influence of the air spring volume. In other words, the system stiffness at high frequencies is primarily the stiffness of the air spring volume alone.

Mass Displacement versus Base Input Relationships

Next, the dynamics of the suspended mass will be included in the formulation. Noting the following relationships:

$$h = h_e + (x - q)$$
$$\dot{h} = (\dot{x} - \dot{q})$$

and substituting the expression for $\dot{h}$ into (2.29) and expressing the suspended mass equation (2.32) with respect to equilibrium, the state space formulation can be expressed as

$$\begin{bmatrix} \dot{P}_{sp} \\ \dot{P}_{ac} \\ \dot{z} \end{bmatrix} = \begin{bmatrix} -1/C_{sp}R_f & 1/C_{sp}R_f & -K_{sp}/A_s \\ 1/C_{ac}R_f & -1/C_{ac}R_f & 0 \\ A_s/M & 0 & -c_b/M \end{bmatrix} \begin{bmatrix} P_{sp} \\ P_{ac} \\ z \end{bmatrix}$$

$$\dot{x} = \begin{bmatrix} 0 & 0 & 1 \end{bmatrix} \begin{bmatrix} P_{sp} \\ P_{ac} \\ z \end{bmatrix} + \begin{bmatrix} K_{sp}/A_s \\ 0 \\ c_b/M \end{bmatrix} \dot{q} \tag{2.52}$$

where the state variable $z = \dot{x}$ is the velocity of the mass.

Taking the Laplace transform of (2.52) representing the displacement of the mass relative to the displacement of the base produces

$$\frac{x(s)}{q(s)} = C(sI - A)^{-1}B \tag{2.53}$$

Carrying out the symbolic operations represented by (2.53), along with some algebraic manipulations, results in the linear transfer function

$$\frac{x(s)}{q(s)} = \frac{\frac{C_{ac}R_f c_b}{K_{sp}} s^2 + \left(\frac{c_b}{K_{sys}} + C_{ac}R_f\right) s + 1}{\frac{C_{ac}R_f}{\omega_{sp}^2} s^3 + \left(\frac{1}{\omega_{sys}^2} + \frac{C_{ac}R_f c_b}{K_{sp}}\right) s^2 + \left(\frac{c_b}{K_{sys}} + C_{ac}R_f\right) s + 1} \tag{2.54}$$

where $\omega_{sp} = \sqrt{K_{sp}/M}$ and $\omega_{sys} = \sqrt{K_{sys}/M}$ are the natural frequencies of oscillation of the mass with the valve closed (air spring only) and with the valve fully open (air spring + accumulator), respectively.

As before, it is instructive to look at the limiting conditions. First, assume $c_b = 0$, and divide the numerator and denominator of (2.54) by R_f. Now, observe the limiting condition as $R_f \longrightarrow \infty$, which is equivalent to closing the valve, and produces

$$\lim_{R_f \to \infty} \left| \frac{x(s)/R_f}{q(s)/R_f} \right| = \frac{1}{\frac{M}{K_{sp}} s^2 + 1} \tag{2.55}$$

An inverse Laplace transform of (2.55) leads to a linear second order differential equation

$$M\ddot{x} + K_{sp}x = K_{sp}q \tag{2.56}$$

of which the natural frequency of oscillation is associated with the air spring only

$$\omega_{sp} = \sqrt{\frac{K_{sp}}{M}} \tag{2.57}$$

If the bag damping c_b is included in the formulation, a linear damped second order equation results as

$$M\ddot{x} + c_b\dot{x} + K_{sp}x = c_b\dot{q} + K_{sp}q \tag{2.58}$$

which can be expressed in the familiar form

$$\ddot{x} + 2\zeta\omega_{sp}\dot{x} + \omega_{sp}^2 x = 2\zeta\omega_{sp}\dot{q} + \omega_{sp}^2 q \tag{2.59}$$

where ζ is the damping ratio defined as

$$\zeta = \frac{c_b}{2M\omega_{sp}} \tag{2.60}$$

Since c_b is typically small, which leads to an under-damped system, the linear equation indicates free vibration at the damped frequency given by

$$\omega_{d(sp)} = \omega_{sp}\sqrt{1-\zeta^2} \tag{2.61}$$

Second, observe the limiting condition $R_f \longrightarrow 0$ with $c_b = 0$, which approximates the valve fully open (assuming minimal flow resistance at the fully open position), and produces

$$\lim_{R_f \to 0} \left|\frac{x(s)}{q(s)}\right| = \frac{1}{\frac{M}{K_{sys}}s^2 + 1} \tag{2.62}$$

Following the same procedure as before leads to a second order differential equation

$$\ddot{x} + \frac{K_{sys}}{M}x = \frac{K_{sys}}{M}q \tag{2.63}$$

where the natural frequency of oscillation is

$$\omega_{sys} = \sqrt{\frac{K_{sys}}{M}} \tag{2.64}$$

This corresponds to free oscillation at a frequency composed of the combined effects of the air spring and accumulator volumes. If the bag damping is included, the same equations as (2.58) through (2.61) result with K_{sp} and ω_{sp} replaced with K_{sys} and ω_{sys}, respectively.

Summary

Based on the above analyses, the limiting conditions can be summarized as follows:

1) At *low frequencies*, for a given value of R_f, the system stiffness approaches a value that is composed of the sum of the air spring and accumulator volumes. Intuitively, this makes sense because, for a fixed value of R_f at low enough frequencies, the pressures have time to approximately equalize (i.e., $P_{sp} \approx P_{ac}$) on each up and down stroke. This implies that as much air flow as possible has passed between volumes, thus giving the effect of both volumes being joined together. This has the same effect as reducing the restriction to air flow by opening the valve.
2) At *high frequencies*, for a given value of R_f, the system stiffness approaches a value composed only of the air spring volume. Intuitively, this occurs because, as the mass oscillates, there is not enough time between strokes to equalize the pressure, which has the same effect as restricting air flow. In other words, during each half cycle, the air spring reverses from compression to tension, or vice versa, before the air flow has a chance to reach its full potential relative to the pressure drop across the valve. This has the same effect as increasing the restriction to air flow by closing the valve.
3) As the valve approaches fully closed ($R_f \longrightarrow \infty$), air flow is restricted, the system stiffness approaches a value that represents the air spring alone, and the system can be described by a *linear* 2nd order differential equation.
4) As the valve approaches fully opened ($R_f \longrightarrow 0$), restriction to air flow is reduced, and the system stiffness approaches a value that represents the air spring and accumulator combined, and the system can be described by a *linear* 2nd order differential equation.
5) The linear flow resistance is both amplitude and valve opening area dependent.

2.3.2 Frequency Response

The linear frequency response from (2.54) for various values of R_f is shown in Figure 2.11. The vertical axis values represent the magnitude of the output amplitude divided by the input amplitude. The parameters used for this analysis are listed in Table 2.1. As indicated in

the prior analysis, as $R_f \longrightarrow 0$ (valve open) the frequency response peak amplitude is close to the natural frequency of the total system ω_{sys}. As $R_f \longrightarrow \infty$ (valve closed) the frequency response peak amplitude is close to the natural frequency of the air spring ω_{sp}. *Therefore, as the valve orifice opening is adjusted, both the damping and the natural frequency of the system are affected.*

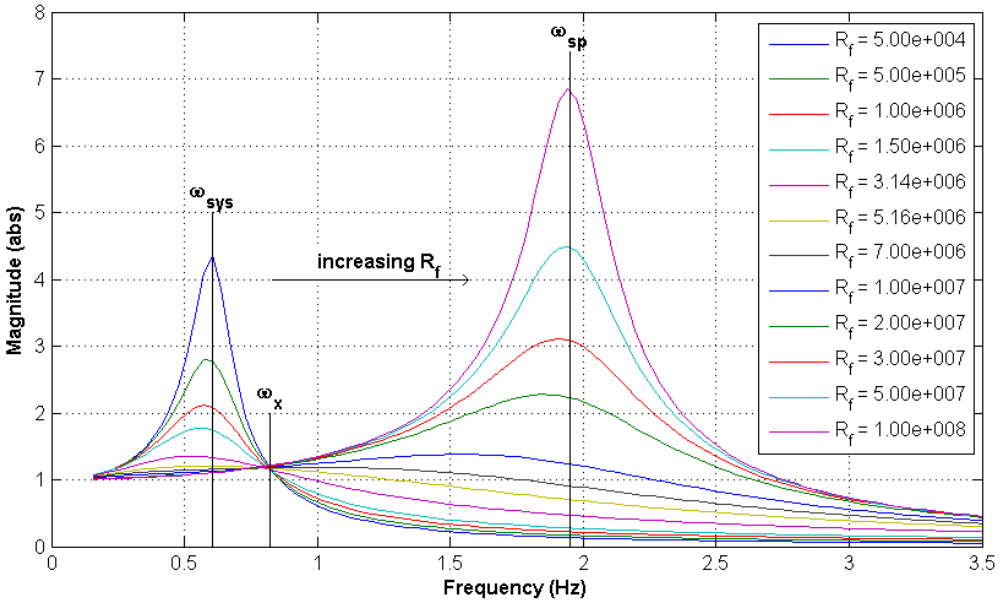

Figure 2.11 Linear frequency response

Table 2.1 Data for linear frequency response

Description	Symbol	Value	Units
Bag damping	c_b	171	(N-s)/m
Air spring stiffness	K_{sp}	30529	N/m
System stiffness	K_{sys}	2961	N/m
Air spring natural frequency	ω_{sp}	1.95	Hz
System natural frequency	ω_{sys}	0.607	Hz
Air spring capacity	C_{sp}	1.039e-008	kg/(N/m^2)

Accumulator capacity	C_{ac}	9.672e-008	kg/(N/m^2)
Cross-over frequency	ω_x	0.8202	Hz

It is instructive to note the response as the valve is adjusted from fully open to fully closed. At fully open (R_f small) the system oscillates with minimal air flow restriction and the primary damping is due to bag damping. As the valve closes, the peak amplitudes decrease as damping increases due to restriction of air flow. Initially, the system approximates a damped second order differential equation of the form shown in (2.59) with $\omega_n = \omega_{sys}$. At a frequency defined as ω_x, the system makes a transition as the valve continues to close and R_f increases. The system damping reaches a maximum value, and then starts to decrease as the system natural frequency has shifted from ω_{sys} toward ω_{sp}. At the limit (R_f large), the system approximates a damped second order differential equation given by (2.59) with $\omega_n = \omega_{sp}$.

The value of R_f corresponding to the lowest peak amplitude (maximum damping) can be determined by finding the value of R_f that minimizes the infinity norm of the transfer function given by (2.54). The infinity norm of a SISO (Single-Input, Single-Output) transfer function is the maximum peak of the transfer function over all frequencies. In other words, in symbolic notation

$$|H(s)|_\infty = \max_\omega |H(j\omega)| \tag{2.65}$$

It is desired to find R_f that minimizes (2.65). This can be easily accomplished by using a standard minimization algorithm along with an infinity norm algorithm, such as the "fminbnd" and "norm" functions found in the Matlab Optimization and Control System Toolboxes, respectively. Using the data in Table 2.1, with the transfer function in (2.52), and applying the previous mentioned algorithms, it is found that the minimum peak response curve occurs for $R_f = 6105173$. The peak amplitude occurs at $\omega = 0.7$ Hz. The minimum peak response curve is shown in Figure 2.11 as the thick black line.

In addition to directly calculating the minimum peak response, it is observed that all curves appear to pass approximately through a cross-over point (or region). It is also

observed that this point is very close to the peak of the calculated minimum peak response (maximum damping) curve. The frequency at this point will be defined as ω_x, which defines a point at which the system is making a transition from the lower to the higher natural frequency. Note that both natural frequency and damping shift in the neighborhood of this point. The damping shifts from a maximum value and starts to decrease as the natural frequency shifts from the lower to the higher value. If the area in the figure around the cross-over frequency is enlarged, it is found that that all lines do not pass through a mathematically exact point. Natural system damping (bag damping) seems to slightly shift the lines away from the point. Nevertheless, an analytical approximation for ω_x will be developed below.

The cross-over frequency can be approximated as follows. First, set the bag damping equal to zero ($c_b = 0$), and note that the responses for the valve fully open and for the valve fully closed can be represented by the following two equations, which are of the same form as (2.59)

$$\ddot{x} + \omega_{sys}^2 x = \omega_{sys}^2 q \qquad R_f \longrightarrow \infty$$

$$\ddot{x} + \omega_{sp}^2 x = \omega_{sp}^2 q \qquad R_f \longrightarrow 0$$

Second, notice that ω_x lies between ω_{sys} and ω_{sp}

$$\omega_{sys} < \omega_x < \omega_{sp}$$

The transfer function for the first equation can be written as

$$\left(\frac{x(s)}{q(s)}\right)_{sys} = \frac{\omega_{sys}^2}{s^2 + \omega_{sys}^2}$$

Substituting $s = j\omega_x$ to obtain the frequency response function leads to

$$\left(\frac{x(s)}{q(s)}\right)_{sys} = \frac{\omega_{sys}^2}{-\omega_x^2 + \omega_{sys}^2} \qquad \omega_x > \omega_{sys}$$

where the inequality constraint implies

$$\left(\frac{x(s)}{q(s)}\right)_{sys} = \frac{\omega_{sys}^2}{\omega_x^2 - \omega_{sys}^2} \qquad \omega_x > \omega_{sys} \tag{2.66}$$

Following the same procedure for the second equation, the frequency response function can be written as

$$\left(\frac{x(s)}{q(s)}\right)_{sp} = \frac{\omega_{sp}^2}{\omega_{sp}^2 - \omega_x^2} \qquad \omega_x < \omega_{sp} \tag{2.67}$$

Equating (2.66) to (2.67) and then solving for ω_x leads to

$$\omega_x = \sqrt{\frac{2\,\omega_{sys}^2\,\omega_{sp}^2}{\omega_{sys}^2 + \omega_{sp}^2}} \tag{2.68}$$

where ω_{sp} and ω_{sys} are defined by (2.57) and (2.64), respectively. Applying (2.68) to the above system leads to $\omega_x = 0.8$ Hz, which is close to $\omega = 0.7$ Hz calculated using the infinity norm minimization.

For a passively designed system, with a defined load, the location of ω_{sp} is determined by the sizing of the air spring. Once the size of the air spring has been selected, the location of ω_{sys} is controlled by the sizing of the accumulator. These two values determine the location of the cross-over frequency ω_x, which approximates the frequency location of the maximally damped response, provided the proper value of R_f is maintained. However, as has been demonstrated, the linear air flow resistance coefficient R_f is a function of both valve opening and amplitude of vibration. Therefore, the design of an optimal passive system is not trivial, since a priori knowledge of both frequency and amplitude content is required. If a design amplitude along with the corresponding pressure drop amplitude has been selected, then the valve opening to achieve a specified optimal R_f, as previously demonstrated, can be determined by solving for the valve opening area percentage $A\%$ in (2.28).

Obviously there are tradeoffs and limitations to any passively designed system, which cannot automatically adjust itself to a changing environment. This is the primary reason for developing an automatic control methodology for a system. If a controller cannot significantly improve the performance of a system over what can be achieved with a passive design, then there is no compelling reason to add a controller to a system. Later in this thesis, a control methodology will be developed and compared to the passively designed system.

2.4 Nonlinear Analysis

Useful information about the system was obtained from a linear analysis of the passive system. A nonlinear analysis of the system was performed and compared to the linear analysis. A nonlinear simulation model based on (2.13) through (2.16) was constructed for this purpose. The model was tuned to match experimental data, and the following simulation results were obtained from the tuned model. The lab test results will be presented in a later section.

2.4.1 Frequency Response as a Function of Valve Opening

The nonlinear steady state frequency response simulation results are shown in Figure 2.12 for base input amplitude of 5.1 millimeters and selected orifice opening percentages. Input data for the frequency response are provided in Table 2.2.

It is observed that the nonlinear frequency response characteristics are similar to those obtained in the linear analysis. Whereas the linear frequency response curves were generated by varying the steady-state linear flow resistance coefficient R_f, which was defined in (2.25), the nonlinear curves were generated by a nonlinear simulation with constant base input amplitude and variable orifice opening areas.

For small base amplitude input, the nonlinear frequency response curves are similar to the linear response curves where the maximum peak amplitudes occur near the calculated natural frequencies. In the linear analysis, it was observed that the linear flow resistance R_f was a function of both pressure drop amplitude and valve opening area. In the nonlinear simulation, keeping the base amplitude small makes the nonlinear flow resistance primarily a function of valve opening area. However, some interesting results occur when attempting to perform a nonlinear frequency response as a function of pressure drop amplitude. These results are presented next.

.

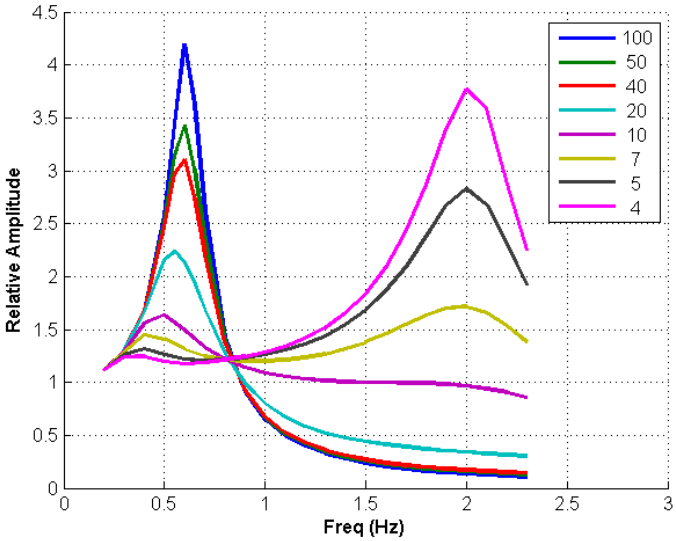

Figure 2.12 Frequency response as a function of valve opening

Table 2.2 Data for nonlinear simulation

Description	Symbol	Value	Units
Suspended Mass	M	184.58	kg
Air spring support area	A_s	0.012817	m^2
Air spring equilibrium volume	$V_{sp(e)}$	0.0012199	m^3
Accumulator volume	V_{ac}	1.136e-002	m^3
Air spring equilibrium pressure	$P_{sp(e)}$	5.624e+005	Pa
Bag damping coefficient	C_b	180.48	N-s/m
Valve orifice maximum area	A_{or} (max)	7.126e-005	m^2
Constant	K	0.12621	null
Test rig tuning coefficient	C_a	0.038	null
Orifice discharge coefficient	C_d	0.62	null
Ratio of specific heats (air)	n	1.3947	null
Temperature	T	293.43	deg K
Specific gas constant	R	286.9	(N-m)/(kg-K)

2.4.2 Frequency Response as a Function of Amplitude

In the preceding section, it was observed that the nonlinear frequency response was similar to the linear frequency response for small base motion amplitudes. As the valve opening area was varied, the natural frequency of oscillation was seen to migrate between ω_{sys} and ω_{sp}. Also, the damping increases as the valve is opened. In terms of the linear flow resistance, which is generally a function of both valve opening area and pressure drop amplitude, small amplitude base motion produces small pressure drop amplitudes, which ensures that air flow resistance is primarily a function of valve opening area with negligible effect from amplitude of vibration.

Observe in Figure 2.13 the results for a fixed valve opening of ten percent (10%) and various input amplitudes. Just as in the variable orifice simulations, the peak relative amplitude of vibration changes based on the amplitude of vibration over the frequency range of interest. The natural frequency varies between ω_{sys} and ω_{sp}. This provides further confirmation that both valve opening area and amplitude of vibration affect resistance to air flow and cause the natural frequency and damping to vary over the frequency range of interest.

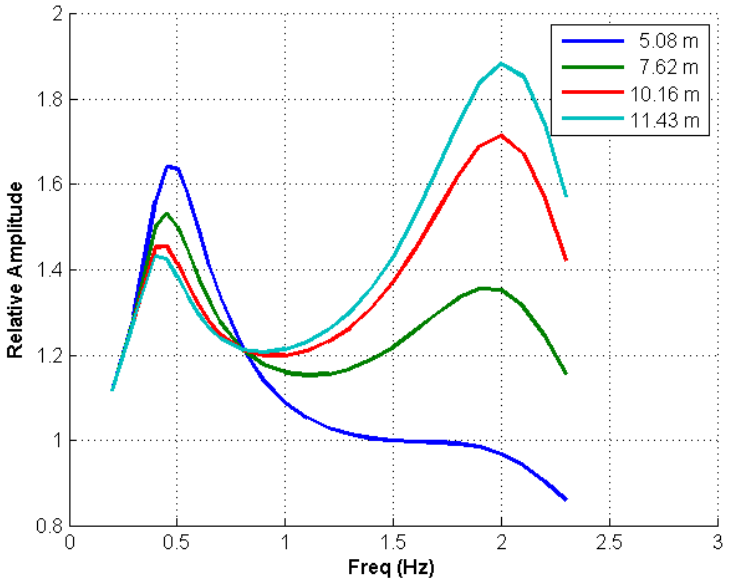

Figure 2.13 Frequency response as a function of amplitude

An interesting phenomenon occurs at higher air flow resistances. At low to moderate resistance levels, the air spring oscillates about the original equilibrium position. However, at higher resistance levels, as vibration amplitude increases, the air spring actually pumps itself up such that the spring oscillates about a higher datum. In addition, as the amplitude level is further increased, this datum increases over time, and the corresponding relative amplitude of vibration changes.

To illustrate this behavior, it is instructive to view a time history plot. Figure 2.14 shows a chart of the displacement versus time for 0.012 meter input amplitude at a frequency of 1.8 Hz and a valve opening area of 30 percent. Note that the mass oscillates about a datum line that is slightly increasing over time, indicating that the air spring is pumping itself up. In addition to the increasing vibration datum, the amplitude, in this particular case, is also increasing. These effects have also been shown to go in the opposite direction under certain conditions. In other words, the air spring vibrates at a lower datum level (not shown).

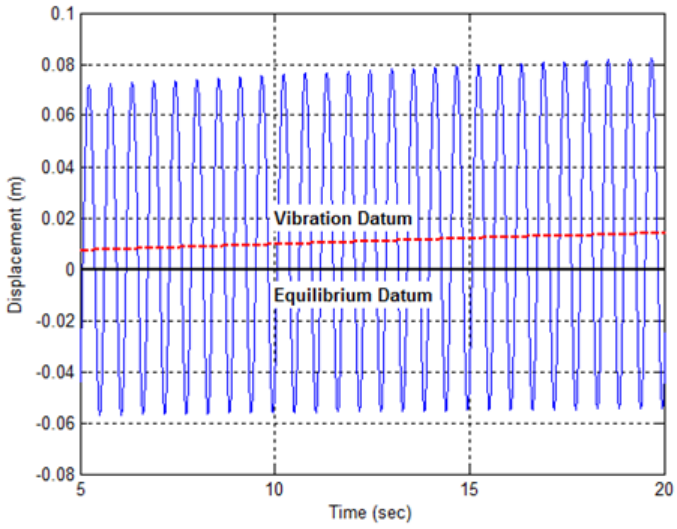

Figure 2.14 Rising vibration datum

2.4.3 Step Response

Frequency Variation

Additional insight into the system behavior can be obtained by observing the step response characteristics. To obtain accurate nonlinear simulation results, the step input is coupled with a first order lag with a time constant of 0.01 seconds.

The step response for 0.010 meter base input for a closed valve is provided in Figure 2.15. By measuring the distance between peaks, it is observed that the damped frequency of oscillation is consistent throughout the simulation and is approximately equal to the natural frequency of the spring (1.9 Hz) calculated from (2.57), and the damping ratio (bag damping) is approximately four percent (4%) as calculated by (2.60). Therefore, a linear equation closely approximates the nonlinear vibration of the air spring without the influence of valve and accumulator dynamics.

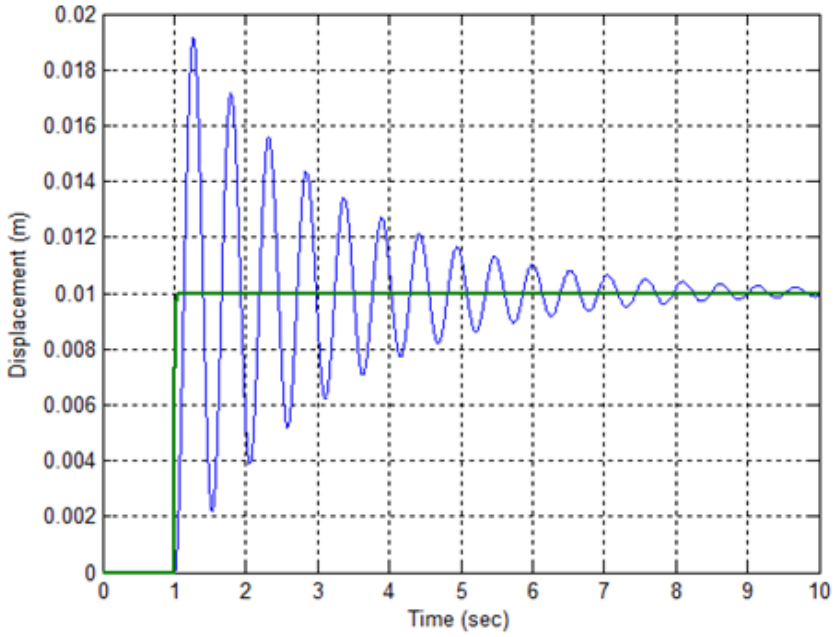

Figure 2.15 Air spring step response

Once the valve is opened such that air flows between the air spring and the accumulator, the step response exhibits nonlinear behavior such that a linear differential equation with constant coefficients is no longer sufficient to accurately describe the behavior of the system. To illustrate this effect, consider the step response shown in Figure 2.16 for a thirty percent (30%) valve opening area and 0.08 meter base input. It appears, at first glance, that the response is similar to a second order linear system response. However, upon closer examination, it is observed that both frequency of oscillation and system damping vary over

time. In the discussion that follows, the frequency variation over time will be analyzed for a typical step response, and then the variation in damping will be studied.

Consider, Figure 2.17 which provides a chart showing the variation in the average frequency of oscillation with respect to time for base input values of 0.02, 0.04, and 0.08 meters at thirty percent (30%) valve opening. The frequencies are determined by measuring the time between successive pairs of peaks. Note that the frequency of oscillation corresponding to the largest amplitudes approaches the calculated value for ω_{sp} (1.9 Hz). As the amplitude decreases over time, the frequency of oscillation decreases to a limiting value of approximately ω_{sys} (0.87 Hz). In addition, note that the curves shift to the right as the base input values increase. This is due to the fact that higher step input magnitudes induce larger amplitudes of oscillation leading to a greater number of relatively high peaks at the beginning of the response. The higher peaks (amplitudes) produce higher pressure drops across the valve, leading to a shift in system natural frequency toward ω_{sp}, along with a corresponding decrease in the time measured between peaks. As the amplitude decreases over time, the natural frequency shifts toward ω_{sys}, and the time measured between peaks increases.

The chart in Figure 2.18 provides the frequency variation for a constant step input magnitude of 0.04 meters and valve opening areas of 10, 20, and 30 percent, respectively. It is noted that smaller valve opening areas achieve a similar result as larger input amplitudes.

In both cases above, by changing the base input magnitude and valve opening area, it was demonstrated how the frequency of oscillation varies over time for the response due to a base step input. In addition, note that there is a point where the frequency rapidly diminishes. This occurs at the cross-over frequency location as previously defined. The natural frequency of the system shifts rapidly between the two system natural frequencies. As previously stated, the system damping also varies over time. This will be demonstrated in the following discussion.

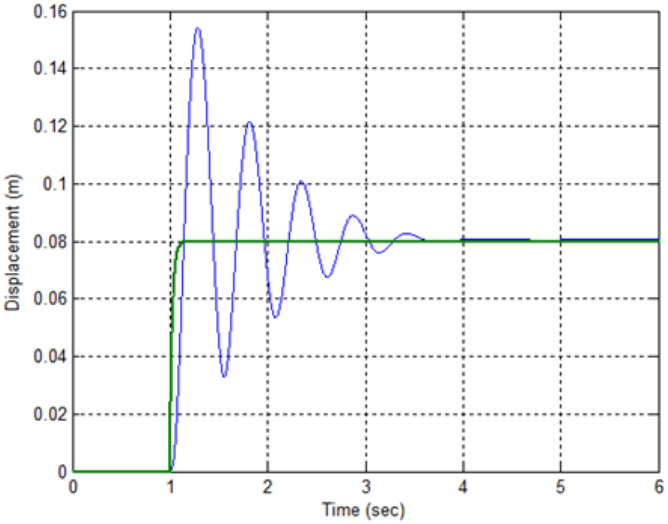

Figure 2.16. Step response for 30% valve opening and 0.08 m base input

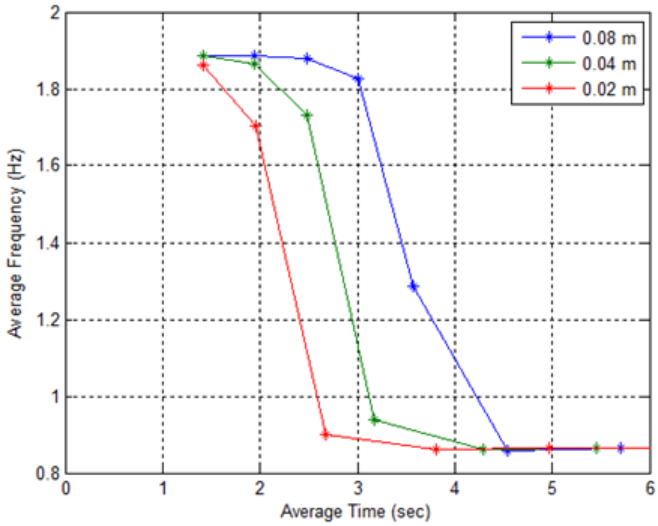

Figure 2.17 Average frequency variation at selected input amplitudes

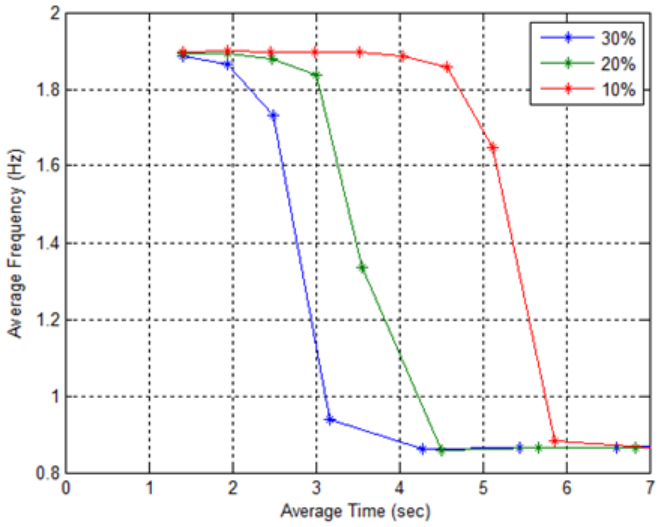

Figure 2.18 Average frequency variation at selected valve openings

Damping Variation

Recall that a single degree-of-freedom, linear second order system can be characterized by a unique natural frequency and associated damping constant. These two parameters are related by the damping ratio in (2.60). In the linear analysis, it was observed that the limiting cases corresponding to infinite resistance and zero resistance produced second order differential equations, which had associated natural frequencies of ω_{sp} and ω_{sys}, respectively. The damping ratio was attributed to bag damping (c_b) in both cases, which was assumed to be linear in nature. Also, the reader should recall that the steady-state linear flow resistance (R_f) is a function of both valve opening area and pressure drop amplitude.

In the nonlinear case, the system damping is also a function of amplitude and valve opening area. At the limiting conditions, which correspond to high flow resistance (large amplitude and small valve opening) and low flow resistance (small amplitude and large valve opening), the damping approaches a linear second order system damping ratio that is associated with the assumed bag damping. Between these two extremes, the nonlinear damping is not associated with a unique natural frequency and damping constant, which are characteristic of a second order linear equation with constant coefficients. As a matter of fact, in the prior linearization it was shown that the system is more accurately described by a third order linear equation. *Therefore, for this nonlinear system, it does not make sense to speak of*

a damping ratio or percent damping in the classical sense, which applies only to a linear second order system.

However, to study the damping variation of the nonlinear response with respect to time, it is proposed to approximate damping by a piecewise linear fit between each pair of peaks in the response. To accomplish this, note that the well-known solution for the standard homogeneous differential equation for under-damped free vibration, subject to a set of initial conditions, is given by

$$x(t) = e^{-\gamma t}[A\cos(\omega_d t) + B\sin(\omega_d t)] \tag{2.69}$$

where the constants are defined as

$$\begin{aligned} A &= x(0) \\ B &= \frac{1}{\omega_d}[\gamma x(0) + \dot{x}(0)] \end{aligned} \tag{2.70}$$

and the damping exponent (exponential decay rate) is given by

$$\gamma = \zeta \omega_n \tag{2.71}$$

where ζ is the damping ratio, ω_n is the natural frequency, and ω_d is the damped frequency of oscillation.

The idea is to apply (2.69) to each pair of peaks to approximate an average damping ratio and natural frequency over the associated time interval. After the system has been set into motion by the initial excitation of the step input, the response can be treated as a free vibration response, and the homogeneous solution can be applied.

To accomplish this, with reference to Figure 2.19, a change of variables can be applied to (2.69) and (2.70). For each pair of peaks, the first peak is considered occurring at $t = 0$, and the zero reference line, $x(t) = 0$, will be taken as the final value x_f of the step input.

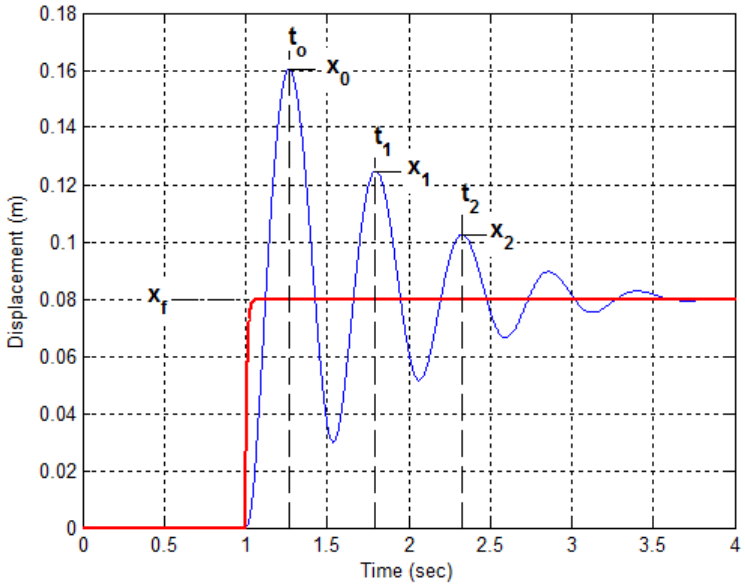

Figure 2.19 Variables for piecewise linear approximation

With this understanding, the following variables are defined:

$$\begin{aligned} \Delta t_i &= t_i - t_{i-1} \\ \omega_{di} &= 2\pi/\Delta t_i \\ y(t_i) &= x(t_i) - x_f \\ y(0) &= y(t_{i-1}) \end{aligned} \tag{2.72}$$

The subscript index, $i = 1,2,\ldots,n$, is the peak pair number, and n represents the number of desired peak pairs for consideration.

Noting that $\dot{x}(0) = 0$ and substituting variables (2.72) into (2.69) and (2.70) leads to

$$y(t_i) = y(t_{i-1})\, e^{-\gamma_i \Delta t_i} \tag{2.73}$$

Solving (2.73) for γ_i leads to an expression for the decay rate between two peaks

$$\gamma_i = -\frac{ln[y(t_i)/y(t_{i-1})]}{\Delta t_i} \tag{2.74}$$

The natural frequency is related to the damped frequency and damping ratio by the well-known equation

$$\omega_{ni} = \frac{\omega_{di}}{\sqrt{1 - {\zeta_i}^2}} \tag{2.75}$$

Substituting (2.75) into (2.71) and solving for the damping ratio produces

$$\zeta_i = \sqrt{{\gamma_i}^2/({\omega_{di}}^2 + {\gamma_i}^2)} \tag{2.76}$$

Equations (2.72) through (2.76) can be used to estimate an average natural frequency and damping ratio between each successive pair of peaks produced by a base step input. This will be a linear piecewise approximation to the nonlinear response.

Before analyzing the step response damping and natural frequencies, it is instructive to revisit Figure 2.11 and Figure 2.12 for the linear and nonlinear frequency responses. Beginning with the high resistance condition (e.g., closed valve), the natural frequency approximates ω_{sp} with small damping. As the resistance is decreased (e.g., opening valve), the damping initially increases with the natural frequency remaining near ω_{sp}. As the resistance further decreases, damping continues to increase until the natural frequency begins to shift toward ω_{sys}, and then the damping begins to decrease as the resistance continues to decrease. A similar situation is observed in the step response.

Figure 2.20 and Figure 2.21 provide a sampling of the piecewise linear natural frequencies and damping ratios for various valve openings at 0.08 meter step input. Each marker in the figure corresponds to a peak pair of the step response, and each curve corresponds to a valve opening percentage as indicated. The first peak in an under-damped response has the largest magnitude, followed by progressively decreasing peak magnitudes. Note that the natural frequencies start near ω_{sp} where peak values are higher, and then move toward ω_{sys} as the peak values decrease over time. Keep in mind that higher peak values, and thus higher pressure drops across the valve, lead to higher resistance. Likewise, smaller valve openings lead to higher resistance. Therefore, similar to the linear frequency response, as resistance increases, due to higher amplitudes and smaller valve openings, the natural frequency moves toward ω_{sp}. However, as resistance decreases, due to lower amplitudes and larger valve openings, the natural frequency moves toward ω_{sys}. In Figure 2.20, at smaller valve openings, the damping is smaller and the oscillations, which are greater in number,

remain large enough to maintain a relatively high pressure drop and corresponding high flow resistance. As the amplitude and corresponding flow resistance decreases, eventually the natural frequency rapidly shifts toward ω_{sys}.

Figure 2.21 provides the piecewise linear damping ratios corresponding to the natural frequencies in Figure 2.20. At smaller valve openings and larger amplitudes (high resistance), the damping starts low and increases as the amplitudes and corresponding resistance decrease. At some point, the amplitude is small enough (low resistance) to cause a shift in the natural frequency and the corresponding damping ratio rapidly drops off. Again, this is the same effect observed in the linear frequency response.

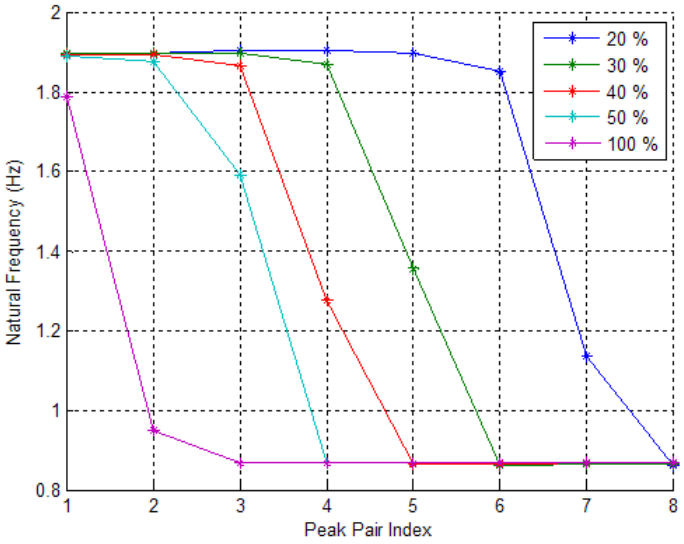

Figure 2.20 Piecewise linear natural frequencies for 0.08 step input response

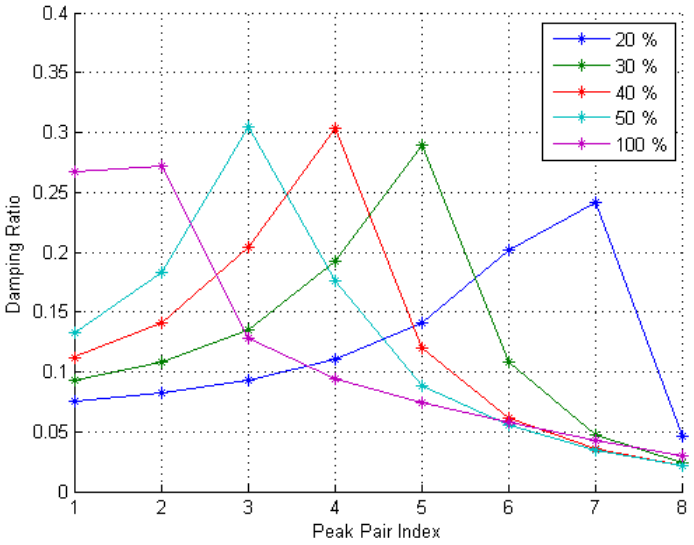

Figure 2.21 Piecewise damping for 0.08 step input response

It is interesting to observe the results of a refined analysis between the 40% and 50% valve opening areas. Figure 2.22 provides the natural frequencies and Figure 2.23 provides the corresponding damping ratios. It is easy to see in the damping ratio chart a cross-over area at about the 45% valve opening area. This occurs at the cross-over frequency location as previously defined.

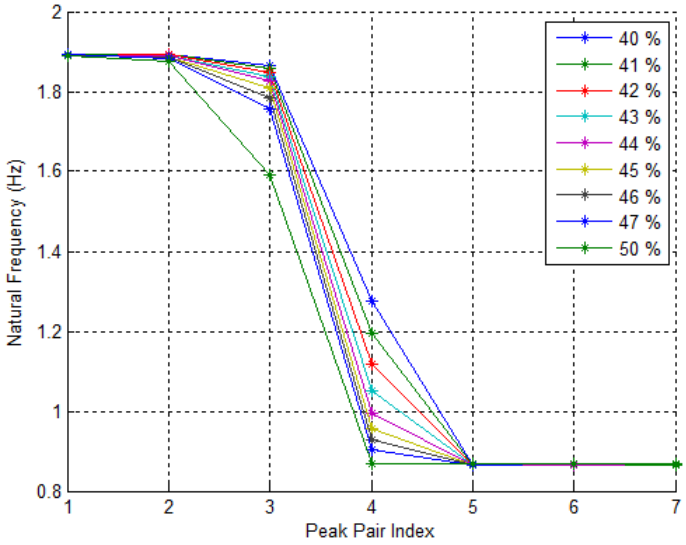

Figure 2.22 Piecewise linear frequency

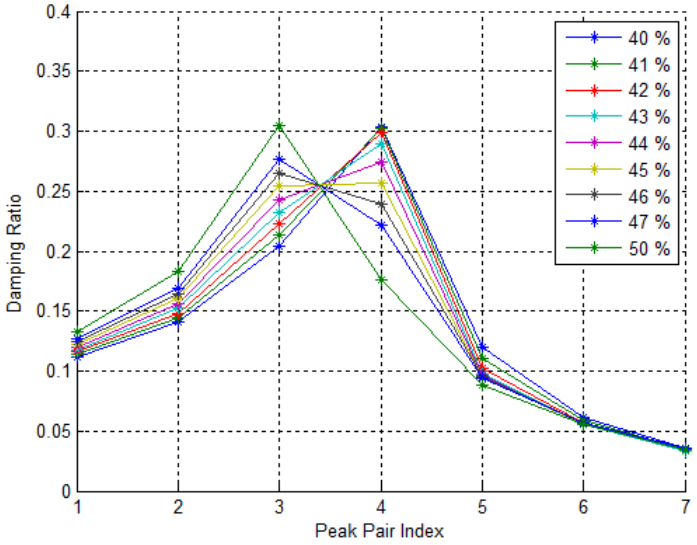

Figure 2.23 Piecewise linear damping

Another way to measure damping effects in the nonlinear system is to observe the settling time. Instead of using a piecewise analysis as was done above, the settling time provides one number as descriptive of the entire time response. The settling time is typically studied as a part of linear system theory and controls; however, it can also be applied to nonlinear systems when appropriate. As damping increases in the nonlinear (or linear) system, the settling time decreases, and vice versa. The settling time is typically expressed as the time it takes for the system step response amplitude to settle down and stay within a band about the final value. This band is typically expressed as a plus or minus percentage of the final steady-state value. The actual percentage of final value is not standard. Examples of common values are $\pm 5\%$ and $\pm 2\%$.

Consider the previous step response at thirty percent (30%) valve opening and 0.08 meter base input. Figure 2.24 illustrates the settling time relative to a $\pm 2\%$ band. The asterisk (*) indicates the point at which the displacement enters and stays within the band. The time measured from the point of initiation (1.0 second) of the step input up to this point is referred to as the settling time. In this case, the settling time is 2.53 seconds.

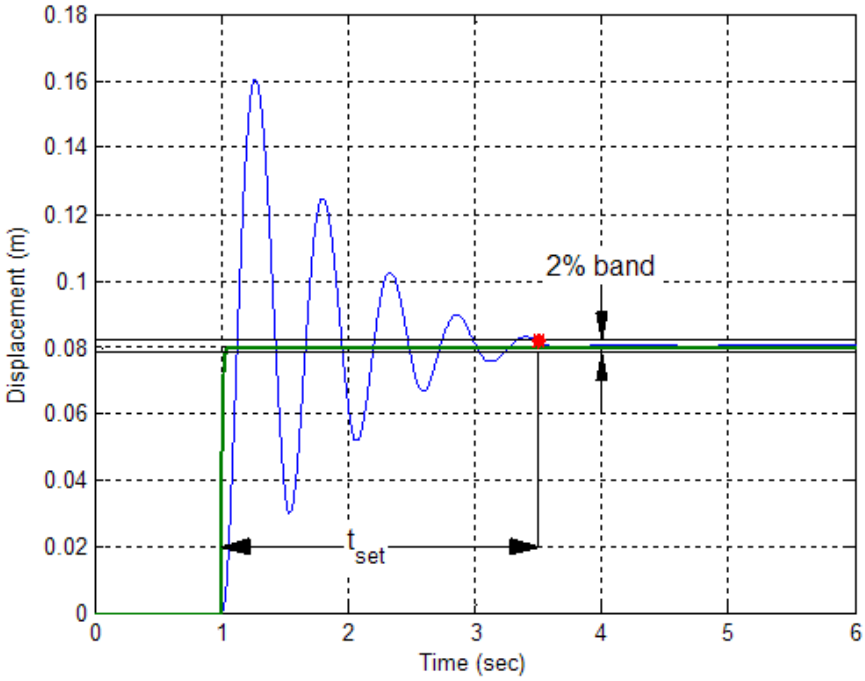

Figure 2.24 Settling time with 2% band

Figure 2.25 provides the settling times versus the valve opening areas for various base step input values. Beginning on the left-hand side of the chart, at the higher resistance levels (smaller valve openings and higher amplitudes), it is observed that the settling times are higher, indicating smaller damping. As the resistance levels are lowered (larger valve openings and lower amplitudes), the settling times decrease, indicating higher damping. In the 40% to 50% opening area range, a cross-over point is observed. As mentioned before, this corresponds to the natural frequency shift from the higher to lower natural frequency. As the resistance levels continue to decrease, settling time rises, and damping decreases.

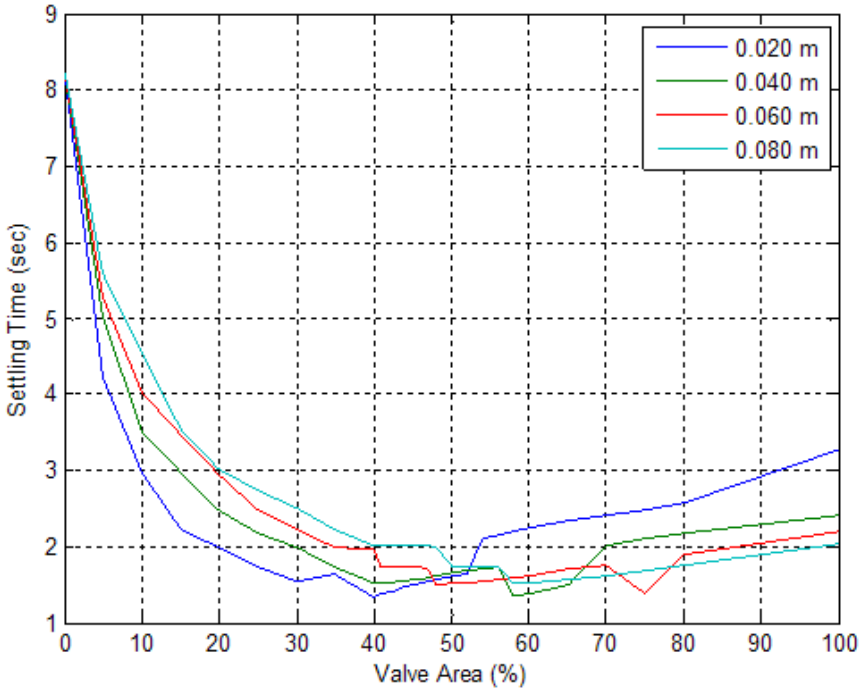

Figure 2.25 Settling time for 2% band

2.4.4 Additional Considerations

The linear and nonlinear frequency response and the nonlinear step response analyses were affected by varying the valve resistance. In the linear analysis, the valve resistance coefficient was defined in (2.24) and (2.25), which is a measure of the resistance to air flow through the valve. Increasing values of the resistance coefficient lead to higher restrictions to the mass flow rate of air through the valve for a given pressure drop. For the nonlinear analysis, the resistance to air flow was varied by controlling the opening area of the valve.

In (2.9) it is observed that the opening area is not the only variable that affects resistance. Another important variable is C, which is composed of the coefficient of discharge and the valve tuning coefficient. This coefficient multiplies A in (2.9). The valve tuning coefficient was introduced to handle the unknown resistances, such as produced by unknown valve construction details and other piping within the system. It is obvious that the frequency and step responses will be affected by any additional resistances introduced into a practical system, such as piping and other line losses. Therefore, these losses should be seriously considered during the design of a production system.

2.5 System Identification

All simulations and analysis in the previous sections used a tuned model based on lab test results. This section will present the laboratory test results and model correlation procedure.

Figure 2.26 provides a picture of the lab test stand. The stand consists of a reversible sleeve air spring connected to an accumulator through a solenoid actuated, continuously adjustable, valve that is regulated by a computer algorithm. The air spring supports a sled, which supports metal plates that can be added or removed to adjust the load acting on the air spring. Matlab real-time software running on dSpace hardware is used to monitor sensor data and provide algorithmic control signals to the valve solenoid.

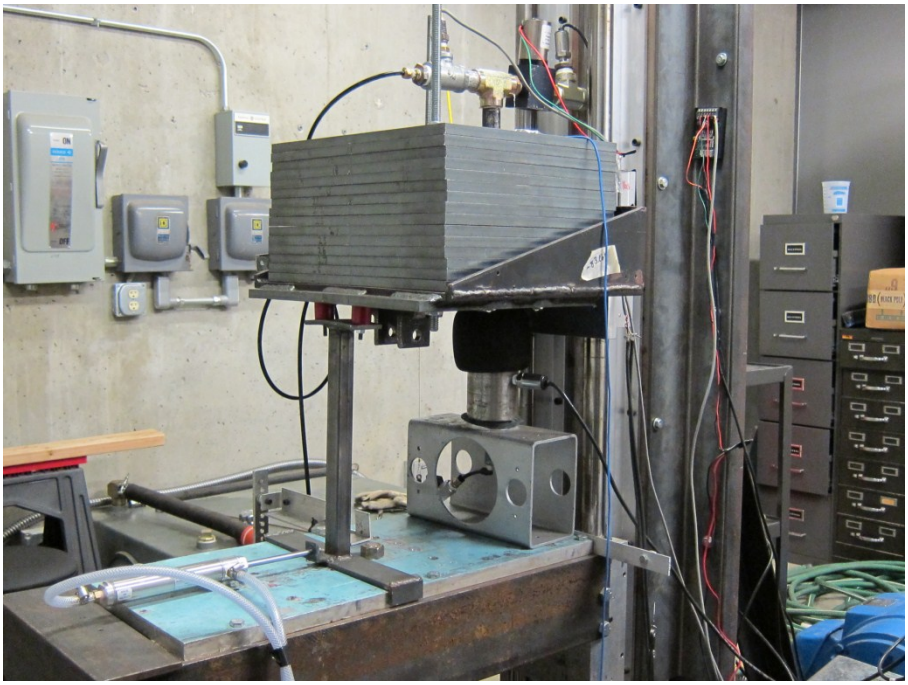

Figure 2.26 Laboratory test rig

2.5.1 Static Tests

Volume Calculations

Direct measurement of the internal volume is difficult, and the current test stand does not have the capability to perform this measurement. Therefore, an effective internal volume

must be indirectly estimated based on other measurements along with application of the fundamental ideal gas laws.

To calculate the air spring volume based on direct pressure measurements, the air spring was initially loaded with a total load of 1994 N, and the pressure was adjusted to place the air spring at a chosen equilibrium operating height. The individual weights were then gradually removed from the sled, and the corresponding displacements, pressures, and heights of the spring were recorded. At the final position, the spring was fully extended and only contained the weight of the sled. Since the spring was fully extended, a physical estimate of the internal volume could be calculated by measuring the diameter and height of the air spring. This measurement provided the initial volume calculation. The volumes for all other positions were calculated from the ideal gas equation, assuming an isentropic relationship, where the equation relating two states in the process is given by

$$P_1 V_1^n = P_2 V_2^n \tag{2.77}$$

Solving for V_2 yields

$$V_2 = V_1 \left(\frac{P_2}{P_1}\right)^{(-1/n)} \tag{2.78}$$

An estimate of the volume at each steady state point as weights are added to the sled, starting with the initial measured volume estimate with the air spring completely extended, is calculated by (2.78)

It is easier to measure relative displacement and to correlate the model to test data if the volume of the air spring is expressed as a function of relative displacement instead of height. Figure 2.27 provides a plot of the static air spring volume versus relative displacement, including an initial condition (relative position). The solid blue line data points are the actual measured points on the test rig. The dashed line points are additional points that were extrapolated from the test data. Since the test facility did not contain enough weights to generate these points, extrapolated data points were added to ensure coverage of the complete dynamic operating range and to provide a more robust table lookup function for computer simulation. The slope of this curve evaluated at the equilibrium point provides a value for ν in (2.21).

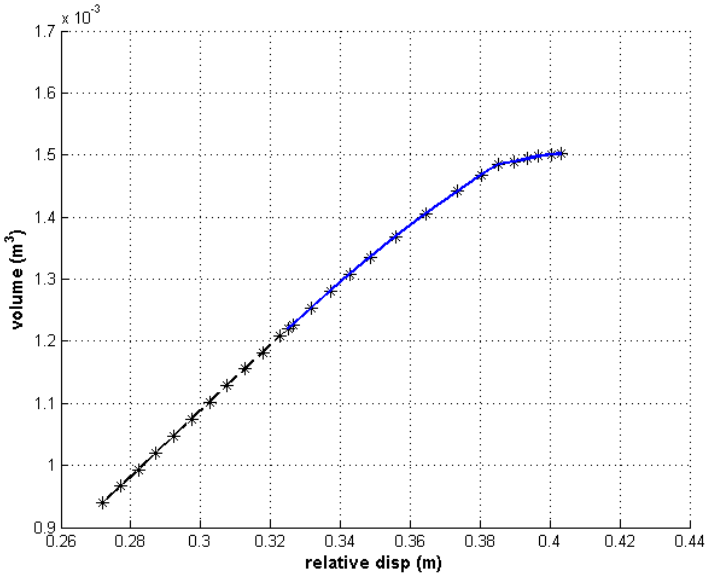

Figure 2.27 Air spring volume vs. relative displacement

Static Pressure

The topic of pressure composition was introduced above during the development of the nonlinear equations of motion. Test data was presented in Figure 2.4. Additional interpretation relative to the volume data will now be presented.

The lower weight portion of the curves in Figure 2.4 corresponds to the upper (higher volume) portion of the curve in Figure 2.27. As weight is initially added to the air spring, notice that the total pressure remains relatively constant, and there is an exchange of "spring" pressure for "weight" pressure. The change in volume during this time is also relatively small. One way to think about this is that the initial inflation pressure was the result of the elastic bag material expanding and absorbing a certain amount of energy due to air expansion inside the bag. As weight is added externally to the bag, some of the elastic potential energy is converted to potential energy to support the added weight, thus relieving some of the "extra" pressure that initially went into bag expansion.

As the weight is increased, a knee forms in the curve, and the total pressure curve becomes steeper as the spring pressure curve flattens out, which indicates a direct relationship between the change in internal air pressure and the change in weight. During this time, the volume is also decreasing at a relatively steep rate. It was observed in the tests that

the knee in the curve occurs at the point where the bag material starts to roll over and along the edge of the piston as weight is continually added to the sled. Also, as the weight is increased, the diameter of the spring initially increases with a slight decrease in volume until the bag material starts to roll along the side of the piston, at which time the diameter remains relatively constant, but the volume sharply decreases as the piston rides up into the air spring. During the time that the bag material is riding up and down the piston, the pressure associated with the elastic behavior of the spring remains relatively flat, and the change in air pressure is mostly a function of the change in weight.

2.5.2 Step Response Tests

Step response tests were used to tune the plant model. The bag damping c_b in (2.16), the test rig tuning coefficient C_a in (2.9), and the valve effective orifice opening area A in (2.9) relative to the solenoid supply voltage were determined by the step response tests.

For control algorithm implementation, the valve opening area versus the solenoid supply voltage needs to be determined. Since the valve does not have an internal sensor to provide an area measurement, this relationship needs to be calculated by indirect measurements. The step response tests results can be used for this purpose; however, before this is possible, c_b and C_a need to be determined.

The test rig contains linear displacement sensors that measure the absolute displacement of the supported mass and the shaker base. Weights are added to the sled such that the total weight supported by the air spring is approximately 1.994 kN.

Bag Damping Coefficient

To determine the bag damping coefficient, a base step input is provided with the air valve fully closed. Under this condition, $C_a = 0$ and $A = 0$ since there is no air flow through the valve. As previously demonstrated, with no valve effects and small amplitudes, the vibration approximates a linear second order system response with a natural frequency approximately equal to the calculated value of ω_{sp} (1.95 Hz).Test results indicated a natural frequency between 1.9 and 2.0 Hz, which is close to the calculated value. The primary damping is assumed to be linear and contributed only by the air spring bag. However, this ignores any

test rig friction and nonlinear effects of the air spring material. The initial assumption is to assume these unknown quantities as negligible; however, as will be seen later, introducing a simple model for friction into the simulation produces a closer match with experimental data. With these assumptions, the bag damping constant can be estimated by the well-known logarithmic decrement method [6]. For convenience, the formulas for this method are provided below.

For an under-damped system, the logarithmic decrement is defined as

$$\delta = \ln \frac{x_1}{x_2} \tag{2.79}$$

where x_1 and x_2 are the amplitudes of two adjacent peaks, which are measured relative to the step response final value (equal to the step input value). The damping ratio is given by

$$\zeta = \frac{1}{\sqrt{1 + (2\pi/\delta)^2}} \tag{2.80}$$

and the natural frequency is given by

$$\omega_n = \frac{2\pi/T}{\sqrt{1 - \zeta^2}} \tag{2.81}$$

where T is the time between the two peaks. The bag damping constant is then calculated by

$$c_b = 2\zeta\omega_n M \tag{2.82}$$

where M is the supported mass. Using these formulas, it is found that $\zeta \cong 0.0428$ and $c_b \cong 174.0$ N-s/m.

Model Tuning (Valve Closed)

Note that the nonlinear differential equations representing the system model are (2.13) through (2.16). The solution to (2.13) provides the total absolute air spring pressure P_{sp}, which must be transformed to the gauge pressure P_w in (2.16), which produces the actual force on the suspended mass when multiplied by the support area A_s. However, the solution P_{sp} to (2.13) requires the air spring volume $V_{sp}(t)$ and time rate of change of volume $\dot{V}_{sp}(t)$ as inputs. Also, the solution to (2.16) requires P_w, which is a function of P_{sp}, and $\dot{h}$, which is the relative velocity between the suspended mass and the base.

To solve the system of equations, the volume needs to be related to the displacement. This relationship was provided above in Figure 2.27, which provides a plot of the static volume versus a relative spacing of the mass and base. An absolute spacing measurement, instead of displacement from equilibrium, is used here for convenience with direct measurements on the test rig. For a numerical simulation, where an interpolation table can be used to represent these values, there will be an initial condition value related to this spacing.

The results in Figure 2.4 can be used to establish P_w as a function of P_{sp}. This relationship is shown in Figure 2.28.

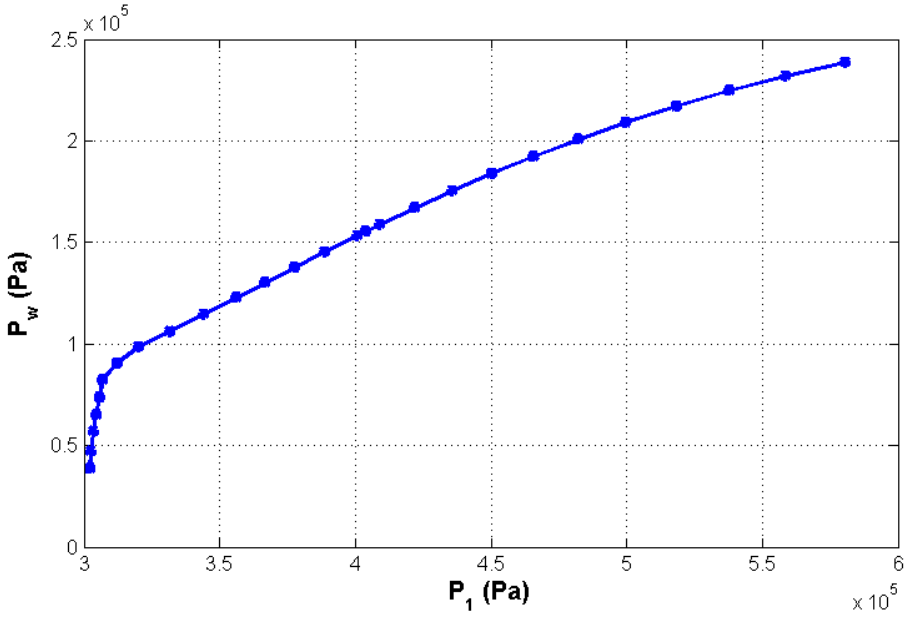

Figure 2.28 P_w vs. P_{sp}

As previously discussed, the relationship established with the data represented in Figure 2.27 and Figure 2.28 is established for static (steady-state) conditions. The unknowns and assumptions behind this data have been discussed. Unfortunately, the static data, along with the unknowns and assumptions behind this data, does not produce the fidelity needed for a dynamic model. However, this data does establish a "ballpark" region from which model tuning to dynamic data can take place.

A comparison of the test results and the model simulation results for displacement and pressure based just on the static data is presented in Figure 2.29 and Figure 2.30, respectively. The plots represent the response to a base step input. The simulation is driven

by the actual base test input. There is an initial startup transient on the simulation pressure curve due to the pressure filter, which is the same as the filter on the test rig. Note that some additional tuning can be done to obtain a better match between the model and the experimental results. This will be discussed below.

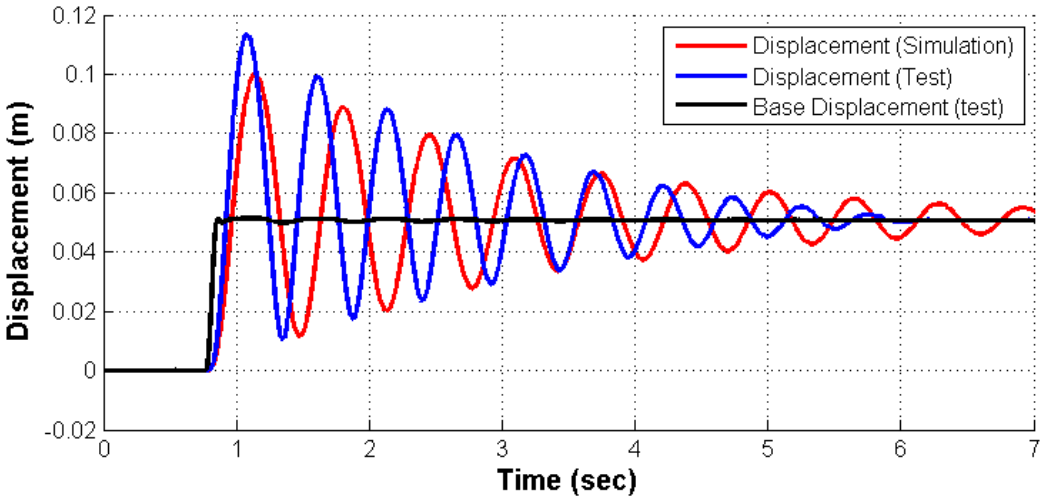

Figure 2.29 Un-tuned displacement

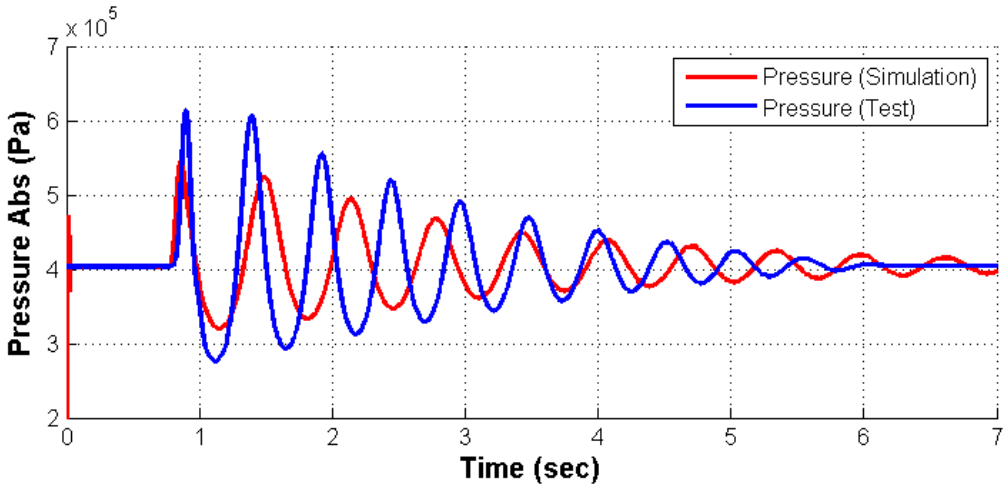

Figure 2.30 Un-tuned pressure

As noted above, the volume, displacement, and pressure relationships were established based on static steady-state tests. In addition, the actual volume could not be directly measured, but had to be estimated based upon the assumption of an isentropic system. Also, the effects of air bag elasticity are unknown. An interesting discovery was that the model could be effectively tuned to the dynamic data by scaling the relative displacement axis of

the static volume data in Figure 2.31. Note that the scaling produced a curve that was rotated counter-clockwise about the initial equilibrium point. This is not a true rotation, but rather a lateral shifting of the data points such that they remain at the same vertical location. In other words, only the scale on the x-axis has changed. The x-axis was scaled according to the following equation:

$$x_{new} = (x_{old} - x_{init})fac + x_{init} \tag{2.83}$$

where

x_{init}= initial equilibrium point

fac = 0.625 (scaling factor)

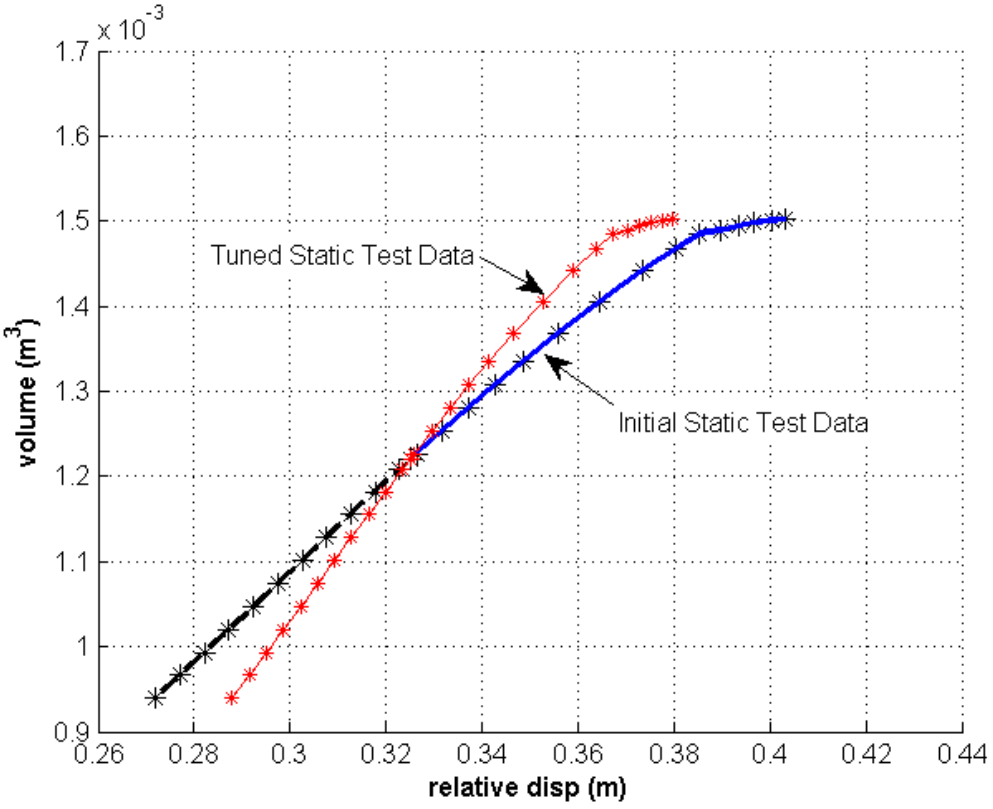

Figure 2.31 Tuned static data versus initial static data

Figure 2.32 and Figure 2.33 provide displacement and pressure plots of the simulation and test results using the tuned data. A much better match to the test data was obtained by this transformation. However, note that the test results die out quicker toward the end of the

data record. This is assumed to be due to friction in the test rig that was not included in the model.

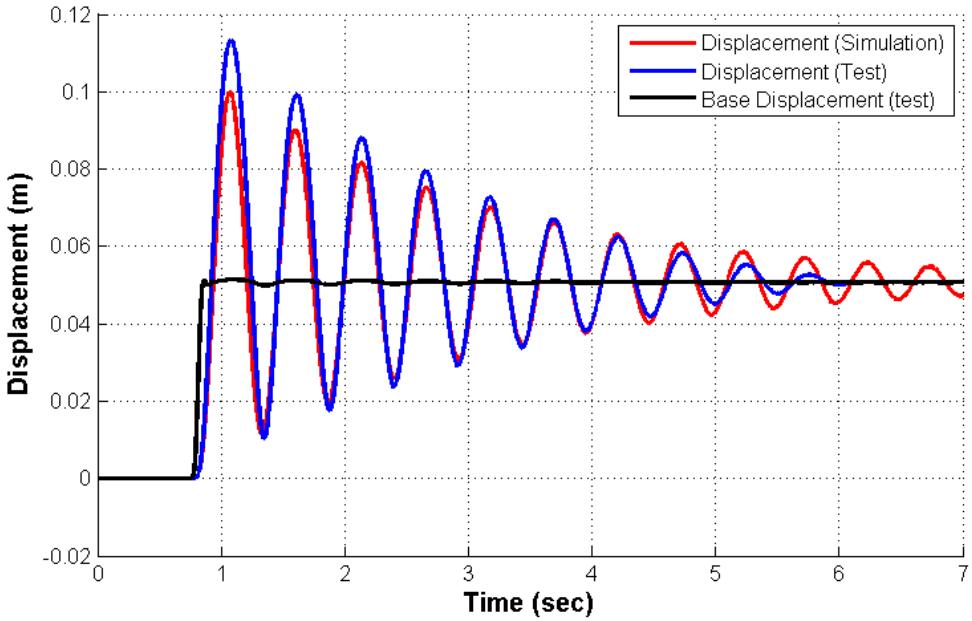

Figure 2.32 Tuned simulation displacement vs. test

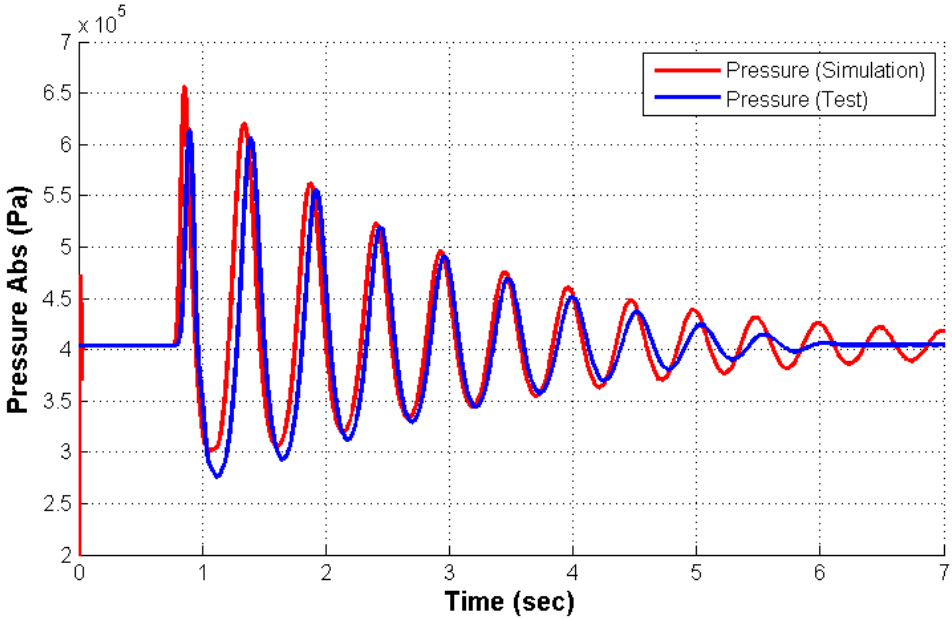

Figure 2.33. Tuned simulation pressure vs. test

To account for friction in the test rig, a simple friction component was added to the model and tuned to obtain a better response. The friction model used was a linear function of velocity that only operates when velocity drops below a certain value. With this addition, the simulation and test results are provided in Figure 2.34 and Figure 2.35.

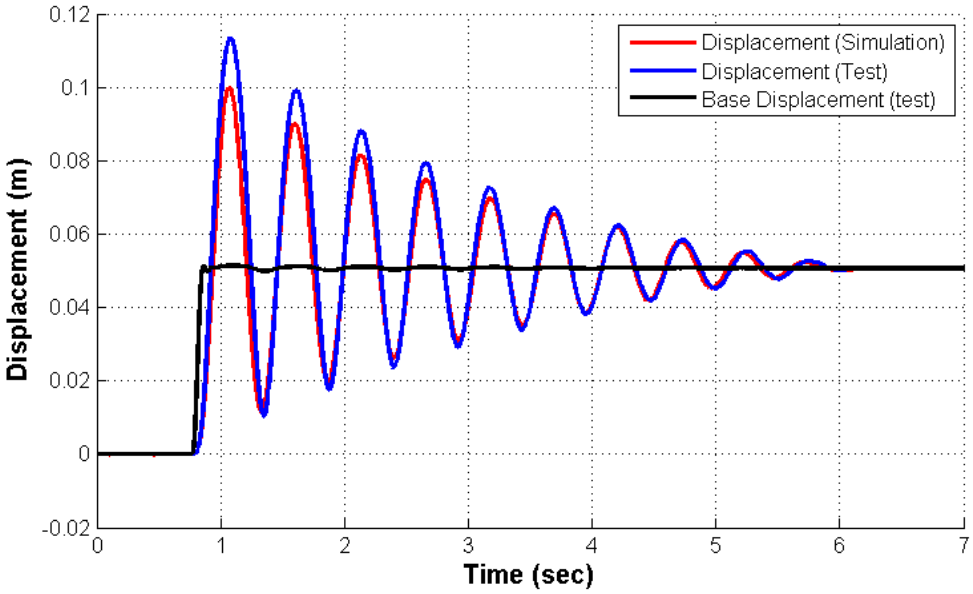

Figure 2.34 Displacement (tuned model including friction)

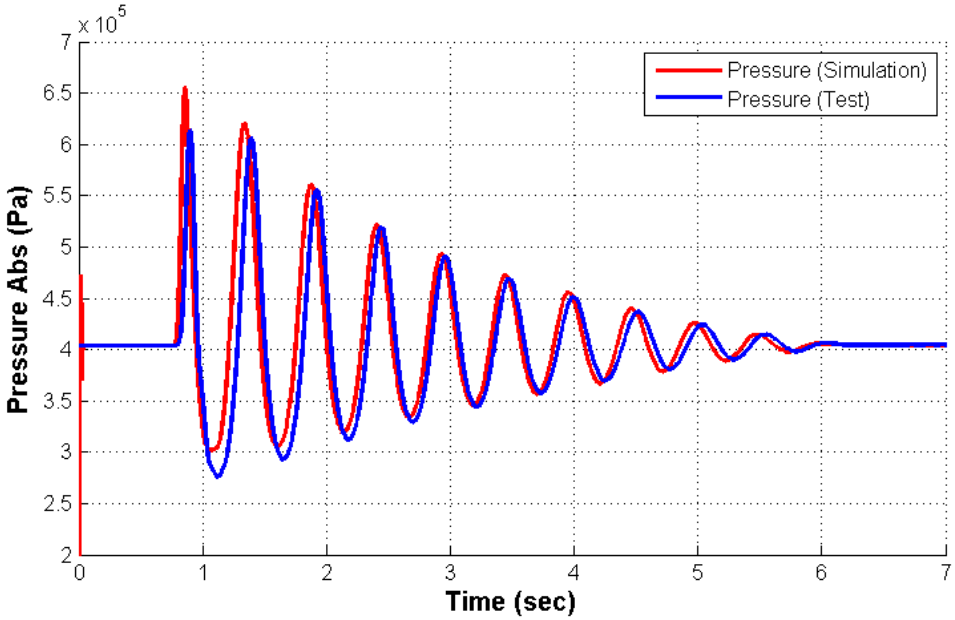

Figure 2.35 Pressure (tuned model including friction)

With the model tuning adjustments, including friction, as discussed above, a credible model, which closely matches test data for the air spring, has been constructed. The following sections will provide details on valve tuning.

Valve Tuning Coefficient

Once the bag damping coefficient has been determined, the next step is to determine the tuning coefficient. As previously explained in the section dealing with the development of the valve equation, there are various unknown quantities or restrictions that influence the mass flow rate of air through the valve. The valve under consideration has an advertised maximum orifice opening diameter of 0.375 inches, which translates to a maximum opening area of 7.1256e-005 m^2. The orifice opening is controlled by a solenoid/poppet type apparatus. The construction of the valve contains air passage ways of unknown length and diameter. In addition, the passages bend the air at 90 degree angles, which may add significant restriction to the air flow. Another unknown is the coefficient of discharge, which was set to a typical nominal value of $C_d = 0.62$. To deal with these unknowns, in addition to any additional piping restrictions in the system, a tuning coefficient C_a was introduced into the air mass flow equation (2.9).

To determine a value for the tuning coefficient, the valve was fully opened to 100%, which established a known value for the opening area A in (2.9). The Simulink Design Optimization software was used to automatically adjust the parameter C_a until a best fit match between the experimental step response and the simulation step response was obtained. The final value obtained was $C_a = 0.038$, which is a significant reduction in air flow due to unknowns. This result highlights the importance of testing a manufacturer's valve before making a final design determination for any particular application. A comparison of the simulation and experimental results is provided in Figure 2.36.

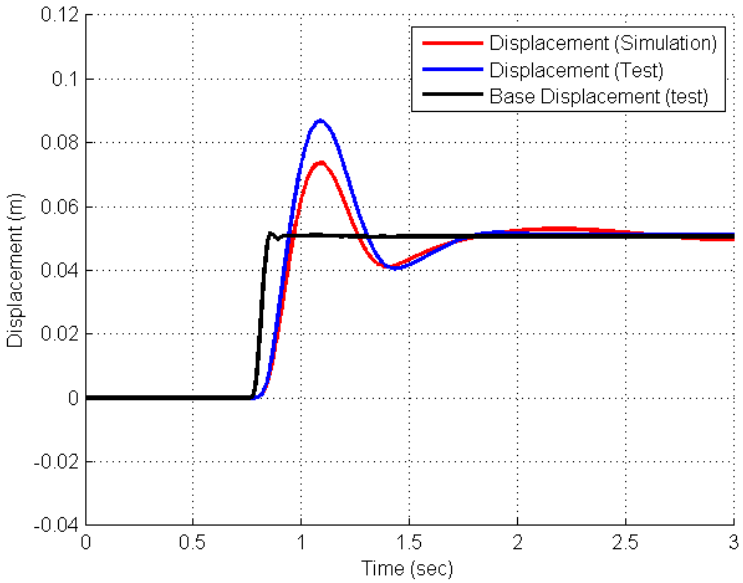

Figure 2.36 Step response with 100% valve opening

Valve Opening Area Calibration

To calibrate the valve opening percentage to the solenoid voltage input, the valve opening percentage of the model was adjusted so that the step response curve from the simulation data optimally matched the corresponding response curve from the test data for each voltage input setting. The Simulink Design Optimization algorithm was used to automatically make these adjustments. The previous Figure 2.36 corresponds to 7.0 volts. Figure 2.37 to Figure 2.40 provide selected results. Figure 2.41 provides the percent area versus solenoid input voltage for the complete range of simulations and tests.

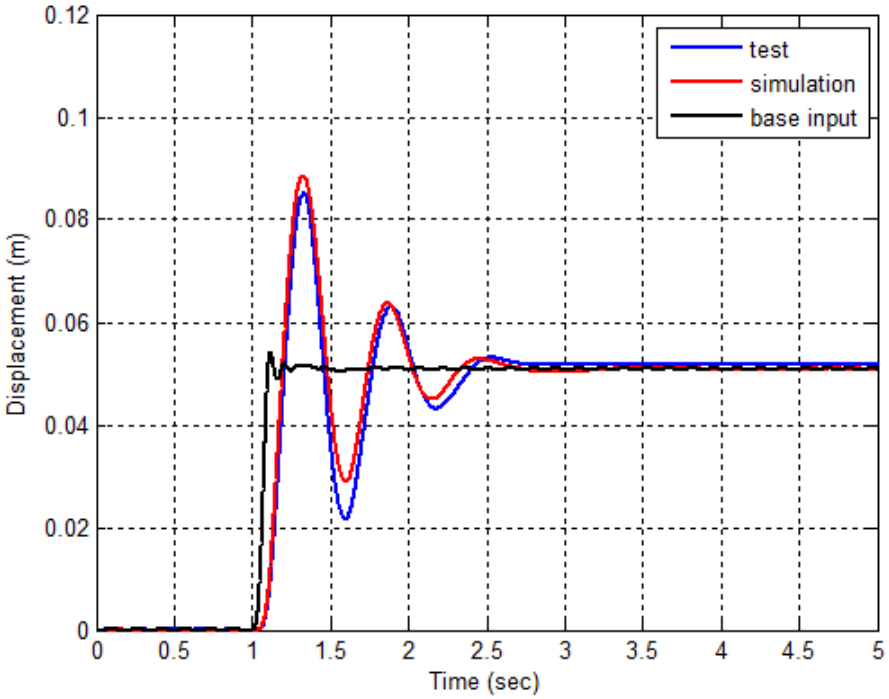

Figure 2.37 Step response – 7 volts (76.8 % area)

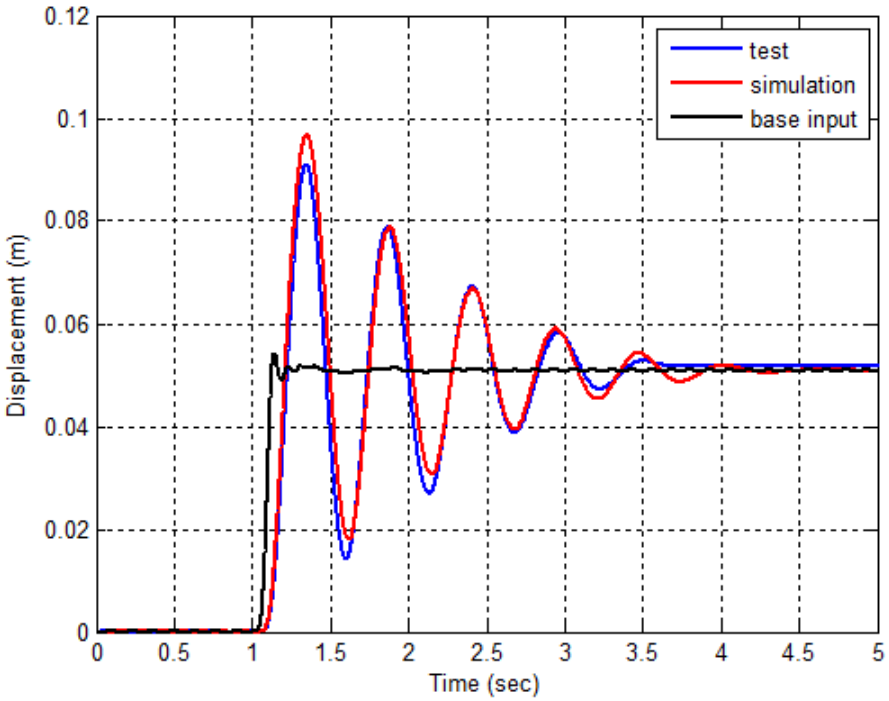

Figure 2.38 Step response – 5 volts (17.3 % area)

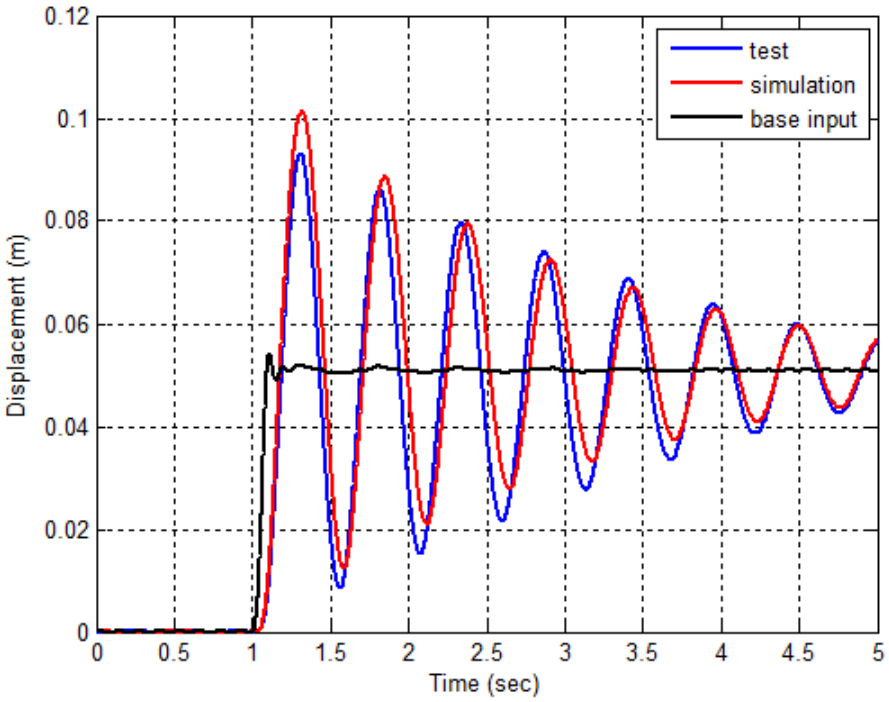

Figure 2.39 Step response – 4 volts (2.21% area)

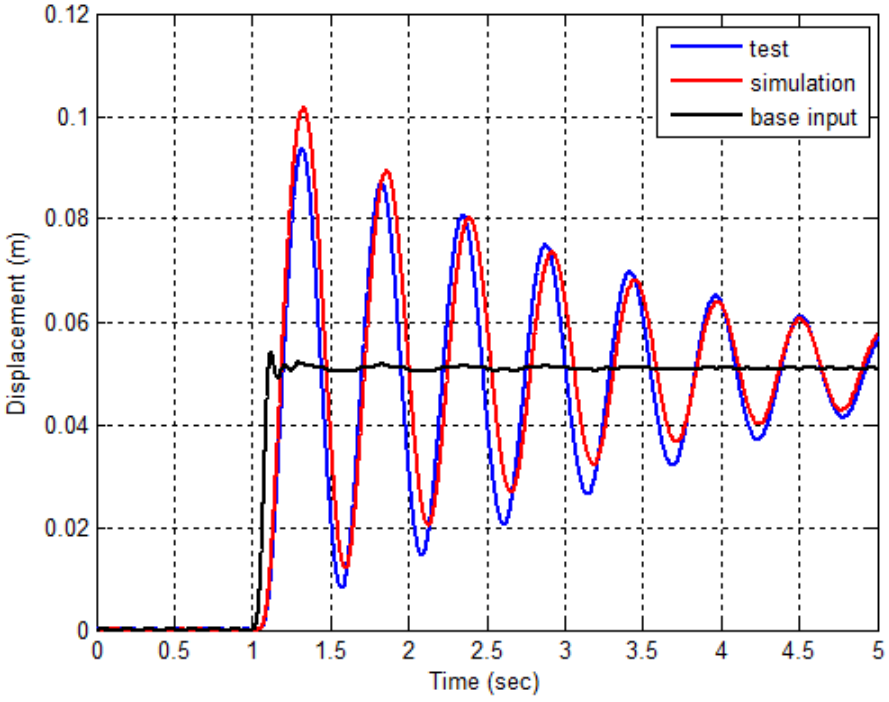

Figure 2.40 Step response – 3 volts (1.27% area)

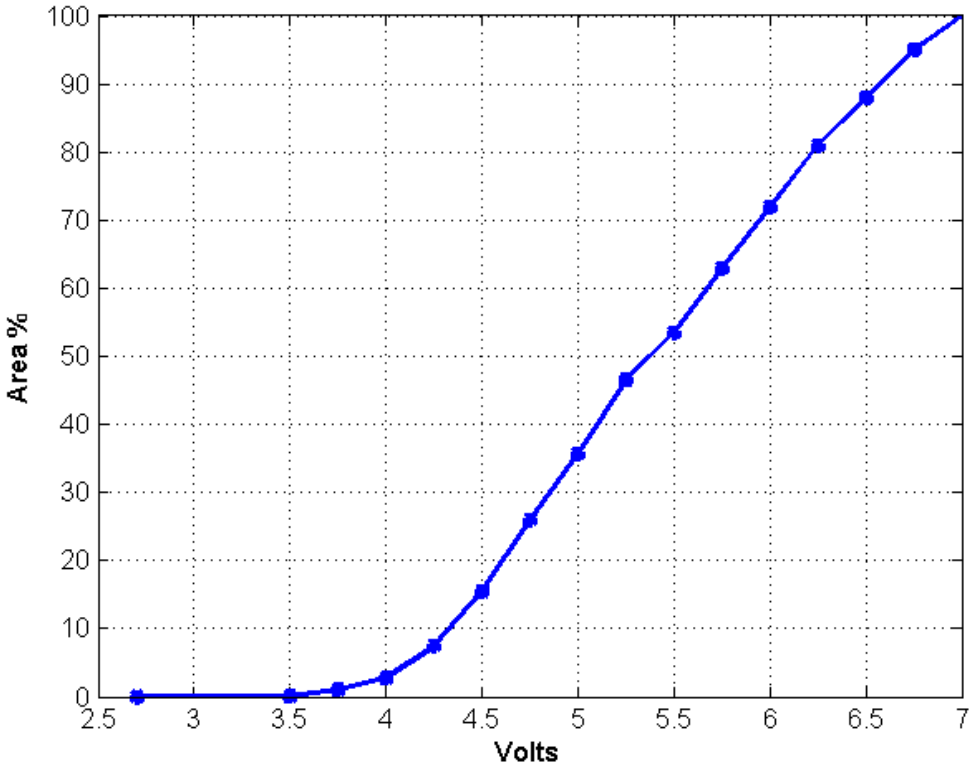

Figure 2.41 Valve area % versus input voltage

CHAPTER 3. CONTROLLER DEVELOPMENT

3.1 Introduction

In the previous chapter a plant model of the air spring, valve, and accumulator (reservoir) system was developed and tuned to the experimental data, where the air flow between the air spring and the accumulator is controlled by a solenoid operated valve. The end result was a validated model that could be used in the development of real-time semi-active control algorithms for vibration suppression. This chapter is dedicated to the development of controller algorithms.

An explanation of the various types of suspension systems was presented in Chapter 1. It was explained that actively controlled systems use an external energy source to directly add or extract energy from the system as a means to damp the vibrations. On the other hand, a semi-actively controlled system is one in which an inherent system parameter is automatically adjusted to allow the energy to dissipate. No additional external energy is used to directly apply an arbitrary damping force, for example. The only control energy used is that which controls the adjustment of the parameter. Another way to think about this is that an adjustment is being applied to the system in such a way that it makes it easier for the system to dissipate its own energy. It is important to understand this fundamental concept when thinking about the inherent limitations of semi-active system control, and also deciding on directions of future research activity, which will be explained later.

Research in both types of control, active and semi-active, is ongoing at present. Specifically, pertaining to semi-active suspensions, which is the focus of this thesis, a significant amount of the more recent research revolves around MR (Magneto-Rheological) dampers [7]-[13]. References to semi-active control of purely air suspension systems are scarce.

In [14] a concept for varying natural frequency and damping using an air spring-valve-accumulator type system was proposed. The variations in natural frequency and damping were achieved by adjusting the valve opening and the size of the accumulator. Experimental studies were conducted to determine the influence of valve opening and accumulator volume on the natural frequency and damping of the suspended mass system. The accumulator used

in the experiments did not have variable volume capability and hence the system frequency was not continuously adjustable in the experiment. The system frequency varied between two fixed values, one related to closed-valve condition and one related to open-valve condition. The work was primarily focused on modeling and validation of the model, and no control methodology was presented in that research.

A semi-active control methodology for varying the valve opening of an air spring-valve-accumulator system using a sliding mode controller with a reference "skyhook" model was demonstrated in [15]. The controller used feedback of the inertial coordinates to achieve the control objective. A mathematical model of the plant, similar to the one in [14], was used in this work as well.

In the remainder of this thesis, the development of a semi-active control methodology will be presented, along with simulation and test results. It will be demonstrated how the control valve size plays an important role in the performance of the controller. This highlights the importance of properly sizing the valve for these types of applications. For the cases when controller design requires the size of the valve to be greater than what is available in the market, simulation results will be used to demonstrate how a properly sized valve can achieve a desired performance and hence motivate the need for the new design of the valve.

3.1.1 Motivation for Research

As mentioned previously, much of the recent research in semi-active control methodology has focused on MR dampers. Typically, MR dampers, as well as other semi-active fluid dampers, act as a replacement for the damping element in a suspension system. The spring element is usually a separate member of the suspension.

As mentioned in the introduction to this thesis, pneumatic systems containing air springs are already in wide spread use. Depending on construction, these systems have the ability to handle large variation in loads. Adding the ability to automatically control an air spring system allows for greater flexibility in vibration control for these systems. In an air spring system, the same fluid (air) provides both the spring function and the damping function. Therefore, controlling this air flow provides the ability to change both the damping and the spring (natural frequency) characteristics in one system package. In addition, if an adjustable

accumulator were possible to construct, as suggested in [14], additional flexibility in automatic frequency adjustment is possible, providing an even wider range of control. Various configurations of this type system for improving performance can be easily conceptualized for future investigation.

3.1.2 Approach

One of the features of MR dampers, around which controllers are developed, is an approximately piecewise linear force versus relative velocity profile, depending on the electrical current setting, as shown in Figure 3.1. This profile can be used to establish a damping value proportional to the electrical current sent to the MR damper. Controllers adjust the current to obtain damping values that attempt to minimize, in some sense, the suspension vibration. The damping value provided by the MR damper is quickly realized as the commanded current changes. Since the damper is separate from the spring element, system natural frequencies remain unchanged. Due to the semi-active nature of MR damper control, a switching logic is employed to determine when the force can be applied.

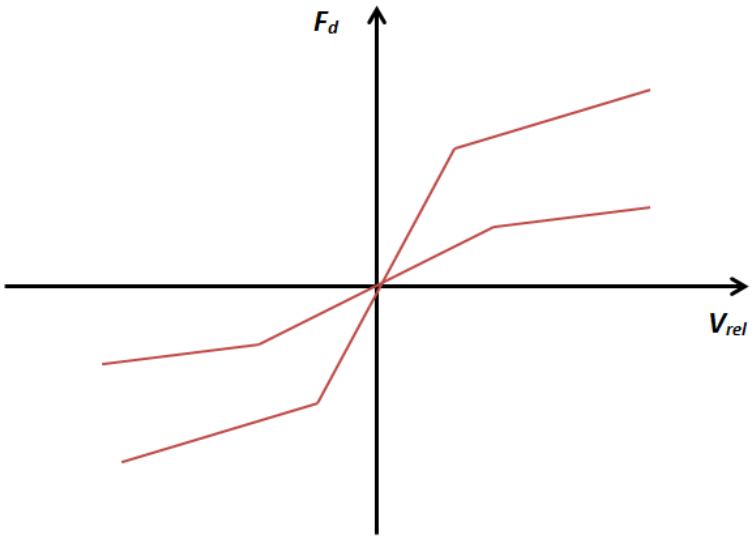

Figure 3.1 MR damper characteristic

In the pneumatic air spring-valve-accumulator system, the natural frequency and damping vary as a function of relative amplitude and valve opening. Damping force is not a piecewise linear function of relative velocity. Thus, the valve opening area, which is the

control mechanism, cannot be easily correlated to specific damping coefficients. Therefore, a different approach will be taken with this system.

The following sections detail the development of the pneumatic semi-active controller methodology for the air spring-valve-accumulator system. Three separate controllers will be developed and compared.

3.2 Review of Covariance Control Fundamentals

3.2.1 Introduction

This section will provide a brief review of the fundamentals of Covariance Control Theory. A subset of this theory will be used to develop the "active" part of the first semi-active controller. The resulting optimal solution will also be used to aid in setting the gains on the other two controllers, although those controllers do not directly implement the covariance control law.

The Covariance Control Theory does not seem to be widely used or researched at the present time. It is this author's opinion that there are some useful features of this theoretical framework that can be exploited in general for vehicular control related issues. Therefore, more information on this framework will be provided for the benefit of the reader than is required to implement the controllers in this thesis in order to suggest possible future research and development directions. The remaining sections will provide the details of the controller development, along with test and simulation results.

A review of the literature indicates research in the development of covariance control theory began in the early 1980s and extended through early 2000s. Much of this research seems to have been funded by NASA for purposes of developing control methods for flexible space structures. Selected references are provided in [16]-[33].

The first papers introducing the development of a general covariance control theory were published in 1987 for both continuous [16] and discrete systems [17], although the idea was first introduced in 1977 according to statements by Iwasaki [32]. The idea behind covariance control is to generate a linear feedback controller such that the closed-loop system achieves a specified state covariance. Thus, the system performance requirements are naturally specified in terms of variance and covariance, or RMS (root-mean-square) values. One of the

motivations given by the authors for developing a covariance control theory is that the requirements for many engineering systems are naturally stated in terms of variances on the state variables. An example given is the need to have a spacecraft antenna to not exceed a specified RMS deflection at 20 points over the surface of the parabolic dish, to remain pointed within a specified degrees RMS to an earth receiver station, and to not exceed a specified RMS value of strain at a critical point in the structure. The reader might note that these are multi-objective formulations, which are captured by covariance control theory.

Similar to the above example, it is not hard to conceive of casting requirements within industrial and vehicle control in terms of RMS values. For example, given a particular roadway disturbance input model, formulated in terms of RMS inputs to the wheels of a vehicle, it might be desired to achieve RMS bounds on displacements, velocities, and/or accelerations at various points on the vehicle, including keeping the RMS acceleration to the driver below specified levels. Some prior vehicular control research in active control has revolved around the use of state covariance matrices and optimization, including the modeling of road disturbances [34]-[38]. Most of this research could be recast into a Covariance Control theoretical framework.

Another motivation given by the authors is that a theory of covariance control may help unify the modeling and control problem, since various theories of system identification, estimation, and model reduction use covariance as a measure of performance.

An interesting feature of covariance control theory is that specifications can be formulated “deterministically” as well as “stochastically.” One of the authors of the 1987 papers mentioned above published a book in 1988 titled, *Dynamic Systems Control* [18], where the fundamentals of deterministic covariance control were provided. The author demonstrated that the deterministic formulation is mathematically equivalent to the covariance analysis of stochastic processes. The optimal control problem cast in this framework was termed Linear Quadratic Impulse (LQI) control, since the theory for deterministic covariance (or correlation) is based on impulses interjected one-at-a-time into the system.

Over the next decade after 1988, research continued in covariance control theory, and several algorithms were designed to solve the optimal control problems formulated in terms

of covariance assignment in one form or another. In addition, applications, primarily related to flexible space structures, demonstrated the practical use of covariance control [26];[27]. Another book was published in 1998, titled *A Unified Algebraic Approach to Linear Control Design* [33], which realized, to some extent, the second motivation of the authors mentioned above, which was to unify the modeling and control problem under one theory. In fact, a major contribution of this book was to demonstrate that some 18 control problems reduce to a single linear algebra problem. In addition, the book suggested the direction for future research in this area of control.

The earlier deterministic formulation of optimal covariance control, LQI, will be used in this paper. The following section provides some mathematical background fundamentals of LQI control. The complete theoretical development is found in [18].

3.2.2 Mathematical Preliminaries

The time correlation of two vector functions of time, $v_1(t+\tau)$ and $v_2^T(\tau)$, which forms the definition of "deterministic" covariance, where the superscript T indicates the transpose of the vector, is given by

$$C_{v_1 v_2}(t) = \int_0^\infty v_1(t+\tau)\, v_2^T(\tau)\, d\tau \tag{3.2}$$

Using this definition, time correlation matrices of the system *state* variables, system *inputs*, and system *outputs*, respectively, can be defined as

$$C_{xx}(t) = \int_0^\infty x(t+\tau)\, x^T(\tau)\, d\tau \tag{3.3}$$

$$C_{uu}(t) = \int_0^\infty u(t+\tau)\, u^T(\tau)\, d\tau \tag{3.4}$$

$$C_{yy}(t) = \int_0^\infty y(t+\tau)\, y^T(\tau)\, d\tau \tag{3.5}$$

Of particular interest in the development of covariance control theory are the following fundamental quantities, which are the result of impulsive inputs and initial conditions applied one at a time to the system represented by

$$\begin{aligned} \dot{x} &= Ax + Bu + Dw \\ y &= Cx \end{aligned} \tag{3.6}$$

where the vectors x, u, w, and y are the state, input, disturbance, and output vectors, respectively, and A, B, D, and C are the respective distribution matrices.

If impulsive inputs are applied one at a time into each input channel of u, while all other inputs are set to zero, and the results are summed, the *state covariance matrix* (deterministic sense) is defined by

$$X = \sum_{i=1}^{n_u} \int_0^\infty x^i(t) x^{i^T}(t)\, dt \tag{3.7}$$

where $x^i(t)$ is the state impulse response due to $u_i = \mu_i \delta(t)$, where μ_i is the magnitude of the impulse, and $\delta(t)$ is the Dirac delta function. The state covariance matrix satisfies the following linear matrix equation:

$$0 = XA^T + AX + BUB^T \tag{3.8}$$

where $U = \begin{bmatrix} \mu_1^2 & 0 & 0 \\ 0 & \ddots & 0 \\ 0 & 0 & \mu_{n_u}^2 \end{bmatrix}$ is the matrix of input impulse magnitudes (intensity) squared. Likewise, if impulses are applied one at a time in each of the disturbance channels, the state covariance matrix is the summed effects due to disturbance impulsive inputs ($w_i = \omega_i \delta(t)$), and is defined by

$$X_w = \sum_{i=1}^{n_w} \int_0^\infty x^i(t) x^{i^T}(t)\, dt \tag{3.9}$$

which satisfies

$$0 = X_w A^T + AX_w + DWD^T \tag{3.10}$$

where $W = \begin{bmatrix} \omega_1^2 & 0 & 0 \\ 0 & \ddots & 0 \\ 0 & 0 & \omega_{n_w}^2 \end{bmatrix}$ is the matrix of disturbance impulse magnitudes squared. If initial conditions are applied one at a time, then

$$X_x = \sum_{i=1}^{n_x} \int_0^\infty x^i(t) x^{i^T}(t)\, dt \tag{3.11}$$

which satisfies

$$0 = X_x A^T + A X_x + X_o \tag{3.12}$$

where $X_o = \begin{bmatrix} x_{o_1}^2 & 0 & 0 \\ 0 & \ddots & 0 \\ 0 & 0 & x_{o_{n_x}}^2 \end{bmatrix}$ is the matrix of initial condition magnitudes squared. Finally, the total summed effects of all excitations applied one at a time satisfies

$$0 = X_{uwx} A^T + A X_{uwx} + B U B^T + D W D^T + X_o \tag{3.13}$$

where $X_{uwx} = X + X_w + X_x$. In addition, the output covariance matrix is defined as

$$R_o = C X C^T \tag{3.14}$$

where X is the solution to (3.8).

The above fundamental definitions form the basis for the development of covariance control theory. The following sections will provide the modeling and control solutions for the LQI optimal solution. A subset of the following, namely state feedback, will be used in the present research; however, the expanded results are presented to highlight some possibilities for casting future research in vehicular control within the covariance control framework.

3.2.3 LQI Plant Model and Control Formulation

The plant to be controlled is in the form of

$$\begin{aligned} \dot{x} &= Ax + Bu + Dw, \qquad w_i(t) = \omega_i \delta(t) \\ y &= Cx \\ z &= Mx + v, \qquad v_i(t) = \upsilon_i \delta(t) \end{aligned} \tag{3.15}$$

with the dynamic controller

$$\begin{aligned} u &= G x_c \\ \dot{x}_c &= A_c x_c + F z \end{aligned} \tag{3.16}$$

where A, B, D, C, and M are the usual distribution matrices, z is the measurement vector, and $w_i(t)$ and $v_i(t)$ are the impulsive inputs with intensities ω_i and υ_i, respectively, as previously defined. The last equation in (3.16) is the dynamic state variable formulation for the controller, of which the solution is a special optimal form of a state estimator. The LQI

optimal solution to this problem produces G, F, and A_c. For purposes here, the state estimator will be assumed full order (same order as the plant). If full state feedback is used, then (3.16) is not needed.

3.2.4 Disturbance Modeling

Due to the unique formulations using disturbance impulsive inputs applied one at a time, it is possible to naturally include disturbance modeling within the deterministic (or stochastic) covariance control framework. As an example, in vehicular control, [36] presents a road profile disturbance model, which is modeled as a zero-mean, white noise process. In fact, the model can be cast within the deterministic formulation, since the mathematics are the same in each case [33]. The road profile input to one tire of a vehicle has been shown to be of the form

$$\dot{x}_w = A_w x_w + B_w \xi \tag{3.17}$$

where $E[\xi(t)\xi(t-\tau)] = \kappa\delta(t)$, where E is the expectation operator, and κ is the intensity of the impulse. The parameters here are unimportant for present purposes, but have been defined in the reference. Appending (3.17) to (3.15) leads to

$$\begin{aligned} &\begin{bmatrix} \dot{x} \\ \dot{x}_w \end{bmatrix} = \begin{bmatrix} A & 0 \\ 0 & A_w \end{bmatrix} \begin{bmatrix} x \\ x_w \end{bmatrix} + \begin{bmatrix} B \\ 0 \end{bmatrix} u + \begin{bmatrix} 0 \\ B_w \end{bmatrix} w, \qquad w(t) = \kappa\delta(t) \\ &y = [C \quad 0] \begin{bmatrix} x \\ x_w \end{bmatrix} \\ &z = [M \quad 0] \begin{bmatrix} x \\ x_w \end{bmatrix} + v, \qquad v_i(t) = v_i\delta(t) \end{aligned} \tag{3.18}$$

This formulation would be for one tire/road input, but (3.17) would be expanded in size to include additional tires. The LQI optimal control solution would then contain an optimal state estimator that included an estimate of the disturbance states, as a natural part of the solution. The optimal controller would then operate on both estimates of the plant states and estimates of the disturbance states. This opens the possibility of disturbance accommodation (utilization, cancellation, etc.) as part of the control law.

A separate line of research, known as DAC (Disturbance Accommodating Control) Theory [39];[40] has developed over the years, beginning before the development of Covariance Control Theory. One of the key ingredients of DAC is using a state observer to

estimate the state of the disturbances in a deterministic sense. The usual method advocated for constructing an observer of the disturbance states, separate from the control law, is an ad hoc procedure whereby eigenvalues are place in the far left-half plane to ensure fast convergence to the states. The Covariance Control Theory seems to form a natural framework within which to merge DAC. A side benefit of this is that the state estimator is automatically generated in the solution of the optimal controller, and the gain F on the estimator, which affects the speed of convergence, is strictly determined by the plant and measurement disturbance, $w(t)$ and $v_i(t)$. Future research would need to verify this claim for merging the two lines of research.

As a side note, if A_w for a disturbance model includes any zeros on the diagonal (this particular one does not), then a technique outlined in [18] needs to be employed, whereby any "offending" zeros are replaced by small numbers to render the matrix stabilizable.

3.2.5 Optimal Solution

Various algorithms to solve the LQI problem have been proposed in the literature, given various objectives and ways of specifying the controller and system requirements. In a typical control optimization problem, a performance index to minimize is selected based on chosen values for a pair of matrices (or weights), for example, *R* and *Q*, which apply to the control inputs and the states (or outputs), respectively. The algorithm then calculates the controller gain *G* that minimizes this performance index, and thus attempts to minimize a combination of control energy and some weighted combination of the states. In the LQI control problem, the algorithms actually iterate on *R* or *Q* to calculate a gain *G* to achieve the performance objectives in terms of the designer specified RMS values of the outputs (or states). If a state estimator (dynamic controller) is part of the formulation, then the solution also includes the optimal estimator gain *F* and the associated optimal estimator state matrix A_c.

LQI Optimal (Estimated States)

Given the system defined by (3.15) and (3.16), where it is assumed all impulsive disturbances, $w_i = \omega_i \delta(t)$ and $v_i = v_i \delta(t)$, are applied one at a time as previously stated,

and given the scalar objective function with specified weights, R and Q, on the inputs and outputs defined by

$$\gamma = \sum_{i=1}^{n_x+n_z} \int_0^\infty [u^T(i,t)Ru(i,t) + y^T(i,t)Qy(i,t)]dt, \qquad R > 0, Q > 0 \tag{3.19}$$

it can be shown that γ is minimized by the choice of parameters G, A_c, and F which satisfy the following matrix algebraic equations:

$$A_c = A + BG - FM \tag{3.20}$$

$$G = -R^{-1}B^T X_2 \tag{3.21}$$

$$0 = X_2 A + A^T X_2 - X_2 B R^{-1} B^T X_2 + C^T Q C \tag{3.22}$$

$$F = X_1 M^T V^{-1} \tag{3.23}$$

$$0 = X_1 A^T + A X_1 - X_1 M V^{-1} M X_1 + D W D^T \tag{3.24}$$

where $V = \begin{bmatrix} v_1^2 & 0 & 0 \\ 0 & \ddots & 0 \\ 0 & 0 & v_{n_z}^2 \end{bmatrix}$, and all other quantities have been previously defined. Note that (3.22) and (3.24) are Riccati type equations, which are solved with standard software algorithms, such as are found in Matlab software. The minimum value of the cost (objective) function is

$$\gamma = tr(X_1 + X_3)C^T Q C + tr(X_3)G^T R G \tag{3.25}$$

where *tr* indicates the trace of the matrix, X_1 solves (3.24), and X_3 is the solution to the following Lyapunov equation:

$$0 = X_3(A + BG)^T + (A + BG)X_3 + F V F^T \tag{3.26}$$

This formulation is a somewhat standard optimization problem cast into the covariance control framework. However, it is desired to recast this problem such that requirements can be specified in terms of upper bounds on the RMS values of the outputs. Therefore, the problem can be recast as follows. Given the objective function with weighting R on the control inputs defined by

$$\gamma = \sum_{i=1}^{n_x+n_z} \int_0^\infty [u^T(i,t)Ru(i,t)]dt, \qquad R > 0 \tag{3.27}$$

and upper bounds on the RMS values of the outputs defined by

$$y_{\alpha,rms} = \left[\sum_{i=1}^{n_x+n_z} \int_0^\infty y_\alpha^2(i,t)\, dt \right]^{1/2} \leq \sigma_\alpha \,, \alpha = 1,2,\ldots,n_y \tag{3.28}$$

find G, A_c, and F that minimize (3.27) and achieve (3.28). An algorithm was proposed in [18] that automatically iterates on the Q matrix in (3.22) to achieve these objectives. This algorithm was called *Weight Selection for Dynamic Output Constrained Controller (DOC)* algorithm in [18], and the problem was later referred to as the *Output L_2 Constraint (OL_2)* problem in [29]. This algorithm will not be repeated here, but a similar algorithm will be provided below for the state feedback solution, which will be used in this thesis. A schematic of the optimal LQI measurement feedback controller [18] is shown in Figure 3.2.

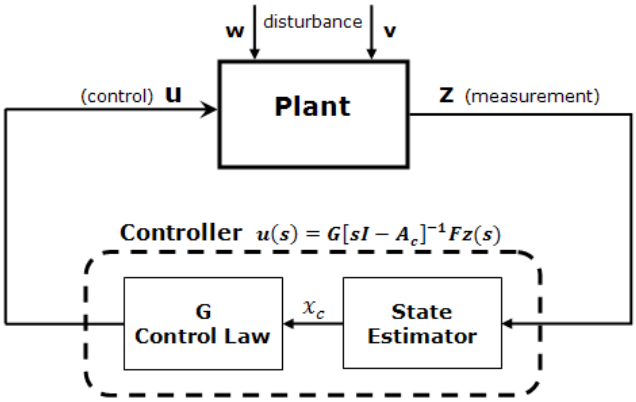

Figure 3.2 LQI optimal measurement feedback controller

Before moving on to the state feedback case and the semi-active controller development, it is instructive to review a few interesting observations in the literature pertaining to the optimal LQI measurement feedback controller and the resulting state estimator. First, note that the optimal controller and the estimator were simultaneously calculated as part of the minimization process. The author in [18] states that the appearance of a state estimator in the LQI controller remains a surprise. Second, the G obtained using measurement feedback is the same G that would be obtained assuming state feedback. It has been proven that the control and the state estimation are separable. Third, the LQI controller consists of two parts: the

control law, u = Gx, and the *state estimator*, $\dot{x}_c = Ax_c + Bu + F(z - Mx_c)$, which has states $x_c(t)$ that converge to the states $x(t)$. The rate (speed) of convergence of $x_c(t) \rightarrow x(t)$ is governed by F, and F is completely determined by the intensities, ω_i and ν_i, of the plant and measurement impulse disturbances. Therefore, F is independent of G or the Q and R parameters that dictate G. Thus, G is optimal no matter what the time constants of convergence are for the estimator. The author points out that this fact contradicts an argument that has been put forth in some literature that rationalizes a relatively fast state estimator (observer) in ad hoc juxtaposition of a state estimator and an optimal control law. For the LQI optimal control, this is not a valid argument.

LQ Optimal (State Feedback)

When state feedback is used (i.e., all states available for feedback), and it is assumed that the impulsive disturbances $w_i = \omega_i \delta(t)$ are applied one at a time, and/or initial conditions $x_i(0)$ are either applied one at a time *or* simultaneously, the solution to the optimal control problem represented by

$$\begin{aligned} &\dot{x} = Ax + Bu + Dw, \qquad w_i(t) = \omega_i \delta(t), x_i(0) = x_{i0} \\ &y = Cx \end{aligned} \tag{3.29}$$

is given in [18] by

$$u = Gx \tag{3.30}$$

$$G = -R^{-1}B^T K \tag{3.31}$$

where K solves the algebraic Riccati equation

$$0 = KA + A^T K - KBR^{-1}B^T K + C^T QC \tag{3.32}$$

and the minimum value of the cost function is

$$\begin{aligned} \gamma &= trK(DWD^T + X_o) \\ &= trX(C^T QC + G^T RG) \end{aligned} \tag{3.33}$$

where X solves

$$0 = X(A + BG)^T + (A + BG)X + DWD^T + X_o \tag{3.34}$$

If only disturbances $w_i = \omega_i \delta(t)$ are applied or initial conditions are zero, then X_o = 0. If initial conditions $x(0)$ are applied *simultaneously*, then $X_o = x(0)x^T(0)$. If initial conditions are applied one at a time, then X_o is as defined for (3.12).

The state feedback case presented here is called LQ (Linear Quadratic) instead of LQI because the solution has meaning whether the excitation comes from an initial state applied simultaneously, or from impulsive disturbances.

Output L_2 Constraint Algorithm

It is desired to solve the state feedback case using the formulation represented by (3.27) and (3.28), whereby the designer specifies *R* and the RMS upper bound on each individual output signal. As previously stated, this formulation is "multi-objective" and provides a more natural way to specify the requirements for many engineering systems. Historically, in most controls optimization problems of this type, the procedure has been to specify, for example, the weighting matrices *R* and *Q*. This leads to a solution that achieves a performance that is optimal in some sense over the total output or state vector, but does not guarantee that all *individual* outputs of interest behave in an acceptable way. The covariance control formulation allows for the specification of individual objectives.

The Output L_2 Constraint algorithm iterates on the diagonal of Q to achieve the objectives specified by (3.27) and (3.28). The algorithm from [24] is as follows, but has been expanded to provide some additional explanation:

1) Given the specified RMS upper output bounds, $\sigma_i,\ i = 1, 2, \ldots, n_y$, and a diagonal weight matrix $R > 0$, construct the initial $Q_o > 0$ matrix diagonal with the inverse square of the RMS values (variance), and the off-diagonal terms may be set to zero if unknown:

$$Q_o = \begin{bmatrix} 1/\sigma_1^2 & 0 & 0 \\ 0 & \ddots & 0 \\ 0 & 0 & 1/\sigma_{n_y}^2 \end{bmatrix} \tag{3.35}$$

   If R is unknown, a recommended starting point is to set R = identity matrix.

2) Solve Ricatti equation (3.32) for *K*.
3) Solve for controller gain *G* in (3.31).
4) Solve Lyapunov equation (3.34) for covariance matrix X_k.

5) Form the following factor matrix:

$$Y_k = CX_kC^T \tag{3.36}$$

6) Check for convergence of the diagonal elements:

$$\text{if } |[Y_k - Y_{k-1}]_{ii}| < \varepsilon \text{ for all i, stop.} \tag{3.37}$$

7) Extract the diagonal elements $\left(Y_{jj}\right)_k,\ j = 1,2,\dots,n_y$.

8) Form a scalar factor by dividing each variance into the respective Y_{jj}:

$$Z_{jj} = Y_{jj}/\sigma_j^2 \tag{3.38}$$

9) Form the updated Q matrix by multiplying each diagonal element:

$$\left(Q_{jj}\right)_{k+1} = Z_{jj}\left(Q_{jj}\right)_k \tag{3.39}$$

10) Go to step 2 and repeat.

In [21], there is also a "convergence" exponent applied to (3.38) to assist speed of convergence. However, for the present case, this exponent was set to 1.0 with good convergence speed. As a matter of fact, the original formulation in [18] did not contain this exponent.

3.3 Semi-Active Controller Development

3.3.1 Introduction

Generally, the following steps are proposed to achieve semi-active control of this system. As with most semi-active controllers, a switching logic will be applied to this system to ensure the control force is applied in the appropriate direction. Controller gains will be determined such that an optimal ideal or desired force can be tracked. The actual force in the system will be measured directly through pressure measurements, which is a key feature to how all these controllers work. When the switching logic indicates the force can be generated in the right direction, the control algorithm will then adjust the valve opening area by applying a commanded voltage to the valve solenoid, and drive the actual force toward the ideal force in a defined manner. If the switching logic indicates the force cannot be generated in the proper direction, the controller will open the valve to minimize force generation.

Three controllers will be developed and compared. The first controller, referred to as the *LQI with Semi-Active Tracking Controller*, works with inertial measurements of the states, which are displacement and velocity, leading to full state feedback, and a pressure measurement. The second controller, referred to as the *Modified Skyhook with Semi-Active Tracking Controller*, works with measurements of inertial velocity, relative velocity, and pressure. The third controller, referred to as the *Relative Position with Semi-Active Tracking Controller*, works with measurements of relative displacement and pressure.

Both experimental and simulation results will be presented. The simulations are with an experimentally tuned model of the system.

3.3.2 Switching Logic

For semi-active dampers, it is well known that the constitutive law for the mechanical power dissipated is [41]

$$P_d = F_d V_{rel} \geq 0 \tag{3.40}$$

where F_d is the damping force, and $V_{rel} = V_2 - V_1$ is the relative velocity between the two attachment points of the damping element. When F_d is plotted relative to V_{rel}, it is obvious that (3.40) is only satisfied in the first and third quadrants, as shown in Figure 3.3. Therefore, if a control strategy calls for a desired F_d, the semi-active damping force can only dissipate power if the sign of F_d and V_{rel} are the same.

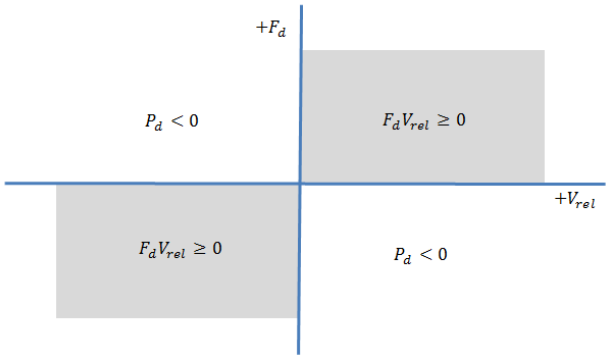

Figure 3.3. Damper force – relative velocity plane

3.3.3 LQI with Semi-Active Tracking Controller

Figure 3.4 provides a free body diagram of the suspended mass. F_b is a bag damping force, which is assumed to be a linear function of relative velocity, and represents any material damping in addition to any other unaccounted-for damping introduced by the test rig or suspension components. P_w is the component of air spring pressure that creates force on the mass. This is the quantity that will be controlled by adjusting the valve opening that controls air flow between the air spring and the accumulator. The diagram is drawn assuming that displacements start from an equilibrium position. Therefore, the mass weight is not included, and P_w represents the change in pressure from an equilibrium condition. Given the assumed configuration, the equation of motion for the suspended mass can be written as

$$M\ddot{x}_m = P_w A_s - c_b(\dot{x}_m - \dot{q}_b) \tag{3.41}$$

where c_b is the bag damping coefficient. This equation will be expanded below for control purposes. Note that, as defined here, P_w is taken relative to an equilibrium value. P_w is positive when the air spring is in compression (V_{rel} negative) and negative when the air spring is in tension (V_{rel} positive). From a simulation perspective, it makes no difference what sign convention is used provided it is consistent and the proper interpretation is assigned.

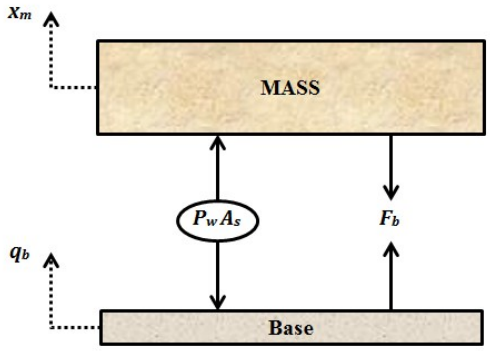

Figure 3.4 Free body diagram of suspended mass

In many semi-active controller applications, such as the MR damper, some form of the *skyhook* control strategy is implemented [6]-[13]. In its simplest form, the switching logic, which satisfies (3.40), can be expressed as

$$\begin{cases} \dot{x}_m \dot{x}_{rel} > 0 & F_d = G_s \dot{x} \\ \dot{x}_m \dot{x}_{rel} < 0 & F_d = 0 \end{cases} \tag{3.42}$$

where G_s is a gain (damping constant) that is chosen such that the damping force F_d approximates a "passive" desired damping force achieved by a fictitious damper attached from the suspended mass to the "sky," which serves as an inertial reference. The term "sky" distinguishes the inertial attachment point of the fictitious damper from a "ground" inertial attachment, which is used in "ground-hook" control where the fictitious damper is instead attached between the tires mass and ground in a two degree of freedom suspension system. The damping constant G_s is chosen based on the characteristics of the MR damper. These characteristics are determined by the force-velocity curves as illustrated in Figure 3.3. As indicated in (3.42), to control an MR damper based system, it is typically required to measure or estimate both the absolute velocity and the relative velocity.

As previously stated, the air spring-valve-accumulator system does not have well defined damper characteristic curves; thus, setting specific damping values as a control strategy is not the best way to approach the control of this system. In addition, both the natural frequency and damping vary as a function of both amplitude of vibration and the air restriction through the valve. This was illustrated Chapter 2. With these considerations in mind, the first controller will be based on measurement of pressure along with feedback of inertial coordinates that can be measured on the test rig. The logical sequence of steps is as follows:

1) Directly measure the force acting on the mass. This can be achieved in a cost effective way by installing a pressure gauge to directly measure the air spring pressure P_{sp}, which can then be transformed to P_w by the relationship shown in Figure 2.28. The force acting on the mass is then obtained by multiplying this value by the air spring support area A_s.
2) Calculate the *ideal* optimal damping control force using an "active" linear control law to minimize vibration. This would be the control force that could be achieved if energy could be added to the system.
3) Use the switching logic (3.40) to determine when the system is able to generate a force in the direction determined by the ideal damping control force.

4) When the switching logic determines that the system is able to generate a proper directionally oriented force, adjust the valve opening area by controlling the solenoid voltage to drive the measured force toward the ideal force determined by the online controller as quickly as possible, and then track the ideal force.
5) If the switching logic in determines that the system cannot generate a proper directionally oriented force, set the valve to 100% open to minimize additional force generation.

To calculate the ideal control force, (3.41) needs to be expressed in terms of state variables. To achieve this, first note that this system cannot immediately generate the ideal force. The system can only move the actual force toward the ideal force as the air spring compresses or expands over a finite period of time. Therefore, during the time interval of control ($F_d V_{rel} \geq 0$), the valve is going to be initially commanded closed in order to drive the actual force toward the ideal force as quickly as possible. Second, note that for small valve openings approaching a closed valve and/or for large amplitudes of vibration, the system stiffness and natural frequency are defined in (2.39) and (2.57), respectively. Therefore, during the time interval of control, the system can be approximated by a 2nd order linear differential equation. *It should be noted that this particular feature of this system, which is not intuitively obvious, is the primary reason that a linear controller can be utilized as part of the control methodology*. During the time interval of no control effort ($F_d V_{rel} < 0$), the valve will be set to constant 100% open, so it does not matter what the describing equations are during this interval. Given this understanding, (3.41) can be replaced by the linear differential equation

$$M\ddot{x} = -k_{sp}(x - q) - c_b(\dot{x} - \dot{q}) - F_d \tag{3.43}$$

where F_d is the commanded damping control force that will be determined by the active controller, k_{sp} is calculated from (2.39), and c_b is the external bag damping coefficient determined through testing for the particular system. Equation (3.43) can be expressed in the form of (3.29) as

$$\dot{x} = \begin{bmatrix} 0 & 1 \\ -k_{sp}/M & -c_b/M \end{bmatrix} x + \begin{bmatrix} 0 \\ -1/M \end{bmatrix} F_d + \begin{bmatrix} 0 & 0 \\ k_{sp}/M & c_b/M \end{bmatrix} q$$
$$y = \begin{bmatrix} 1 & 0 \\ 0 & 1 \end{bmatrix} x \tag{3.44}$$

where $x = [x_m \; \dot{x}_m]^T$, $q = [q_b \; \dot{q}_b]^T$, and $F_d = Gx$ is the damping control force. The LQ optimal algorithm will be used to solve for the control gain matrix *G*.

One of the benefits of covariance control is the ability to specify requirements in terms of output RMS values on each individual output of interest. In the present case, there are no a priori specifications established, since the project is still in the research phase. Therefore, the attitude that will be taken is to find the smallest RMS values possible. To do this the output RMS values of the open loop plant can be established as a starting point. Then the controller will be designed to decrease these values as small as possible, with the objective of minimizing the corresponding acceleration. This will necessarily require some iteration between controller design and simulation (and/or test) to determine what is possible for the system under study. The LQ optimal algorithm assumes active control; however, a semi-active system typically cannot achieve the performance of an active system, since controlled energy cannot be supplied to the system.

Observation of (3.34) for the closed loop system will indicate that the RMS values (or variances) are a function of the disturbances *W* and/or the initial conditions X_o. Therefore, from an absolute system RMS *specification* viewpoint, some knowledge of the disturbance environment (magnitudes) is desired. However, this is not strictly necessary to obtain a good controller design for the system, due to the assumption of linearity. In other words, iterating between controller design and simulation is going to establish a possible *G*, no matter what the exact assumption is on the magnitudes of the disturbances, provided these are held constant during the design process.

Solving the Lyapunov equation (3.34) with $G = 0$ will supply the open loop output RMS values, which are defined as

$$(y_{rms})_{ii} = \sqrt{(CXC^T)_{ii}} \tag{3.45}$$

where the subscript *ii* indicates the diagonal elements of the matrix. For the present case, the open loop RMS values written as a row vector are

$$(y_{rms})_{OL} = [0.01963 \quad 0.23998] \tag{3.46}$$

To establish the desired (or target) output RMS values (closed loop), one way to approach the design process, without any a priori information, is to simply scale this vector by a number less than one. Alternatively, the individual elements of the vector could be scaled separately. However, for this problem, the elements are correlated, since they represent displacement and the associated velocity, respectively. So, scaling one element will also affect the other. Continue to decrease this number to find out how small the values can be made, and still obtain an acceptable controller gain *G*. If the desired RMS values become too small, the LQ optimal algorithm will not converge to a solution. However, before this happens, in the case of an active controller, there will be a bound on the physical control energy available from the actuator element that will limit what can physically be achieved. For a semi-active system, there will also be a bound on what the system can physically achieve. In the present case, this bound will become evident through simulation or test. Therefore, the desired closed loop RMS values can be represented by

$$(y_{rms})_{desired} = (y_{rms})_{OL} k_f, \;\; 0 < k_f < 1 \tag{3.47}$$

Before designing the controller, which will provide a desired optimal damping force, the methodology for driving the measured instantaneous force toward the desired force, and then tracking the force, needs to be specified. The proposed methodology is to initially close the valve in order to drive the measured force F_p quickly toward the desired force F_d. When F_p is within a pre-specified distance from F_d, a Proportional plus Integral (PI) control law will be implemented to track F_d. Therefore, this part of the total controller can be referred to a *Set-Point + PI Tracking Controller*. The PI control law can be expressed in the continuous time domain as

$$or\ \% = K_p * \left(F_d - F_p\right) + K_i * \int_{t_1}^{t_2} \left(F_d - F_p\right) dt \tag{3.48}$$

where or % is the orifice opening percent, and K_p and K_i are the proportional and integral control gains. A digital version of (3.48) is implemented in the controller. In addition, or % is scaled between 0 and 100. Proportional and Integral gains are set through simulation and/or testing.

Based on the open loop RMS values, $k_f = 0.52$ in (3.47) was tuned by simulation to produce the desired RMS values

$$(y_{rms})_{desired} = [0.010208 \quad 0.12479] \tag{3.49}$$

This produced the closed loop RMS values

$$(y_{rms})_{CL} = [0.010208 \quad 0.12293] \tag{3.50}$$

Note that the algorithm placed the closed loop values very close to the desired values. The tuning was accomplished at 7.62 mm (0.3 inch) base input amplitude at 1.0 Hz base input frequency, with the objective of minimizing the maximum peak magnitude acceleration. The closed loop values only apply to the system with active control, and represent what can ideally be achieved with the corresponding active control gain. The semi-active system cannot produce these values. However, this provides a targeted performance to drive the system toward. The corresponding control gain is

$$G = [1052.1542 \quad 505.05261] \tag{3.51}$$

The performance of the system at 1.0 Hz base input is shown in Figure 3.5, where the desired damping force is

$$F_d = Gx \tag{3.52}$$

and the measured force is

$$F_p = -P_w A_s \tag{3.53}$$

The negative sign is due to the assumed sign convention. The first chart in the figure shows F_p (dashed red line) being driven towards F_d (solid blue line). The second chart in Figure 3.5 shows the commanded orifice percentage (blue line) and the switching signal (black line). Switching signal high indicates the switching condition in (3.40) is activated. The controller immediately commands the valve to close (0 %) until the measured force gets close to the desired force, at which time the controller regulates according to the PI control law to track the desired force. When the switching signal goes lower, the controller opens the valve

(100%) until the next switching instant. The corresponding magnitude of acceleration is shown in the third chart of Figure 3.5.

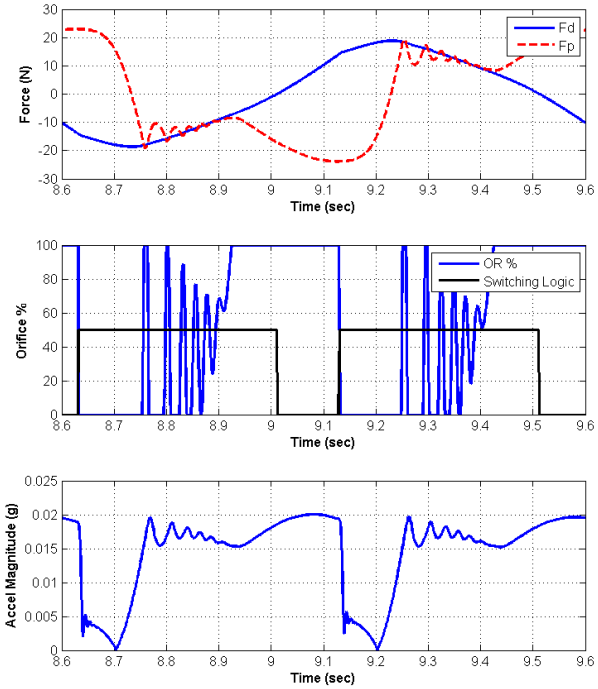

Figure 3.5 LQI semi-active tracking performance controller (a: ideal force vs. measured force; b: orifice area and switching event signal; c: acceleration)

Figure 3.6 expands the left hand portion of the first chart in Figure 3.5. The bottom chart shows the commanded orifice opening and the switching signal along with an overlay of the pressure drop across the valve. F_d is negative, and there is a positive switching event, which indicates $\dot{x}_r$ is negative. Thus, the air spring is compressing. Note that the orifice command migrates to 100% before the switching event ends as F_p migrates away from F_d. At this point, note that the pressure drop *dP* is fast approaching zero. This indicates that the system cannot supply the commanded damping force, which is generated by air flow through the valve. The pressures in the air spring and the accumulator have reached a temporary equilibrium, and no more air flow can be generated. This occurs at a point where the relative velocity in compression is nearing zero at the bottom of a compressive stroke. Therefore, no more energy can be extracted from the system during this switching event.

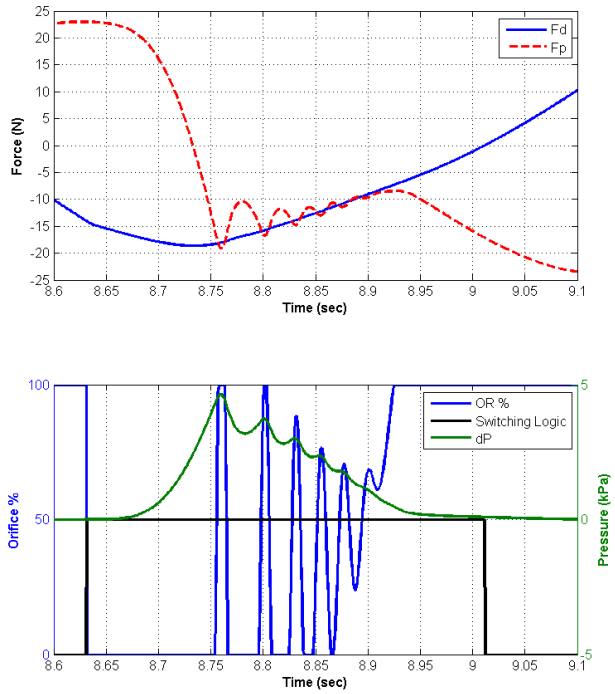

Figure 3.6 LQI semi-active tracking performance controller (a: ideal force and measured force; b: orifice %, switching event signal, and pressure drop)

3.3.4 Modified Skyhook with Semi-Active Tracking Controller

A well-known control strategy for semi-active suspension systems, especially for MR damper systems, as previously mentioned, is the skyhook controller. Equation (3.42) provides one form of the control law for the skyhook damper. The control gain G_s is usually chosen as a damping constant based on the characteristics for the MR damper. The idea is to approximate the damping that could be achieved if a "fictitious" damper were attached from the suspended mass to the "sky" or ground. To implement the skyhook control law, both the relative velocity $\dot{x}_r$ and the inertial velocity $\dot{x}$ need to be measured. The relative velocity can usually be determined by differentiating the signal from a string potentiometer attached between the suspended mass and the base. The absolute velocity is usually estimated based on filtering and integrating an accelerometer signal for vehicular applications. The signal processing and proper selection of a cost effective accelerometer required to obtain good results has its own set of challenges. For stationary applications, the velocity is more easily determined by differentiating the signal of a string potentiometer attached between the

suspended mass and ground. In the present research, to implement a modified form of the skyhook control law, the velocity will be determined by differentiating string potentiometers attached between the suspended mass and ground and the shaker base and ground, since the test rig can function as a stationary application. As previously stated, the air spring-valve-accumulator system has varying damping as a function of amplitude and valve opening area. Therefore, obtaining linear force-velocity characteristics leading to specific damping constants for this system is not possible. To implement the skyhook control law for application to the air spring-valve-accumulator system, the following modifications will be made:

1) The force will be directly measured based on air spring pressure using a pressure transducer,
2) The gain G_s will be determined based on matching the vibration response to the response obtained from the semi-active implementation of the LQI optimal controller as described in the prior section,
3) Switching logic, as previously described, will be employed to determine when the control force can be applied, and
4) Set-Point + PI Tracking control based on (3.48) will be used to cause the measured force to track the desired force defined in (3.42) as

$$F_d = G_s \dot{x} \tag{3.54}$$

where $\dot{x}$ is the absolute (inertial) velocity.

The performance for the modified skyhook is shown in Figure 3.7. Note that the performance is very close to the performance achieved by the state feedback controller. In addition, F_d is very close to the optimally calculated ideal force, as will be shown below.

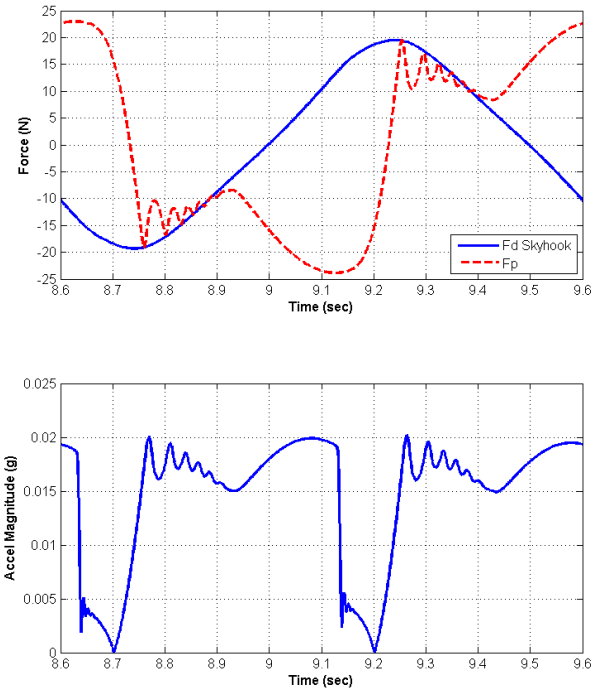

Figure 3.7 Modified skyhook semi-active tracking performance controller (a: ideal force and measured force; b: acceleration)

3.3.5 Relative Position with Semi-Active Tracking Controller

The semi-active controllers developed above were based on tracking a measured force, where at least one of the measurements required an inertial coordinate (displacement and/or velocity). In addition, a control law generated by state feedback in this fashion is usually thought to be the "best" that can be generated, based on an active controller. As previously mentioned, this methodology would not be very costly to implement in a stationary situation. However, the measurement of inertial coordinates for vehicular applications can be relatively expensive and/or require significant attention to the filtering of accelerometer signals to obtain good measurements of the required quantities.

It will be demonstrated for this particular system that a controller, based only on relative displacement and pressure measurements, may perform acceptably well. The following development will assume that only relative displacement between the suspended mass and the base is measured, and relative velocity is determined by differentiating the relative displacement signal.

The general procedure for designing this controller is as follows:

1) The force will be directly measured based on air spring pressure using a pressure transducer,
2) The gain G_x will be determined based on matching the vibration response to the response obtained from the semi-active implementation of the LQI optimal controller as described in the prior section,
3) Switching logic, as previously described, will be employed to determine when the control force can be applied, and
4) Set-Point + PI tracking control based on (3.48) will be used to cause the measured force to track the desired force defined as

$$F_d = G_x x_r \tag{3.55}$$

where x_r is the relative displacement between the suspended mass and base.

The performance for this controller implementation is shown in Figure 3.8. For short hand convenience, the controller will also be referred to as the F_x controller.

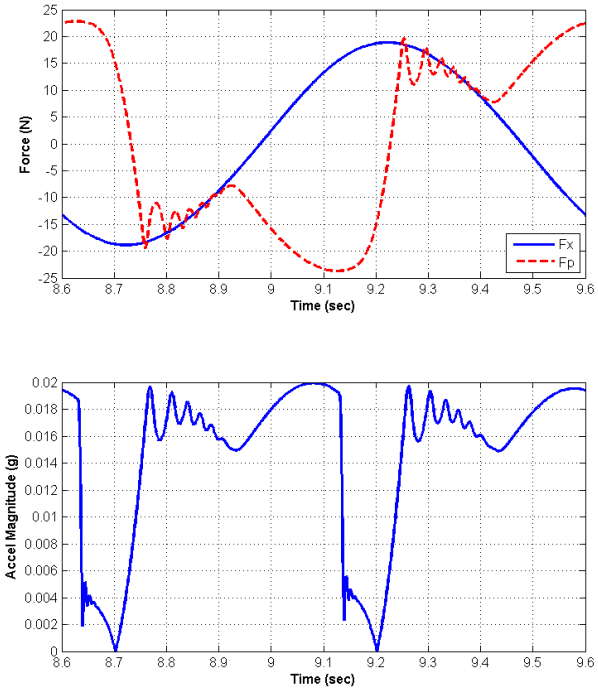

Figure 3.8 Relative position semi-active tracking performance controller (a: ideal force and measured force; b: acceleration)

3.3.6 Semi-active Controller Comparisons

Figure 3.9 provides a comparison of all three controllers, with inclusion of the acceleration due to an open valve (no control) in the second chart, and mass displacement in the third chart. Note that the calculated ideal (desired) forces lie very close to each other for each controller. The open valve configuration is the best performance possible for the passive system. There is an optimal valve setting that will lower the peak amplitude at the expense of raising the amplitude response at higher frequencies, as previously mentioned. However, the frequency response with the controllers is better in the range shown for any combination of valve openings in the passive system. The displacement of all three controllers is also closely matched.

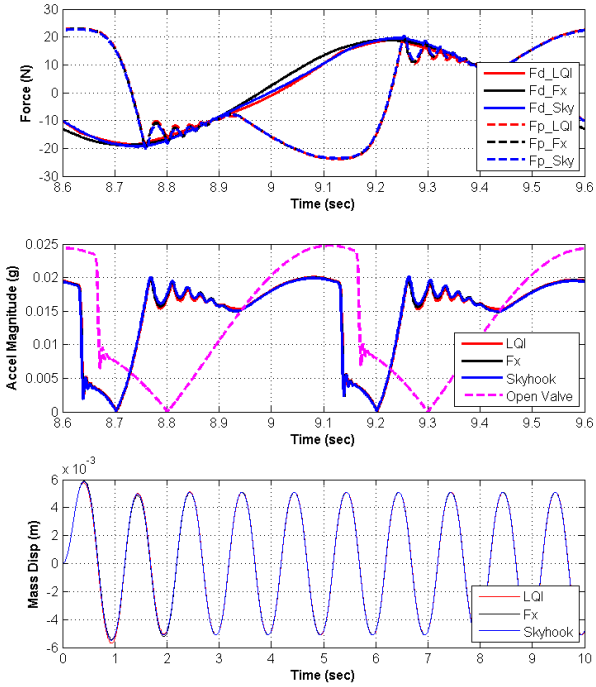

Figure 3.9 All controllers semi-active tracking performance (a: ideal force and measured force; b: acceleration; c: displacement)

Figure 3.10 provides a chart of the nonlinear frequency response. Note that all controllers perform well up to about 1.2 Hz. At higher frequencies, there is little difference between the open valve (no control) and the controllers, although the open valve response is slightly better. This demonstrates that the controllers are only effective in the low frequency region. At higher frequencies, the controllers behave essentially as an open valve by remaining open

most of the time during the switching instant. Therefore, there is nothing to be gained by trying to control in the high frequency region, since an open valve can achieve the same result.

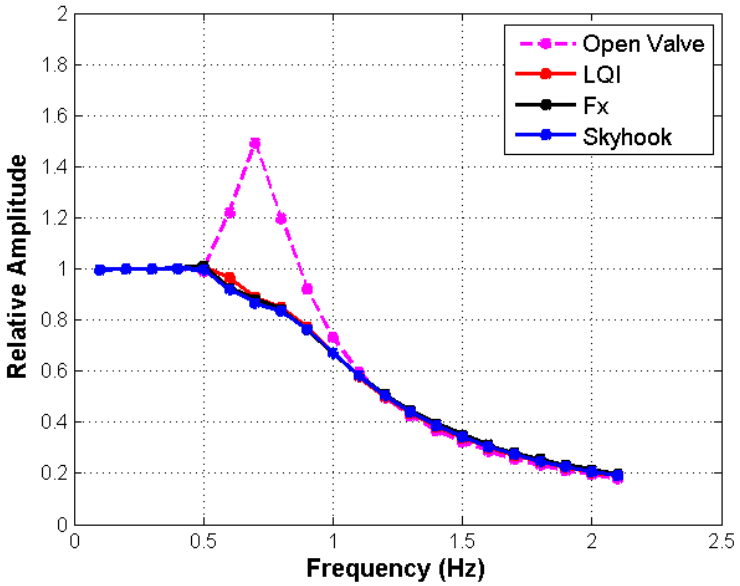

Figure 3.10 Closed loop system frequency response

Figure 3.11 provides a chart of the acceleration magnitudes and mass displacements for mixed frequency and amplitude inputs. This demonstrates the performance for a simulated road input. As expected, all three controllers performed better than the open valve response. Table 3.1 provides the overall RMS values for each controller and the open valve, and Table 3.2 provides the same information expressed as a percent reduction from the open valve response. The *LQI* and *Modified Skyhook* controllers performed roughly equivalent to each other, but better than the F_x controller on acceleration, and the Modified Skyhook performed best on overall RMS displacement, followed by the *LQI* and *Fx* controller, respectively.

All three controllers used the same tracking gains for the PI tracking control and the target value of F_p to determine when to start the PI tracking. These gains were initially tuned specifically to the LQI controller. In practice, these gains would be tuned to the specific controller used. Therefore, a better response could possibly be obtained by the Fx controller with a more judicious choice of tracking gains.

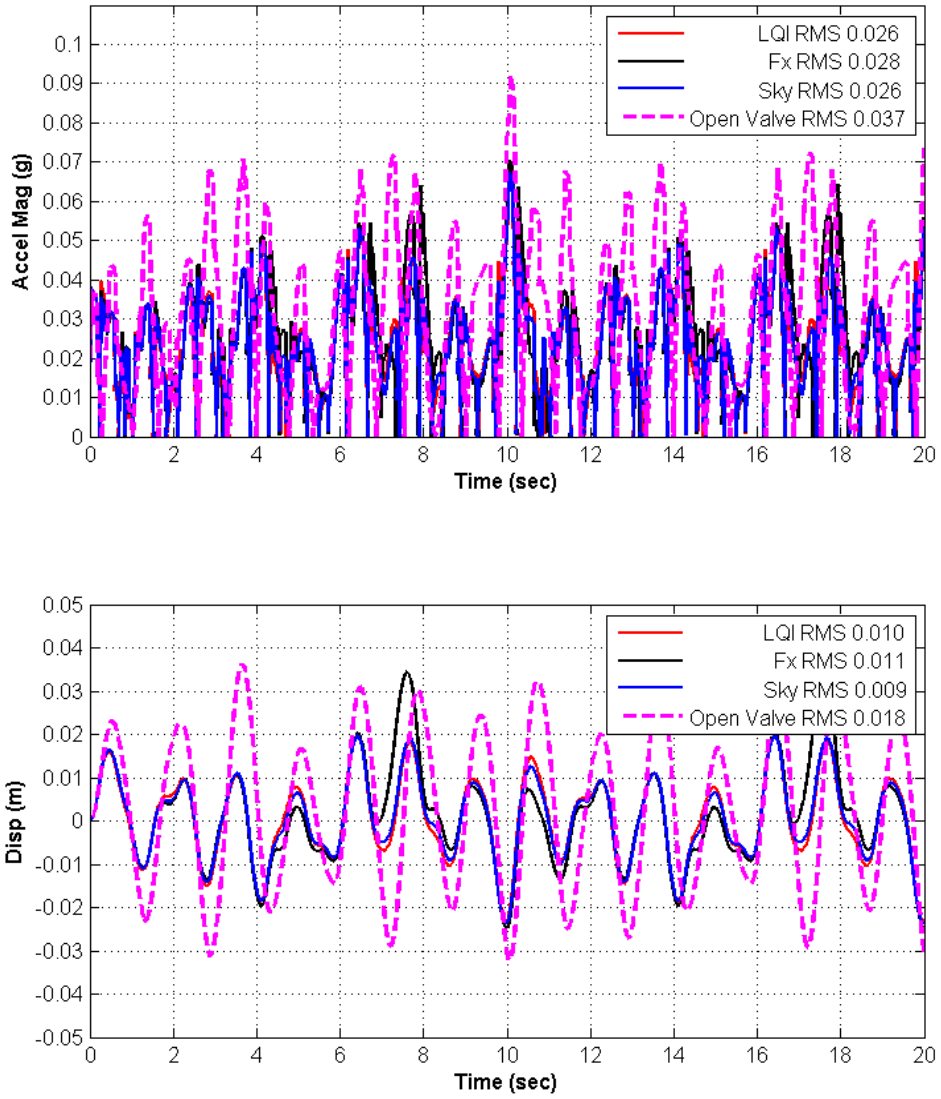

Figure 3.11 Response to multi-frequency input – acceleration and displacement

Table 3.1 Overall RMS simulated controller performance

	LQI	Modified Skyhook	Fx	Open Valve
Acceleration	0.026	0.026	0.028	0.037
Displacement	0.010	0.009	0.011	0.018

Table 3.2 RMS simulated controller performance expressed as a % reduction from open valve

	LQI	Modified Skyhook	Fx	Open Valve
Acceleration	-30%	-30%	-24%	0%
Displacement	-44%	-50%	-39%	0%

3.3.7 General Observations on Semi-Active Control

Unlike an active controller that supplies an external "aid" (energy or force) to the system to achieve the desired performance, the semi-active controller can only help the system generate *its own* damping force, which is dependent on inherent system parameters, both tunable and fixed. In the case of the present system, the opening of the valve is a tunable parameter, and the size of the valve, accumulator, air spring, pipes, hoses, and so forth, are fixed parameters. This would imply that the design of the system components (plant) is just as important for achieving optimal performance in a semi-active system as the design of the controller. To use an old saying, "You can't get blood out of a turnip." This is also true for an actively controlled system, but apparently even more so for a semi-active system, by virtue of the fact that the introduction of external energy cannot be used to potentially overcome any system defects or a less than optimal design.

It should also be emphasized that all controllers for a semi-active suspension system, such as this one, use some form of switching logic to determine when the system can generate a force in the required direction to help dissipate its own energy. Thus, there is only a finite amount of time during each cycle of the system that the controller can do its job, and the system can appropriately respond. This was seen in Figure 3.6 where the switching event is only about 0.37 seconds at 1.0 Hz. The switching instant or "window of opportunity" for control is smaller as the frequency rises. Note that when the controller activates, there is a finite amount of time required for the system to generate the desired force. In other words, no external energy is available to quickly deliver that force. The system itself has to generate it. The design and sizing of the system components influence how quickly the desired action can take place, not only by how fast the controller can react. As the frequency rises, there is a physical limit to how fast the valve can respond, and the forces that are generated are also a function of the proper sizing of the components.

In light of these observations, for purposes of future research on this system, it does not appear prudent to spend much time, effort, and money on developing other control algorithms, without attention to overall system (plant) design. No matter the type, speed, or

complexity of the controller algorithms, the limiting factor is going to be the actual system component design and/or configuration.

These observations were also verified by implementing the controllers on a test rig with a valve size that was not optimal (too restrictive to air flow) and an accumulator configuration that was less than optimal due to additional restrictions between the valve and the accumulator. These will be discussed in the next section.

3.4 Controller Test Implementation on the Test Rig

3.4.1 Introduction

The results given in the previous section were the simulation results using the plant model tuned to the test data. There were two major differences between the simulated results and the experimental test results presented below. Due to the limitations of the test rig, which are explained below, the simulations used a larger valve with an effective valve restriction that is roughly ten times less than the valve on the test rig. In other words, the tuning coefficient C_a in (2.15) was multiplied by a factor of 10. In addition, the effective accumulator size was increased to approximately 0.0114 m^3 (3 gallons), whereas the effective volume on the test rig was approximately 0.0038 m^3 (1 gallon). The test actually contained an accumulator with a volume around 3 gallons. However, due to restrictions introduced by the hose attachment and connections, the effective accumulation capacity was reduced to around 1 gallon. These changes illustrate the importance of system component design for future applications using a controlled orifice. The simulations were performed with better component sizing to illustrate what can be obtained by a properly sized system. Also, for the frequency response results, a larger input amplitude was used in the simulation.

3.4.2 Experimental Results

All controllers were implemented on the test rig. The frequency response is shown in Figure 3.12 for 6.35 mm base input amplitude. All controllers performed acceptably well compared to the open valve response up to about 1.7 Hz. It is interesting to note that the F_x controller performed slightly better than the other two.

Figure 3.13 provides a chart of the acceleration magnitudes and mass displacements for mixed frequency and amplitude inputs. This demonstrates the performance for a simulated road input. Table 3.3 provides the overall RMS values for each controller, and the open valve values. Table 3.4 provides the overall RMS values expressed as a percent reduction from the open valve performance. As expected, all three controllers performed better than the open valve response. On acceleration performance, relative to overall RMS, the *LQI* and F_x performed better than the Skyhook controller. On displacement performance, the *LQI* and *Modified Skyhook* performed better than the F_x.

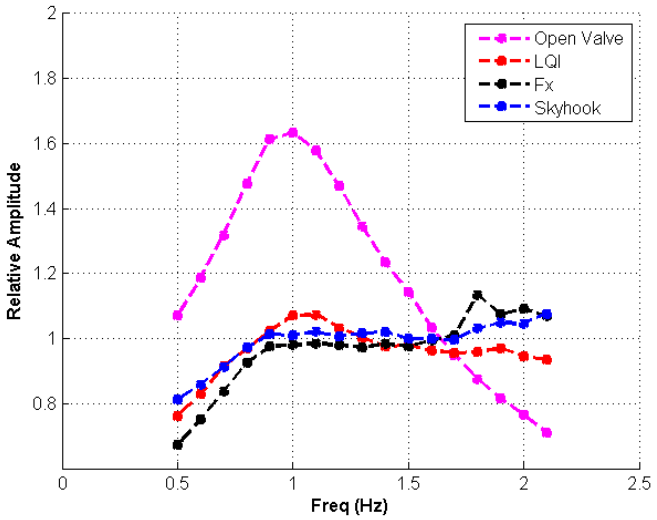

Figure 3.12 Controller tests frequency response

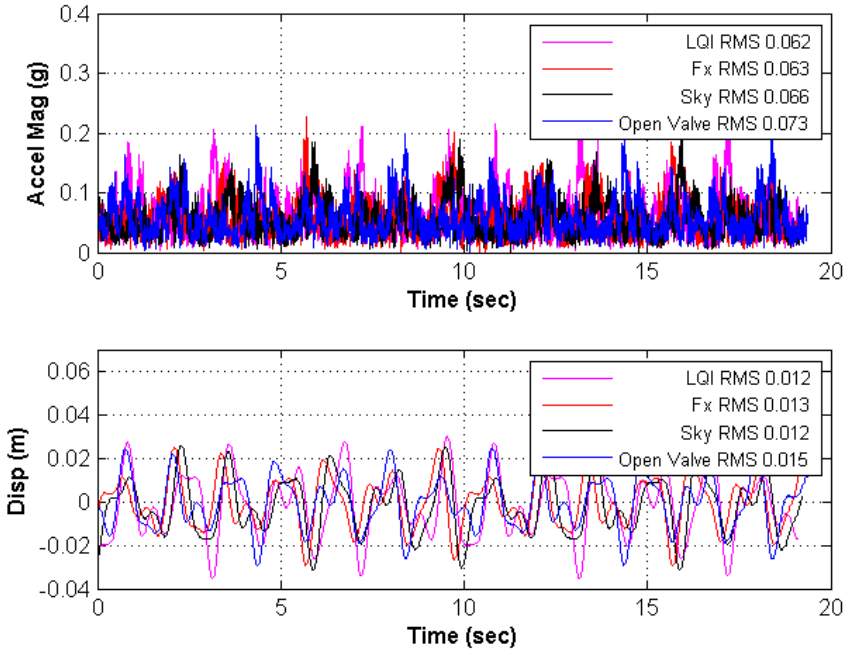

Figure 3.13 Controller test data mixed frequency and amplitude response

Table 3.3 Overall RMS controller test data performance

	LQI	Modified Skyhook	Fx	Open Valve
Acceleration	0.062	0.066	0.063	0.073
Displacement	0.012	0.012	0.013	0.018

Table 3.4 RMS controller test data performance expressed as a % reduction from open valve

	LQI	Modified Skyhook	Fx	Open Valve
Acceleration	-15%	-10%	-14%	0%
Displacement	-33%	-33%	-28%	0%

In summary, the test results provided similar overall behavior (trends) as the simulation results, although the simulation results were for a more ideal system configuration. In addition, the simulation frequency response results were run at higher displacement amplitude in the simulation. Performance on the test rig would be better at higher amplitudes if a more optimal design of components was implemented.

3.4.3 Observations and Design Issues

The valve used in the test rig was highly restrictive. In order for the model to match test data, the valve tuning coefficient C_a was set at 0.038, whereas a valve behaving as a "perfect" sharp-edged orifice would have $C_a \approx 1.0$. The valve is essentially a poppet type valve with passages that bend the air at 90 degree angles, which cause additional significant restrictions. Thus, the air flow is significantly less than would be expected from the advertised orifice size (0.375 inches). The exact details of the valve design are proprietary to the manufacturer. A search for a larger valve that met the requirements of this application was unsuccessful.

A second important sizing and attachment issue is the accumulator. The accumulator on the test rig is attached to the valve by a relatively long section of large hose (1.25 inches OD). The accumulator size was advertised at approximately 0.0151 m^3 (4 gallons). It was discovered that the large hose and piping attachments, in addition to providing some additional resistance, also acted as an accumulator. It is postulated that the large size (diameter and length) of these attachments and thus a relatively large volume of air contained within the components provided an accumulation effect. This effect was not modeled. As is clear from the analysis in this research, resistance alone does not set the location of the lower natural frequency of the system. Only the accumulator volume is responsible for this frequency. Experimental data indicated a higher natural frequency on the low end of the spectrum than what the model predicted using only the advertised volume of the accumulator. Adjusting the air flow resistance numbers in the simulation did not bring the model into conformance with the experimental data pertaining to this lower frequency. However, by adjusting the volume of the accumulator in the model, the simulation frequency response matched the experimental data frequency response for this lower system natural frequency. Therefore, it is postulated that there were effectively two accumulators acting in series. The combined effects effectively reduced the actual accumulation to approximately 0.0038 m^3 (1 gallon). To verify this postulate, future work would need to include a more detailed model of the piping between the air spring and the accumulator.

All tests were performed starting from an equilibrium condition with the valve open. While ensuring system equilibrium, there was a noticeable effect of a relatively long transient

for the stabilization of the pressure in the accumulator. This is believed due to the long hose and associated piping attachments between the valve and the accumulator, which effectively lowered the accumulation capability of the system, as discussed above, and provided some additional hose and piping resistance, as previously discussed.

It is unknown how the combined effects of the extra accumulation and hose/piping resistance dynamic behavior affected the results of the controller experiments. This dynamic effect was not modeled for simulation; however, the lower effective volume (from a static point of view) was accounted for in the simulation. If this effect happens to be significant, the resulting experimental results could be affected as a result of slightly varying accumulation capacity during each experiment as the pressure drop across the valve is constantly changing. A higher fidelity model would need to include this effect if it is desired to more closely approximate experimental results, although higher fidelity modeling does not necessarily lead to better control design in a simulation or model based engineering design environment.

An effective system design needs a valve and effective accumulation that are large enough to generate a force that is small as possible when the valve is fully open. This ensures that a force is not generated in the wrong direction when the switching logic determines that the controller should be turned off. It also ensures that the commanded force during a controllable event can be generated as quickly as possible. The accumulator also determines the lower system natural frequency when the valve is fully open.

Note in Figure 3.6 that the controllable switching event has a width of about 0.37 seconds at 1.0 Hz base input. This is a very small window of opportunity for the controller to do its job and for the system to respond. There is an assumed 0.03 second delay assumed for the valve response time, which is what was advertised but not verified. This underscores the importance of proper valve design. The valve needs to respond quickly to a command input. In addition, the air flow restriction needs to be minimal so that air can pass rapidly between the air spring and the accumulator, so that the *rate* of pressure drop across the valve is high enough to achieve the commanded damping force as quickly as possible during valve open command within a controllable event. This leads to better tracking of the desired force.

An additional issue in testing is the filtering of noisy signals, which typically degrades performance. The simulations used the same filters as on the test rig so that any delays

introduced by filtering would be same. However, for purposes of this research, it was decided that the additional work required identifying the actual noisy signals "seen" by the test rig for simulation purposes was neither cost effective nor necessary to achieve the goals of this research.

Another issue due to noisy signals that needs to be addressed is the effect on the switching events. The switching events are determined by the sign of the commanded damping force multiplied by the relative velocity as shown in (3.40). If these signals are noisy, there could be chattering of the controller at the switching event. Thus, proper filtering of the signals is important; however, the filtering should not introduce too much delay, which could degrade control performance.

The effects of temperature changes on the system during testing were not studied, and thus the effects on the results are not known. In addition to ambient temperature, resistance to air flow and compression/decompression of air in the system causes variations in temperature. In vehicular applications, temperature might become an important environmental variable, depending on climate.

CHAPTER 4. CONCLUSIONS

This chapter provides a summary of the research accomplishments, the major contributions of this research, and suggestions for future research.

4.1 Summary

The research presented in this thesis can be viewed to have two major parts: system or plant analysis and interpretation along with model development and tuning, and semi-active controller development. Simulations with a correlated model and test results were used to demonstrate the system's unique features, which led to the development of the control methodology.

In Chapter 2 a detailed development and in-depth analysis of the primary equations of motion for the system were realized. New results and interpretations were reported. A model of the system was developed with a view toward the utilizing the model for controller development, which set the operating paradigm on how much fidelity to build into the model. New results were reported on how best to tune the model to experimental data. The in-depth understanding and observations of the system led to how best to control the system.

Due to the unique features of the air spring-valve-accumulator system, the well-known methods typically used for semi-active vibration suppression, such as those applied to MR damper systems, cannot be easily applied to this type system in their current form. In particular, it has been demonstrated that the natural frequency and damping of this system vary as a function of relative amplitude and restriction to air flow between the air spring and the accumulator. This research developed and compared three new control methodologies that were shown to be effective at controlling the system. A key feature of each controller is the reliance on direct estimation of the damping force by measuring the air spring pressure. Pressure gauges are cost effective, easily available, and relatively easy to build into the system.

The first controller, referred to as the *LQI with Semi-Active Tracking Controller*, relied on the generation of an optimal "active" control law based on a subset of linear deterministic covariance control theory to calculate a desired damping force, which was assumed to be ideal if the system was being controlled actively. It was shown that the active controller

design could be based on a particular linear representation of the system due to a unique feature of this system. This determined the target or desired damping force. A Set-Point + PI tracking control law was then designed to drive the measured force as quickly as possible toward the desired force and to track the desired force once the initial error signal was sufficiently small. The tracking part of the control is only activated during the appropriate switching instants determined by appropriate switching logic. The active controller requires state feedback of inertial coordinates (mass displacement and velocity). This is easily done and not very costly for a stationary system, such as in a factory. However, the measurement of the two inertial coordinates is usually not practical for vehicular applications.

The second controller, referred to as the *Modified Skyhook with Semi-Active Tracking Controller*, used a modified form of the skyhook methodology applicable to this type system, which requires the measurement or estimate of a relative velocity and an inertial velocity (same as in MR (Magneto-Rheological) damper control). It was discovered that by proper selection of a skyhook gain multiplied by the absolute velocity, the ideal damper force generated by the LQI control law could be approximated. Thus, the LQI controller design can aid in selecting the skyhook gain. The remaining portion of the control is implemented the same as in the LQI Controller case. In the laboratory setting, the inertial velocity is easily calculated by differentiating the absolute displacement. In vehicular applications, the inertial velocity is usually estimated by integrating and properly filtering an accelerometer signal, which has its own set of signal processing issues.

The third controller, referred to as the *Relative Displacement with Semi-Active Tracking Controller*, may be the most promising for vehicular applications. This controller, in addition to the pressure measurement, relies only on a relative displacement and a relative velocity measurement, which is cost effective and easy to implement. The relative displacement is easily determined from, for example, a string potentiometer attached between the suspended mass and the base. The potentiometer signal is then differentiated to obtain the relative velocity. Similar to the modified skyhook controller, it was discovered that the appropriate selection of a control gain multiplied by the relative displacement could approximate the optimal damping force generated by the LQI active control law. Thus the LQI active control law can aid in the selection of the control gain.

For each of the controllers, the PI tracking control gains can be tuned based on simulation and/or testing on the actual system.

The importance of system component design for effective vibration control was highlighted. In particular, the proper sizing and selection of an air flow valve and the sizing and proper attachment of an accumulator were emphasized. The air flow valve should have as little restriction as possible to the air flow, and allow enough air flow that any forces generated in the wrong direction during the switching event when the controller commands a fully opened valve are minimized. In addition, the valve response time needs to be as fast as possible to provide good control over the small switching time frames or "windows of control opportunity." The width of these time frames is a function of the frequencies to be controlled. The accumulator should also be sized appropriately, since it controls the placement of the lower natural frequency of the system. A larger accumulator shifts system natural frequency lower relative to the air spring frequency (valve closed). Also, the accumulator should be attached to the air flow valve with minimal restriction. As discussed, piping restrictions may effectively lower the effective accumulation volume, and thus raise the lower system natural frequency.

As a secondary issue, additional insight was presented on the Covariance Control Theory. To date, this theory has not received wide spread attention, possibly due to being "buried" in the literature, most of the literature dealing with theoretical issues, and the lack of practical application examples outside of the aerospace venue, in particular flexible space structure control, which make it inaccessible to the practicing engineer. This theory, in the author's opinion, has certain benefits that make it amiable for application to vehicular control and design issues. With the algorithms that have already been developed, it is not hard to apply. A subset of the theory was used to develop the controllers in this thesis. Some additional examples were provided of how the theory might be applied, in the future, in the vehicular control area. Also, it was postulated that some prior active control research in vehicular control could be nicely expressed within the Covariance Control framework.

4.2 Primary Research Contributions

The primary contributions of this research are two-fold: those associated with the in-depth and insightful dynamic analysis of the system (plant) and model development and tuning, and those associated with the controller development. The in-depth study of this system generated the ideas for the best methodology to use to control the system, which led to the development of three possible controllers that were demonstrated and compared.

The in-depth dynamic analysis of the plant generated some new interpretations of the fundamental behavior of the plant, the model correlation and tuning procedure, and the reporting of new test data on a reversible sleeve air spring. The key items are:

1) The linear logarithmic relationship of the linear flow resistance to pressure and valve opening was a new result. Further research is needed to determine the utility of these relationships.
2) The understanding of how pressure composition affects the actual force transmitted to the suspended mass, and the resulting interpretation of the static pressure and volume test data in light of this interpretation is new information for this system.
3) The calculation and interpretation of the cross-over frequency is a new result.
4) The calculations and interpretation of the minimum peak frequency response on the behavior of the passive plant is a new result.
5) The procedure whereby static test data (volume vs. displacement) could be tuned so that the model could be correlated to dynamic test data is a new result.
6) The demonstration of the air spring "pumping" effect, whereby it oscillates above or below the initial equilibrium condition is new information on the behavior of this system.
7) The procedures for determining the valve effective orifice area relative to solenoid voltage and the bag damping coefficient is useful information for future design and research on this type system.
8) The reporting of new test data on a reversible sleeve type air spring provides useful data for future comparison to air springs of this type.
9) A number of design issues and recommendations were discussed. These are valuable for future research and design of this type system.

All of the controller developments are new results for this system, with the following highlights:

1) The observation of a special property of this system, whereby the plant can be described by a linear second order differential equation during the desired controllable instances. This allowed the use of a *linear* active control law to generate an ideal or desired optimal force.
2) The observation that a cost effective measurement of pressure allowed for the direct measurement of the damping force on the suspended mass. This overcame an apparent difficulty with this system due to the variable frequency and damping characteristics of the system, which does not exhibit in other semi-active systems, such as MR dampers. This allows the controller to establish a feedback of the damping force related to the commanded control input.
3) The demonstration that all three semi-active controllers could drive a damping force toward an optimally calculated ideal force. This result was made possible by the two observations above.
4) The linear optimal control law, coupled with simulations or test, could be used to set the gains on the other two controllers.
5) The surprising result that the third controller, which only needs a *relative* displacement and pressure measurement feedback can drive the damping close to the ideal optimal. This controller may be the most suited for vehicular applications, since it does not require inertial coordinates, and is very cost effective.
6) The demonstration of the importance of system component design as it relates to the controllability of the system.

4.3 Future Research Directions

Several suggestions are offered for future research and development as follows:

1) Testing with a larger valve and modified accumulator attachment should be implemented to demonstrate the full range of controllability of these controllers. As previously mentioned, a larger size valve is not currently available on the market that meets the optimal requirements of this system. If it is desired to implement this type

of semi-active control in practical applications, then valve design and manufacturing will need to be addressed.

2) To fully understand the behavior of the air spring/mass/valve/accumulator system, a model of the air spring sleeve material should be included. This could possibly be accomplished with the aid of finite element techniques coupled with the thermodynamic relationships.
3) Investigate the possibility of a cost effective *mechanical* solution that approximates the performance of the computer controlled solution.
4) Investigate the possibility of a variable accumulator design where both the air flow valve and accumulation are controlled.
5) Determine the effects of temperature on the system. This is especially important for vehicular applications that might require operating in extreme temperature conditions.
6) Develop a design methodology that generates *jointly* the optimal sizing of system components and controller design variables. It is known that optimizing parts of a system *separately* does not generate the optimum solution for the system as a whole.
7) Investigate various configurations for active control of this type system. For example, an air compressor and/or pressurized containers could be added to the system to supply additional control energy. The benefits of these configurations could then be compared to the semi-active control implementations in terms of performance and costs.
8) Investigate various alternative configurations for the system using semi-active controller methodology. For example, introducing into the system a second spring, which is mechanically attached to the first spring, such that when the suspended mass spring extends, the second spring compresses, and vice versa. This would have an additional "pushing" effect of forcing air through the valve in both directions. The second spring could be attached to the accumulator side of the valve, and air flow could be controlled between all three components in an optimal fashion.
9) Investigate the practical application of Covariance Control Theory to whole vehicle suspension control.

10) From a theoretical viewpoint, investigate merging the Disturbance Accommodating Control Theory with the Covariance Control Theory, with an application view toward whole system vehicular control, both active and semi-active, could be investigated.

BIBLIOGRAPHY

[1] Elbeheiry E. M., Karnopp D. C., Elaraby M. E., and Abdelraaouf A. M. (1995). Advanced Ground Vehicle Suspension Systems – A Classified Bibliography. *Vehicle System Dynamics, 24*, 231-258.

[2] Koeske, P. (2006). How an Air Spring Works. Firestone Industrial Products Company. [online] Available at: www.cargogear.com/imagelibrary/pdf/how-an-air-spring-works.pdf [Accessed 06 June 2012]

[3] Kuhn, T. S. (1970). The Structure of Scientific Revolutions, 2nd Edition. The University of Chicago Press.

[4] Quaglia, G., and Sorli, M. (2001). Air Suspension Dimensionless Analysis and Design Procedure. *Vehicle System Dynamics, 35(6)*, 443-475.

[5] Smith, Chester W. (1946). Calculation of Flow of Air and Diatomic Gases. *Journal of the Aeronautical Sciences*, 309-314.

[6] Beachley, N. H., and Harrison, H. L. (1978). Introduction to Dynamic System Analysis, 110-112, Harper & Row, Publishers, Inc., New York, NY.

[7] Ahmadian, M., Song, X., and Southward, S. C. (2004). No-Jerk Skyhook Control Methods for Semiactive Suspensions. *Transactions of the ASME*, Vol. 126, 580-584.

[8] Song, X., and Ahmadian, M. (2004). Study of Semiactive Adaptive Control Algorithms with Magneto-Rheological Seat Suspension. *SAE Technical Paper Series*, 2004-01-1648.

[9] Ahmadian, M., Song, X., and Southward, S. (2005). Semiactive Suspensions. *Transactions of the ASME*, Vol. 126, 580-584.

[10] Ahmadian, M., Song, X., and Sandu, C. (2005). Designing an Adaptive Semiactive Magneto Rheological Seat Suspension for Heavy Truck Applications. *Proceedings of SPIE*, Vol. 5760, 247-255.

[11] Song, X., Ahmadian, M., and Southward, S. (2007). Analysis and Strategy for Superharmonics With Semiactive Suspension Control Systems. *Journal of Dynamic Systems, Measurement, and Control*, Vol. 129, 795-803.

[12] Ma, X. Q., Rakheja, S., and Su Chun-Yi. (2008). Synthesis of a semiactive suspension seat for attenuation of Whole-Body Vibration and shock. *Int. J. Vehicle Design*, Vol. 47, Nos. 1/2/3/4, 157-175.

[13] Song, X. (2009). Cost-Effective Skyhook Control for Semiactive Vehicle Suspension *Applications. The Open Mechanical Engineering Journal*, 3, 17-25.

[14] Porumamilla, H., Kelkar, A. J., and Vogel, J. M. Modeling and Verification of an Innovative Active Pneumatic Vibration Isolation System (2008). *Journal of Dynamic Systems, Measurement, and Control, Vol. 130*.

[15] Porumamilla, H. Modeling, Analysis and Non-linear Control of a Novel Pneumatic Semi-Active Vibration Isolator: A Concept Validation Study (2007). PhD Dissertation, Iowa State University.

[16] Hotz, A., and Skelton, R. E. (1987). Covariance Control Theory. *Int. J. Control*, Vol. 46, No. 1, 13-32.

[17] Collins, E. G., Skelton, R. E. (1987). A Theory of State Covariance Assignment for Discrete Systems. *IEEE Trans. Automatic Control*, AC-32, No. 1, 35-41.

[18] Skelton, R. E. (1988). Dynamic Systems Control – Linear Systems Analysis and Synthesis. Wiley, New York.

[19] Yedavalli, R. K., (1988). Robust Covariance Control for Linear Uncertain Systems. *ASME Winter Annual Meeting*, Chicago, 88-WA/DSC-10.

[20] Corless, M., Zhu G., and Skelton, R. E. (1989). Improved Robustness Bounds Using Covariance Matrices. *IEEE Conf. on Decision and Ctrl*, Tampa, FL., 2667-2672.

[21] Hsieh, C., Skelton, R. E., and Damra, F. M. (1989) Minimum Energy Controllers with Inequality Constraints on Output Variances. *Optimal Control Applications & Methods*, Vol. 10, 347-366.

[22] Skelkton, R. E., and Ikeda, M. (1989). Covariance Controllers for Linear Continuous-Time Systems. *Int. J.* (198*Control*, Vol. 49, No. 5, 1773-1785.

[23] Hsieh, C., and Skelton, R. E. (1989). Covariance Controllers for Linear Discrete Time Systems. American Control Conf., June 21-23, 1989

[24] Zhu, G., and Skelton, R. E. (1990). Mixed L_2 and L_∞ Problems by Weight Selection in Quadratic Optimal Control. *IEEE Conf. on Decision and Control*, Hawaii, 1990.

[25] Hsieh C., and Skelton, R. E. (1990). All Covariance Controllers for Linear Discrete-Time Systems. *IEEE Transactions on Automatic Control*, Vol. 35, No. 8l, 908-915.

[26] Hsieh, C., Kim J. H., Liu K., Zhu G., and Skelton R. E. (1990). Model Identification and Controller Design for Large Flexible Space Structures – An Experiment on NASA's Mini-Mast. Report prepared for NASA Langley Research Center under grant NAG1-958.

[27] Liu, K., and Skelton, R. E. (1991). Model Identification and Controller Design for Large Flexible Space Structures – An Experiment on NASA's ACES Structure. CSI Guest Investigator Program, Second Year Report.

[28] Skelton, R. E. (1992). Multiobjective Control. Final Report, NASA Grant NAG8-124.

[29] Zhu, G., and Skelton, R. E. (1992). A Two-Riccati, Feasible Algorithm for Guaranteeing Output L_∞ Constraints. *Journal of Dynamic Sys., Meas., and Control*, Vol. 114, 329-338.

[30] Iwasaki, T., and Skelton, R. E. (1993). A Computational Algorithm for Covariance Control: Discrete Time Case. *Proceedings of American Control Conf.*, San Francisco, June 1993.

[31] Zhu, G., Rotea M. A., and Skelton, R.E. (1997). A Convergent Algorithm for the Output Covariance Constraint Control Problem. *SIAM J. Control Optim.*, Vol. 35, No. 1, 341-361.

[32] Iwasaki, T., Skelton, R. E., and Corless, M. (1998). A Recursive Construction Algorithm for Covariance Control, *IEEE Transactions on Automatic Control*, Vol. 43, No. 2, 268-272.

[33] Skelton, R. E., Iwasaki, T., and Grigoriadis, K. (1998). A Unified Algebraic Approach to Linear Control. Taylor & Francis Publishers, PA.

[34] Elmadany, M. M. (1988). Stochastic Optimal Control of Highway Tractors with Active Suspension. *Vehicle System Dynamics*, 17, 193-210.

[35] Elmadany, M. M., and Samaha, M. E. (1989). Optimum Response of a Stochastic Model of a Tractor-Semitrailer Vehicle Part I: Linear and Nonlinear Models of a Passively Suspended Vehicle. *12th Biennial Conf. on Mechanical Vibration and Noise*, Montreal, Quebec, Canada, Sept. 17-21, DE-Vol. 18-5.

[36] Elmadany, M. M., and Samaha, M. E. (1989). Optimum Response of a Stochastic Model of a Tractor-Semitrailer Vehicle Part II: Ride Control of an Actively Suspended Vehicle. *12th Biennial Conf. on Mechanical Vibration and Noise*, Montreal, Quebec, Canada, Sept. 17-21, DE-Vol. 18-5.

[37] Elmadany, M. M., and Abiduliabbar, Z. (1990). Design Evaluation of Advanced Suspension Systems for Truck Ride Comfort. *Computers & Structures*, Vol. 36, No. 2, 321-331.

[38] Beheiry, E. M., and Karnopp, D. C. (1996). Optimal Control of Vehicle Random Vibration with Constrained Suspension Deflection. *Journal of Sound and Vibration*, 189(5), 547-564.

[39] Johnson C. D. (1976). Theory of Disturbance Accommodating Controllers. *Advances in Control and Dynamic Systems*, Vol. 12, Ch.7, Academic Press, New York.

[40] Johnson C. D. (1982). A Discrete-time, Disturbance-Accommodating Control Theory for Digital Control of Dynamical Systems. *Control and Dynamic Systems; Advances in Theory and Applications*, Vol 18, Academic Press, New York.

[41] Karnopp, D. (1990). Design Principles for Vibration Control Systems Using Semi-Active Dampers. *Transactions of the ASME*, Vol. 112, 448-455.

ACKNOWLEDGEMENTS

First and foremost I would like to express my gratitude to my family, Charlyn, Bill, Greg, David, and Ann, for the several years of sacrifice to allow this work to be completed. This work could not have been completed without their patience.

In addition, I would like to thank all the committee members, Dr. Atul Kelkar, Dr. James Bernard, Dr. Judy Vance, Dr. Brian Steward, Dr. Greg Luecke, and Dr. Jerald Vogel for their patience and understanding as I struggled to complete this work in light of holding a full time job, not to mentioned having transferred to different jobs and locations twice before completing this work. Their occasional words of encouragement were appreciated. It has also been a pleasure to work with some of the members of this committee, in a different capacity, on research outside of what is contained in this thesis.

I would also like to extend special thanks to Dr. Atul Kelkar, my major professor, for his guidance and motivation during the entire process. Without his guidance, assistance, and patience, I would not have been able to complete this work. Also, special thanks go to Dr. Jerald Vogel for his assistance and practical insight. In addition, Dr. Kelkar's and Dr. Vogel's entrepreneurial spirit is highly contagious, and it has been a real pleasure to work with these guys.